UNCERTAINTY QUANTIFICATION BY USING STOCHASTIC APPROACH IN PORE VOLUME CALCULATION FOR GEOTHERMAL RESERVOIR

A THESIS SUBMITTED TO
THE GRADUATE SCHOOL OF NATURAL AND APPLIED SCIENCES
OF
MIDDLE EAST TECHNICAL UNIVERSITY

BY

EMRAH GÜREL

IN PARTIAL FULFILLMENT OF THE REQUIREMENTS
FOR
THE DEGREE OF MASTER OF SCIENCE
IN
PETROLEUM AND NATURAL GAS ENGINEERING

FEBRUARY 2016

Approval of the thesis:

UNCERTAINTY QUANTIFICATION BY USING STOCHASTIC APPROACH IN PORE VOLUME CALCULATION FOR GEOTHERMAL RESERVOIR

submitted by EMRAH GÜREL in partial fulfillment of the requirements for the **Degree of Master of Science in Petroleum and Natural Gas Engineering Department, Middle East Technical University by**,

Prof. Dr. Gülbin Dural Ünver _____
Dean, Graduate School of **Natural and Applied Sciences**

Prof. Dr. Serhat Akın _____
Head of Department, **Petroleum and Natural Gas Engineering**

Prof. Dr. Serhat Akın _____
Supervisor, **Petroleum and Natural Gas Engineering Dept., METU**

Examining Committee Members:

Prof. Dr. Nurkan Karahanoğlu _____
Geological Engineering Dept., METU

Prof. Dr. Serhat Akın _____
Petroleum and Natural Gas Engineering Dept., METU

Prof. Dr. Şakir Şimşek _____
Geological Engineering Dept., Hacettepe University

Assist. Prof. Dr. Çağlar Sınayuç _____
Petroleum and Natural Gas Engineering Dept., METU

Assist. Prof. Dr. İsmail Durgut _____
Petroleum and Natural Gas Engineering Dept., METU

Date: 02/02/2016

I hereby declare that all information in this document has been obtained and presented in accordance with academic rules and ethical conduct. I also declare that, as required by these rules and conduct, I have fully cited and referenced all material and results that are not original to this work.

Name, Last name: EMRAH GÜREL

Signature :

ABSTRACT

UNCERTAINTY QUANTIFICATION BY USING STOCHASTIC APPROACH IN PORE VOLUME CALCULATION FOR GEOTHERMAL RESERVOIR

Gürel, Emrah
M.S., Department of Petroleum and Natural Gas Engineering
Supervisor: Prof. Dr. Serhat Akın

February 2016, 113 pages

This study will present the application of a stochastic approach and experimental design techniques to a geologic system in order to quantify the uncertainty of pore volume estimations for a liquid dominated high temperature geothermal reservoir. The pore volume is a key element when defining the total resource available in the field. Alasehir geothermal reservoir pore volume uncertainty has been assessed. The uncertainties being addressed include geometry (top of reservoir and base of reservoir), reservoir continuity and porosity. Porosity of reservoir rocks (marble and schist) that are producing formations of Alasehir reservoir has been calculated using fractal analysis method. Thickness of the reservoir is obtained using drilling logs, seismic and resistivity data interpretations. Areal extent of the reservoir is obtained using reservoir temperature data obtained from static temperature logs of 25 previously drilled wells. Uncertainties were firstly characterized by standard deviations and then evaluated from the statistical distribution using Monte Carlo simulations. Placket and Burman design is performed with Minitab software using the significance at 95% confidence level and to identify the sensitivity of parameters on pore volume calculation. It has been found that porosity followed by the thickness and the area is most uncertain parameters that effect pore volume.

Keywords: pore volume, porosity, fractal characterization

ÖZ

JEOTERMAL REZERVUARLAR İÇİN GÖZENEK HACMİ HESAPLANMASINDA STOKASTİK YAKLAŞIM KULLANILARAK BELİRSİZLİK ÖLÇÜMÜ

Gürel Emrah
Yüksek Lisans, Petrol ve Doğal Gaz Mühendisliği Bölümü
Tez Yöneticisi: Prof. Dr. Serhat Akın

Şubat 2016, 113 sayfa

Bu çalışmada sıvı hâkim yüksek sıcaklıklı jeotermal rezervuar için gözenek hacmi tahmini belirsizliğini belirlemek amacıyla jeolojik sistem için stokastik bir yaklaşım ve deneysel tasarım teknikleri sunulacaktır. Gözenek hacmi toplam mevcut kaynak hesaplaması yapılırken en önemli unsurdur. Bu çalışmada Alaşehir jeotermal rezervuarının gözenek hacmi belirsizliği değerlendirilmiştir. Rezervuar geometrisi (rezervuar girişi ve tabanı), rezervuar sürekliliği ve gözeneklilik ele alınan belirsizliklerdir. Alaşehir rezervuarında üretim kayaçları olan mermer ve şistin gözeneklilikleri fraktal yöntem kullanılarak hesaplanmıştır. Rezervuar kalınlıkları sondaj logu, sismik ve özdirenç verileri kullanılarak hesaplanmıştır. Alan hesaplaması ise sondajı tamamlanan 25 kuyunun taban statik sıcaklıkları kullanılarak hesaplanmıştır. Belirsizlikler öncelikle standart sapma ile karakterize edilmiştir ve ardından Monte Carlo Simülasyonu kullanılarak istatistiksel dağılımlar değerlendirilmiştir. Gözenek hacmi hesaplamasındaki değerlerin hassasiyeti Plackett ve Burman tasarım tekniği 95 % güven düzeyi kullanılarak Minitab yazılımıyla belirlenmiştir. Gözenek hacmi hesaplamasında gözeneklilik, rezervuar kalınlığı ve alan başlıca belirsiz parametreler olduğu tespit edilmiştir.

Anahtar Kelimeler: gözenek hacmi, gözeneklilik, fraktal karekterizasyon.

To my beloved family

ACKNOWLEDGEMENTS

I am sincerely thankful to my supervisor Prof. Dr. Serhat Akın for guidance, advice, criticism, encouragements and insight throughout the research.

I would like to thank Metin Yazman, Erinç Tonguç and Emir Dimici for their valuable support and guidance.

My special thanks go to my wife who supported, encouraged me during my thesis writing period.

TABLE OF CONTENTS

ABSTRACT v

ÖZ vi

ACKNOWLEDGEMENTS viii

TABLE OF CONTENTS ix

LIST OF TABLES xii

LIST OF FIGURES xiii

NOMENCLATURE xvii

CHAPTERS

1. INTRODUCTION 1

2. LITERATURE REVIEW 3

2.1 Resource Terminology 3

2.2 Geothermal Resource Terminology 4

2.3 Geothermal Resource Assessment 5

2.4 Resource Assessment Methods 5

2.4.1 Surface Heat Flux Method 5

2.4.2 Volume Method 5

2.4.3 Planner Fracture Method 6

2.4.4 Magmatic Heat Budget 6

2.5 Volumetric Resource Assessment 6

2.6 Pore Volume Calculation 7

2.7 Stochastic Approach 7

2.8 Uncertainty Quantification 8

3. STATEMENT OF PROBLEM 11

4. GEOLOGY OF ALASEHIR GEOTHERMAL FIELD 13

5. METHODOLOGY 17
5.1 Porosity Estimation 17
5.1.1 Fractal Characterization 17
5.1.2 Fracture Density 21
5.1.3 Porosity with FD 24
5.1.4 Porosity from Well Test 26
5.2 Thickness Estimations 28
5.2.1 Thickness Estimation Using Drilled Wells Data 28
5.2.2 Thickness Estimation Using Seismic Data 30
5.2.3 Thickness Estimation Using Resistivity Data 34
5.3 Area Estimation 37
5.3.1 Proven Area 39
5.3.2 Probable Area 39
5.3.3 Possible Area 40
6. MONTE CARLO SIMULATION 41
7. RESULTS AND DISCUSSIONS 43
7.1 Distribution Selection of Parameters 43
7.1.1 Porosity 43
7.1.2 Thickness 44
7.1.3 Area 45
7.2 Monte Carlo Simulation with @RISK 46
7.3 Sensitivity Analysis 50
7.3.1 Monte Carlo Simulation 50
7.3.2 Experimental Design 50
7.4 Error Analysis 53
7.4.1 Source of Error 53
8.CONCLUSIONS 55
REFERENCES 57
APPENDICES
A. FRACTAL DIMENSION ESTIMATIONS 61

B. FRACTURE DENSITY ESTIMATIONS 75

C. POROSITY ESTIMATIONS 85

D. THICKNESS ESTIMATIONS USING CUTTING SAMPLE LOG 93

LIST OF TABLES

TABLES

Table 1 Fractal Dimension of Outcrop Images 21
Table 2 Fracture Density from Outcrop Images 23
Table 3 Fracture Density from Mud Loss Data 24
Table 4 Porosity calculated with FD 26
Table 5 Porosity Values from Interference Test Result 27
Table 6 Reservoir Thickness Determination of Wells 30
Table 7 Thickness from Seismic 31
Table 8 Thickness from Resistivity Data 36
Table 9 Drilled Wells Bottom Hole Temperatures 38
Table 10 Proven, Probable and Possible Areas 40
Table 11 Thickness from different method 44
Table 12 Area from Contour Map 45
Table 13 Monte Carlo Simulation Input Parameters 46
Table 14 Summary Statistics for Pore Volume 48
Table 15 Simulation Summary 49
Table 16 Reference Model Parameters Chosen for the Experimental Design 51
Table 17 Experimental Design Simulation Run for Pore Volume 52
Table 18 Image Length and Area Calculation 82
Table 19 Fracture Intersection Numbers in X and Y Directions 82
Table 20 Fracture Density for Outcrop Images 83
Table 21 Fracture Density for Borehole 84

LIST OF FIGURES

FIGURES

Figure 1 Classification of Mineral Resources (McKelvey, 1976) 3
Figure 2 McKelvey Box for Geothermal Resources (Muffler and Cataldi, 1978) 4
Figure 3 The Geological Map of Gediz Graben (Yilmazer et. al. 2010) 14
Figure 4 Stratigraphy Schemes for Gediz Graben (Demircioglu, 2009) 14
Figure 5 Cross Section of X-5 Well 15
Figure 6 Outcrop Image Stations 18
Figure 7 Threshold Outcrop Image 19
Figure 8 Design of Fracture Patterns 20
Figure 9 Fractal Dimension 20
Figure 10 Fracture Density from Outcrop Image 22
Figure 11 Mud Loss Data (Akin, 2013) 23
Figure 12 Porosity from ImageJ at Selected Area 25
Figure 13 Threshold Image with Shadow 25
Figure 14 Cutting Sample Log 29
Figure 15 Seismic Profiles in Alasehir Graben (Cifci,2007) 32
Figure 16 Seismic Profile of S-16 Superimposed with X-29 and X-30 Cross Section 33
Figure 17 Site Location Map of Survey Area (Erdogan et.al., 2014) 34
Figure 18 Borehole Section Superimposed on Resistivity Mode (Erdogan et. al., 2014) 35
Figure 19 Porous Interval in Reservoir Basement 36
Figure 20 Three Intervals in Porous Section 37
Figure 21 Area Including Drilled Wells Location 38
Figure 22 Temperature Contour Map 39
Figure 23 Probable Area with 185 ^{o}C 39
Figure 24 Porosity Distribution 44

Figure 25 Thickness Distribution 45
Figure 26 Porosity Lognormal Distribution with Frequency 46
Figure 27 Thickness Triangular Distribution with Frequency 47
Figure 28 Area Triangular Distribution with Frequency 47
Figure 29 Monte Carlo Simulation Result (Pore Volume vs. Frequency) 48
Figure 30 Probability Analysis of Pore Volume 49
Figure 31 Tornado Sensitivity Analysis 50
Figure 32 Pareto Chart of the Standardized Effects 52
Figure 33 Normal Plot of the Standardized Effects 53
Figure 34 Threshold of S-1 Image 61
Figure 35 Fracture Pattern and FD of S-1 61
Figure 36 Threshold of S-2 Image 62
Figure 37 Fracture Pattern and FD of S-2 62
Figure 38 Threshold of S-3 Image 62
Figure 39 Fracture Pattern and FD of S-3 63
Figure 40 Threshold of S-4 Image 63
Figure 41 Fracture Pattern and FD of S-4 64
Figure 42 Threshold of S-5 Image 64
Figure 43 Fracture Pattern and FD of S-5 65
Figure 44 Threshold of S-6 Image 65
Figure 45 Fracture Pattern and FD of S-6 65
Figure 46 Threshold of S-7 Image 66
Figure 47 Fracture Pattern and FD of S-7 66
Figure 48 Threshold of S-8 Image 66
Figure 49 Fracture Pattern and FD of S-8 67
Figure 50 Threshold of S-9 Image 67
Figure 51 Fracture Pattern and FD of S-9 67
Figure 52 Threshold of S-10 Image 68
Figure 53 Fracture Pattern and FD of S-10 68
Figure 54 Threshold of S-11 Image 69
Figure 55 Fracture Pattern and FD of S-11 69
Figure 56 Threshold of M-1 Image 69

Figure 57 Fracture Pattern and FD of M-1 70
Figure 58 Threshold of M-2 Image 70
Figure 59 Fracture Pattern and FD of M-2 70
Figure 60 Threshold of M-3 Image 71
Figure 61 Fracture Pattern and FD of M-3 71
Figure 62 Threshold of M-4 Image 71
Figure 63 Fracture Pattern and FD of M-4 72
Figure 64 Threshold of M-5 Image 72
Figure 65 Fracture Pattern and FD of M-5 73
Figure 66 Threshold of M-6 Image 73
Figure 67 Fracture Pattern and FD of M-6 73
Figure 68 Fracture Density of S-1 75
Figure 69 Fracture Density of S-2 75
Figure 70 Fracture Density of S-3 76
Figure 71 Fracture Density of S-4 76
Figure 72 Fracture Density of S-5 77
Figure 73 Fracture Density of S-6 77
Figure 74 Fracture Density of S-7 77
Figure 75 Fracture Density of S-8 78
Figure 76 Fracture Density of S-9 78
Figure 77 Fracture Density of S-10 79
Figure 78 Fracture Density of S-11 79
Figure 79 Fracture Density of M-1 80
Figure 80 Fracture Density of M-2 80
Figure 81 Fracture Density of M-3 81
Figure 82 Mud Loss in Well-1 83
Figure 83 Mud Loss in Well-2 84
Figure 84 Mud Loss in Well-3 84
Figure 85 Porosity @Lo for S-1 85
Figure 86 Porosity @Lo for S-2 85
Figure 87 Porosity @Lo for S-3 86
Figure 88 Porosity @Lo for S-4 86

Figure 89 Porosity @Lo for S-5 87
Figure 90 Porosity @Lo for S-6 87
Figure 91 Porosity @Lo for S-7 88
Figure 92 Porosity @Lo for S-8 88
Figure 93 Porosity @Lo for S-9 89
Figure 94 Porosity @Lo for S-10 89
Figure 95 Porosity @Lo for S-11 90
Figure 96 Porosity @Lo for M-1 90
Figure 97 Porosity @Lo for M-2 91
Figure 98 Porosity @Lo for M-3 91
Figure 99 Porosity @Lo for M-4 92

NOMENCLATURE

H = heat energy, kJ

$\emptyset$= porosity, fraction

c = specific heat, kJ/kg-°C

ρ= density, kg/m^3

A = area, m^2

h_1 = whole reservoir thickness for heat from rock, m

h_2 = porous reservoir thickness for heat from water, m

T = temperature, °C

P = Pore volume, m^3

FD = Fractal dimension

r = smaller square grids length

N = Number of occupied grids

D = Fractal dimension

F_f = Fracture frequency

$\emptyset_f$ = Porosity at L

L = Side length of a region

$\emptyset_{fo}$ = Porosity at L_o

L_0 = Side length of specified region

E = Euclidean dimension

m = meter

S= Storativity, m/Pa

c = compressibility, Pa^{-1}

P10 = %10 Probability

P50 = %50 Probability

P90 = %90 Probability

ED = Experimental design

PB = Plackett and Burman design

CHAPTER 1

INTRODUCTION

This study will present the application of a stochastic approach and Experimental Design techniques to a geologic system in order to quantify the uncertainty of Pore Volume estimations for a liquid dominated high temperature geothermal reservoir. The Pore Volume is a key element when defining the total resource available in the field. The uncertainties being addressed are geometry (i.e. top of reservoir and base of reservoir), reservoir continuity (i.e. rock type and facies distribution) and Petrophysical property (i.e. porosity) (Asrizal et. al., 2006).

Information from varying sources, which includes data from drilling, production, injection and observation wells, comparable geothermal fields, resistivity surveys and seismic survey are key parameters to develop the range of uncertainty for each of the parameters. In fact, the most important parameters when calculating the volume of the geothermal potential is the distribution of porosity. Porosity is calculated using fractal dimension obtained from fractal characterization (Acuna et. al., 1992). Porosity data for schist and marble outcrop data are compared with well test results (i.e. storage capacity constant). Then, reservoir thickness is determined using drilling logs (i.e. cutting sample logs), resistivity data (i.e. Magnetotelluric) and seismic data. Although 3D resistivity is generally used to determine area, measured bottom hole temperature is used to determine area as well (Sarmiento and Steingrímsson, 2008). Porosity, thickness and area uncertainties are firstly characterized by standard deviations and then evaluated from the statistical distribution of the results of series of measurements. Also, parameters are analyzed

in terms of proven, probable and possible cases (EURACHEM/CITAC Guide, 2012). The results are then used to generate a range of theoretical pore volumes via Monte Carlo simulation. The sensitivity of all parameters is studied using an experimental design technique since it is known as alternative method for sensitivity analysis (Yeten et. al., 2005)

CHAPTER 2

LITERATURE REVIEW

2.1 Resource Terminology

U.S. Bureau of Mines and U.S. Geological Survey (1976) classified total resources as identified and undiscovered based on geologic evidence. While classifying resources, economic feasibility and the degree of geologic assurance are used in creating McKelvey Box (1976). A resource is defined as a mineral or energy resource in terms of geologic aspect, which is a concentration of naturally occurring solid, liquid, or gaseous materials in or on the Earth's crust where economic extraction of a commodity is feasible now or in the future. Reserve is defined as part of a resource that can be economically identified as demonstrated and inferred. McKelvey Box (1976) is generally used for classification of mineral resources (Figure 1).

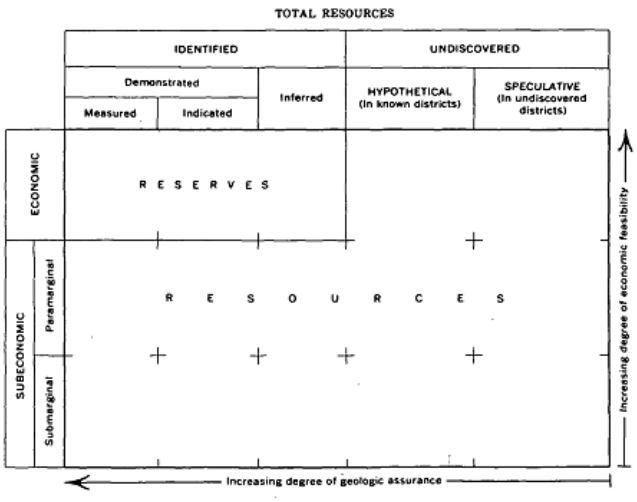

Figure 1 Classification of Mineral Resources (McKelvey, 1976)

2.2 Geothermal Resource Terminology

Muffler and Cataldi (1978) used McKelvey Box to create and categorize geothermal resource (Figure 2). A geothermal resource base definition is used for total resources. It is defined as the heat stored in the earth's crust beneath a specific area and measured from local mean annual temperature. *Geothermal resource* is defined as economical energy extraction in the future. In addition, *reserve* is defined as energy economically and legally extracted now. They classified reserves in two categories in terms of economy aspect, which are economic and sub-economic. Proven, probable and possible definitions are stated in reserve category. *Proven reserves* are heat quantities that are estimated using geoscientific and engineering data and recovered commercially for appropriate operating methods from known reservoir. *Probable reserves* are heat quantities that can be recovered most likely. Sufficiently, there are enough indicators of reservoir temperatures from offset wells. *Possible reserves* are heat quantities that can be recovered in less chance than the probable reserves. Resistivity anomalies, temperature distributions are parameter which can show reservoir existence (Sarmiento and Steingrímsson, 2011).

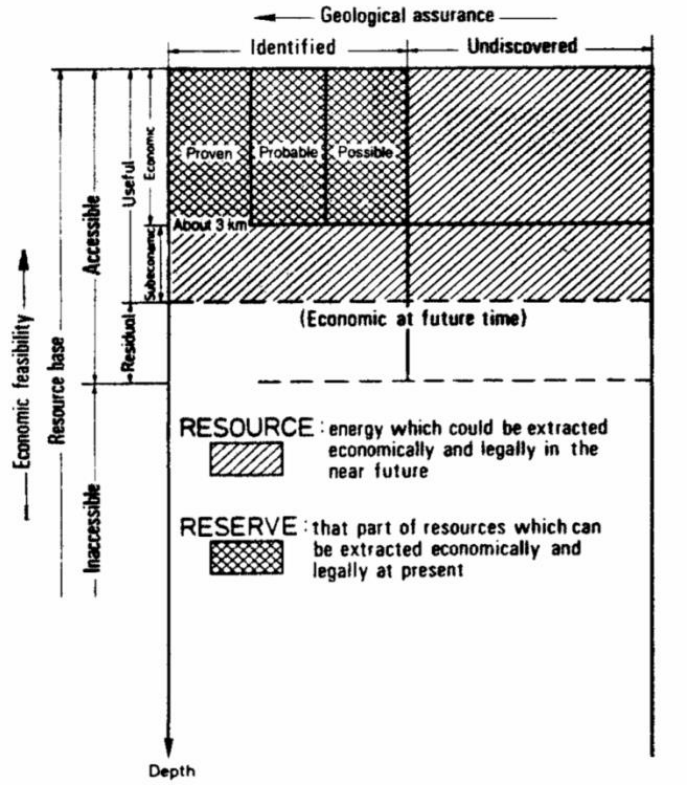

Figure 2 McKelvey Box for Geothermal Resources (Muffler and Cataldi, 1978)

2.3 Geothermal Resource Assessment

Muffler and Cataldi, (1977) defined resource assessment and its importance. Increasing demand for minerals and hydrocarbon is a result of need to estimate both of the quantities that could be produced under present economic conditions and the quantities that have not been discovered yet or that may be produced with improved technology or under different economic conditions. The estimation of future supplies of minerals and hydrocarbon is named as resource assessment. Although it is an extremely powerful tool for calculation of commonly used sources like oil, natural gas, coal etc., increasing demand of renewable geothermal energy resulted in the use of this method for geothermal resource analysis. Yet, changing state of geothermal knowledge, the increasing data with drilled holes number, the improving technology, and the changing economics with respect to other sources of energy necessitated the revise of geothermal resource assessment. Muffler and Cataldi (1977) published a report aiming to summarize the techniques used in geothermal resource assessment, to clarify terminology and assumptions, and to provide a foundation for the development of optimum geothermal resource assessment methodology.

2.4 Resource Assessment Methods

Muffler and Cataldi (1977) grouped geothermal reserve estimation methods in four categories;

1. Method of surface heat flux
2. Volume method
3. Planar fracture method
4. Methods of magmatic head budget

2.4.1 Surface Heat Flux Method

It is the measurement of the rate of thermal energy loss at the ground surface by means of conduction, steaming ground, hot springs, fumaroles, and discharge of thermal fluids directly into streams.

2.4.2 Volume Method

It is the calculation of the accessible resource base using subsurface temperature, volume, specific heat and density. Then, it is multiplied with recovery factor to estimate the recoverable heat.

2.4.3 Planner Fracture Method

It is the calculation of thermal energy where heat is extracted through flow of water along extensive, planar fractures from fractures only by conduction. Since heat is obtained from conductive fractures; fracture area, fracture spacing, initial rock temperature, minimum acceptable outflow temperature, and the thermal conductivity of the rock should be estimated in this method. Essentially, the planar fracture method can be used while calculating the heat extractable from geothermal areas in flood basalt terrains. However, it is not used for large regions or most common geologic situations characterized by folding and faulting.

2.4.4 Magmatic Heat Budget

It is the estimation of thermal energy as a function of the number, size, position and age of young igneous intrusions acting as heat sources for overlying geothermal systems or being themselves targets for exploration and development. Even though this method does not supply a precise categorization of resources, it provides a broad overview of the accessible resource base. Therefore, its result is little quantitative insight into the fraction of this resource base that might be recoverable.

Muffler and Cataldi (1977) pointed out at the end of their study that volume method is more efficient way to calculate resource because its parameters are measured or estimated.

2.5 Volumetric Resource Assessment

The volumetric method is the estimation of the energy content of the geothermal system in question by assessing the reservoir volume and the predominant reservoir temperature above a given cut-off temperature, or rejection temperature, which is based on the energy conversion technology assumed. Then, the recoverable thermal energy is estimated from the thermal energy available in the reservoir with a thermal recovery factor for the producible fraction of the reservoir's thermal energy. There are two assumptions in this method. Firstly, the reservoir rocks are considered as porous and permeable. Secondly, the water mass can be extracted from the reservoir mines the heat from the overall volume of the reservoir (Handoko, 2010).

Muffler and Cataldi (1977) give the formulation of geothermal resource base. In the equation; there are two cases; heat from rock solid and heat from water in pore volumes.

$$H = H_r + H_W \tag{2.1}$$

$$H = c_r \rho_r (1 - \emptyset)(Ah_1)(T_i - T_o) + c_f \rho_f \emptyset (Ah_2)(T_i - T_o) \tag{2.2}$$

where;

H = heat energy, kJ

∅= porosity, fraction

c = specific heat, kJ/kg-°C

ρ= density, kg/m^3

A = area, m^2

h_1 = whole reservoir thickness for heat from rock, m

h_2 = porous reservoir thickness (net thickness) for heat from water, m

T = temperature, °C

Also, other subscripts are *r* for rock, *f* for fluid, *i* for initial and *o* for optimum.

2.6 Pore Volume Calculation

In equation 2.1, the heat from rock and the heat from water in porous volume are two important parameters. While calculating the heat from water in porous volume, porosity, area and thickness are perhaps the most important parameters that affect the result. Multiplications of these three parameters give the pore volume.

$$P = \emptyset(Ah) \tag{2.3}$$

where;

P = pore volume, m^3

∅= porosity, fraction

A = area, m^2

h = porous reservoir thickness, m

2.7 Stochastic Approach

It is possible to use stored heat equation in two approaches, deterministic and stochastic. Both approaches use mathematical formulas to estimate volume. In

deterministic approach, single values are used as input parameters representative of reservoir properties resulting in a single value estimate, which can be defined as best-estimated pore volume. Essentially, the input data are directly related to a physical model. In stochastic approach, continuous probability density functions (PDFs) are used and these distributions are combined for generating a PDF for reserves. The input PDF's can be combined analytically or by random sampling, i.e. Monte Carlo simulation. The result is obtained by central-limit theorem and distribution is generally lognormal, not depending on the type of input variables. Thus, reserves are assumed as in analytical techniques. A large number of iterations should be carried out for stable results in Monte Carlo simulation (Demirmen, 2007).

2.8 Uncertainty Quantification

EURACHEM/CITAC Guide (2012) defined uncertainty as a parameter related with the result of a measurement characterizing the dispersion of the values that could reasonably be attributed to the measured ones. They stated that uncertainty of measurement generally includes many components that can be evaluated from the statistical distribution of the results of series of measurements and characterized by standard deviations as well.

In general, many sources of measurement error such as errors of mathematical models, incomplete data, errors in measurement, deviations of data and missing data may cause uncertainty. A degree of inaccuracy occurs in measurements in the field or in the laboratory due to a consequence objective measurement error or human based errors. Although error occurrence can be reduced with more accurate instruments or careful human efforts, it is never avoided. In fact, creating statically data and producing engineering data may help in assessment of uncertainty and reducing errors. Over the last decade, stochastic models and Monte Carlo simulations have been widely used as they are very useful tools for reserves estimation in oil, gas and geothermal industry. In Monte Carlo simulation, uncertainty of the values of each parameter is evaluated and reserve is calculated. Thus, the stochastic approach provides statistical results for reserves evaluation. A probability distribution function for each parameter and reserves are introduced by stochastic methods. In this methodology, the central limit theorem is used automatically and the sum of probability distributions, regardless of their type will create a normal distribution.

Then, the product of probability distributions, regardless of their type will produce lognormal distribution. The reserves will place best lognormal distribution (Kosova et. al., 2015). The uncertainty in reserve estimation is overcome with the establishment of definitions for reserve categories, which are proved, probable and possible (Elliott, 1995).

CHAPTER 3

STATEMENT OF PROBLEM

Geothermal energy development and investments increased tremendously in the last 10 years in Turkey. That's why resource assessment gained more importance as a tool to make future plans. Essentially, while calculating geothermal potential of a geothermal reservoir, the most important parameters are porosity, area and thickness. Multiplication of these parameters gives geothermal pore volume of field. In this study, pore volume calculation is presented for Alasehir geothermal reservoir with uncertainty quantification by using stochastic approach.

CHAPTER 4

GEOLOGY OF ALASEHIR GEOTHERMAL FIELD

Alasehir Geothermal Field is part of Gediz Graben. Gediz Graben is located in western Turkey from southeast of Alaşehir town to west of Turgutlu town. It is a recent target of the geothermal activities due to high temperature geothermal discoveries. Ciftci (2007) defined the Gediz Graben into two sub-basins as Salihli and Alasehir basins. Thickness and ages of the sedimentary units are essentially distinctive in these sub-basins. The deposition in the Alasehir sub-basin starts with the Alasehir formation compared to Caltilik formation in the Salihli sub-basin. Essentially, thickness of the sediments in two basins is remarkably similar to each other. It can be said that Salihli basin has probably experienced higher rate of subsidence for a relatively shorter period compared to the Alasehir basin. Furthermore, a probable transfer fault between the two basins can cause to accommodate the consequential kinematic differences among them.

Yilmazer et al. (2010) also divided Gediz Graben into three locations based on geothermal activities. They are Alasehir, Salihli and Urganlı (Figure-3). He pointed out that measured reservoir temperature starts from 215 ^{o}C in Alasehir and decreases towards Urganli to 85 ^{o}C.

There are many geological studies to define stratigraphy of Gediz Graben (Figure-4). Basically, studies focus on interpretation of graben fill since hydrocarbon discovery was targeted. Gediz Graben has been mapped in five sections according to lithological characteristics, structure and color. It consists of four main parts according to İztan and Yazman (1990). They are Alluvium, Gediz group, Alasehir and Basement.

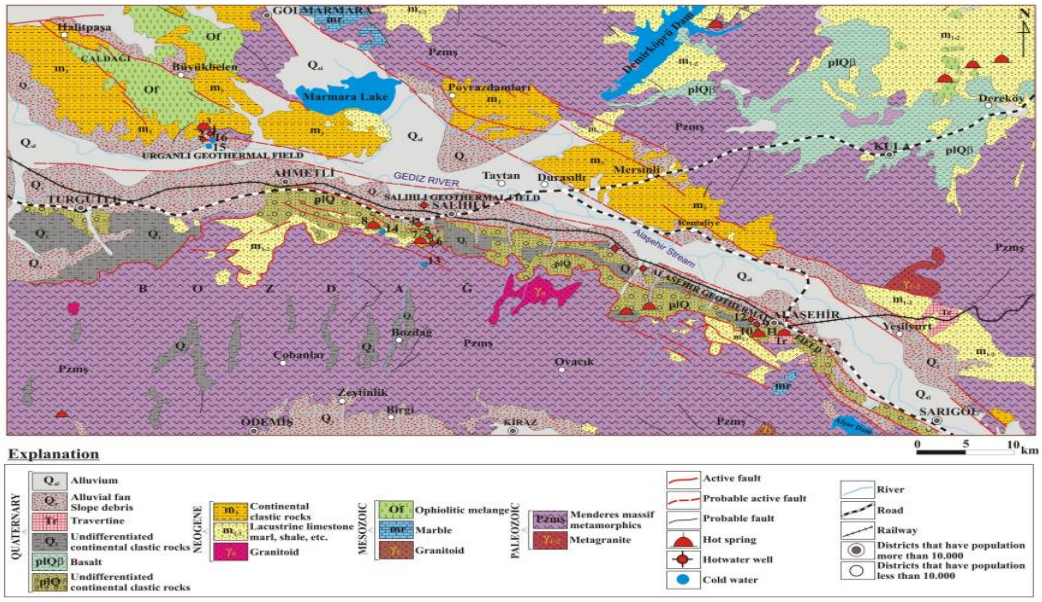

Figure 3 The Geological Map of Gediz Graben (Yilmazer et. al. 2010)

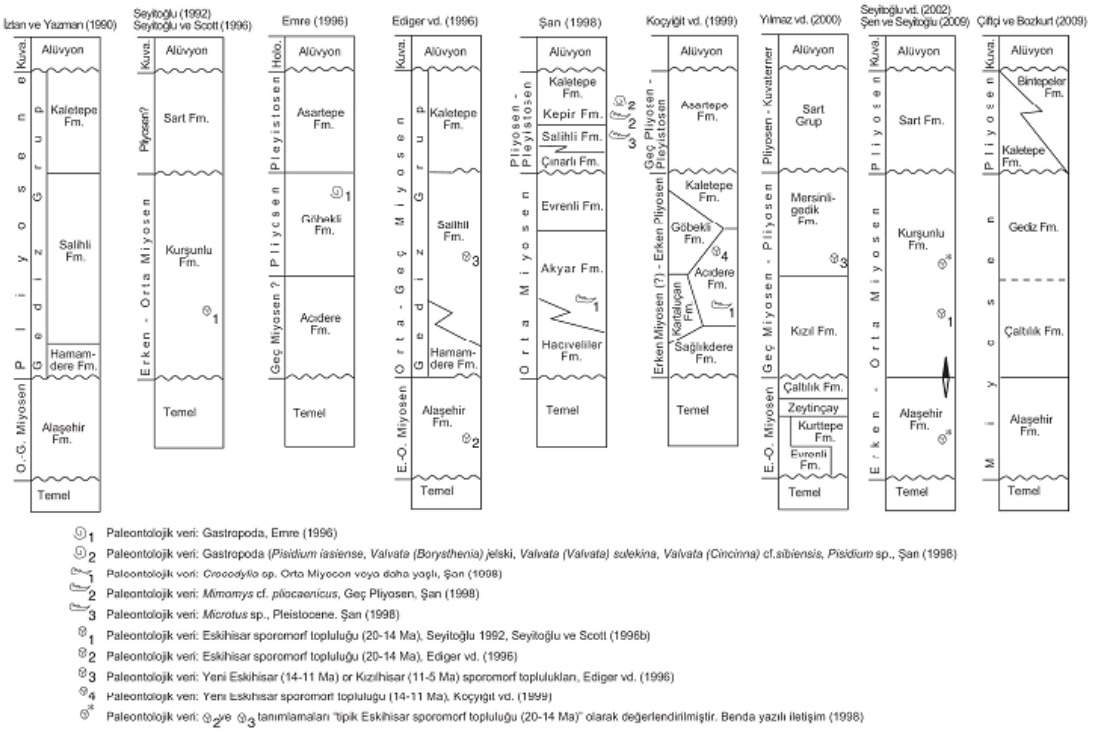

Figure 4 Stratigraphy Schemes for Gediz Graben (Demircioglu, 2009)

Basement section and sediments above basement play important role for geothermal activities. Sediments above basement contain poorly cemented clayey levels and have low permeability acting like cap rocks (Yilmazer et al., 2004). Basement is composed of carbonates of Menderes Massif rocks that are highly fractured and

karstified forming a geothermal aquifer (Baba et al., 2015). Menderes massif rocks are schists, quartzites, phyllites and marbles (Bozkurt and Sozbilir, 2004). Especially, marble and schist are dominantly observed in Alasehir location. For example, Menderes Massif observed in Alkan-1 geothermal well contains marble and schist bands dominant with alternating micaschists. The geological log and well test showed that field has high temperature and pressure (Karamanderesi, 2013). Furthermore, marble, schist, calcschist, gnesis and quartzite are observed in X-5 well (Figure 5).

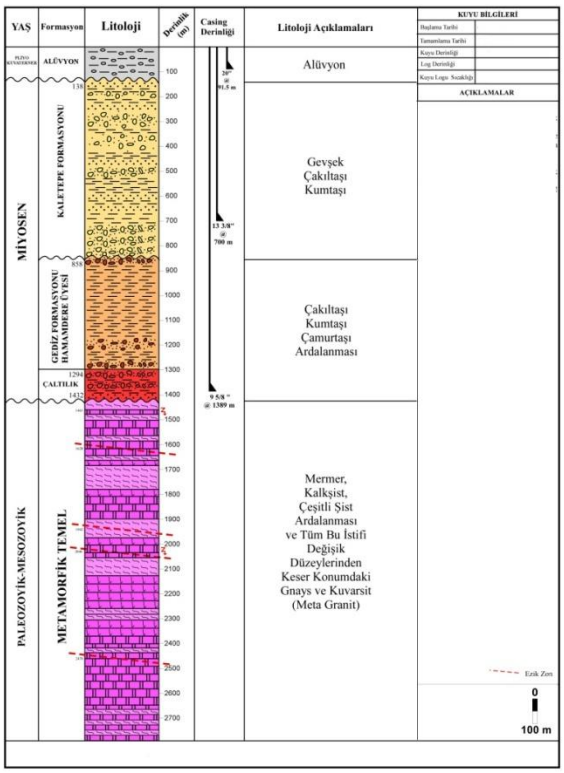

Figure 5 Cross Section of X-5 Well

Tarcanet. al. (2000) pointed out that Menderes Massif rocks have high amount of permeability based on rock and fracture types. In addition to fractured marbles, granodiorite, gneiss, quartz and schist create fractured rock aquifers.

CHAPTER 5

METHODOLOGY

5.1 Porosity Estimation

Perhaps the most important parameter while calculating reservoir volume of a geothermal reservoir is porosity. Essentially, porosity and its distribution should be known for accurate calculation. In Turkey, porosity logging and other characterization tools are generally not used due to high temperature and cost. Coring is not preferable since coring process is extremely difficult due to operational problems. Furthermore, cores taken may not represent whole reservoir section. Generally, calculated geothermal potential is based on flow performance rather than the measured porosity.

When reservoir consists of metamorphic rocks, which are hard and brittle, they have very low matrix porosity. Essentially, storage and flow occurs in natural fractures that are considered as the secondary porosity (Park et. al., 2005). Therefore, detailed characterization is needed to calculate secondary porosity.

In this study, fractal method is used in finding fractal dimensions of outcrops of reservoir rocks. Then, they are used to calculate porosity using a method proposed by Acuna et al. (1992). After that, porosity values obtained from fractal analysis are compared with interference test results, i.e. Storativitiy constant.

5.1.1 Fractal Characterization

Geothermal system of Alasehir is mainly composed of fractures. Since fractures are not heterogeneous and consistent, detailed characterization is needed. In fact, quantitative characterization of fracture network systems is contributing factor in modeling geothermal reservoirs. Thus, fractal geometry is useful way for

quantification. Fractal geometry gives information about a characterization and a quantification of fracture systems. It is very useful while creating representative patterns synthetically. The quantification of natural fracture patterns using fractal geometry is tackled with estimating fractal dimension, FD (Babadagli, 2000).
Jafari (2011) mentioned that there are three basic methods for estimation of FD;

1. Box counting method
2. Mass dimension method
3. Scanline method

In this study, box counting method is selected since it is easy to implement and it is also the most common method used for estimation of FD.

Porous reservoir rocks consist of marble and schist in Alasehir Geothermal Field. It is easy to see reservoir rocks at horst region. Three different locations are selected to collect outcrop images (Figure 6). Firstly, fracture patterns are identified from outcrops of these formations. Then, the resulting images are transferred to computer and fractal characters are analyzed with box counting method by using Image J software (Ferreira and Rasband, 2012).

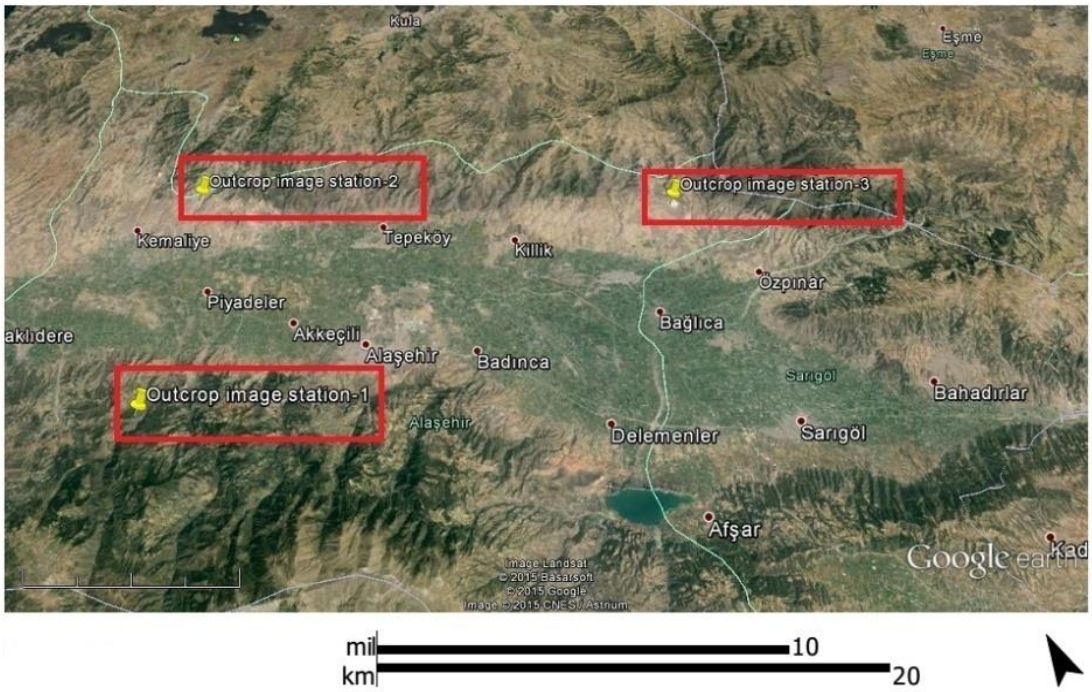

Figure 6 Outcrop Image Stations

Outcrop Images Stations

Station-1 : 38°21'54.95"N - 28°23'45.74"E

Station-2: 38°28'14.23"N - 28°28'0.61"E

Station-3: 38°21'50.96"N - 28°43'4.80"E

5.1.1.1 Box Counting Method

This method basically contains superimposing smaller and smaller square grids of normalized length, which is *r*. It is a box length that is divided the characteristic length of the mapped area. The number of occupied boxes containing one or more fractures is abbreviated as *N*. An array of points in log-log space is fitted with a straight line and its negative slope gives the fractal dimension (FD) value for the fracture pattern (Roy et al., 2007).

$$N(r) \approx r^{-FD} \tag{5.1}$$

The images obtained from three different stations are converted into 8-bit grayscale, and threshold to produce black and white images (Figure 7). In threshold images, fractures appear as black and the matrix is white. Fracture patterns of threshold images are then emphasized manually (Figure 8). Finally, fractal dimension is calculated by using box counting method (Figure 9) (Peitgen et al., 1992). Rest of the calculations for outcrop images are presented in Appendix A.

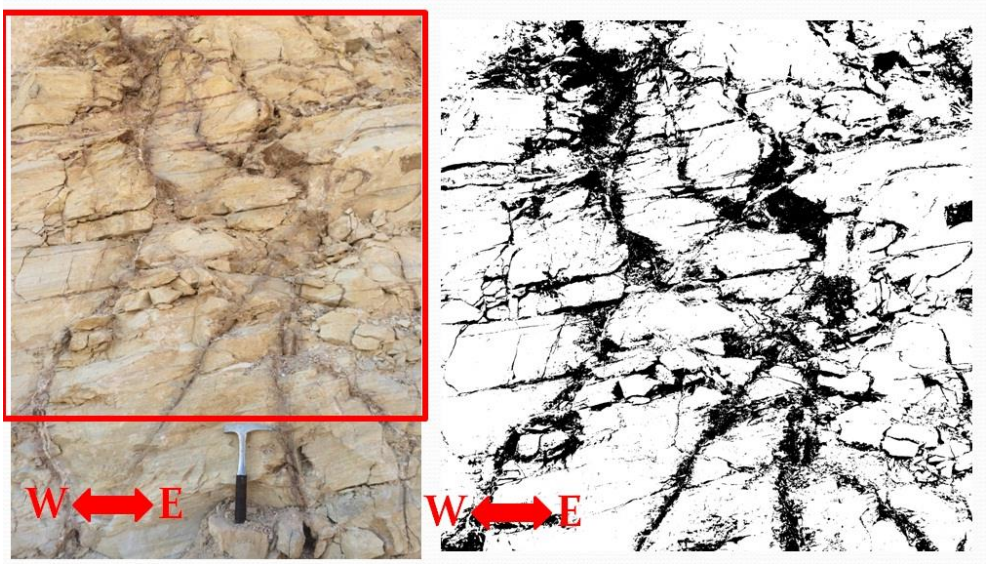

Figure 7 Threshold Outcrop Image

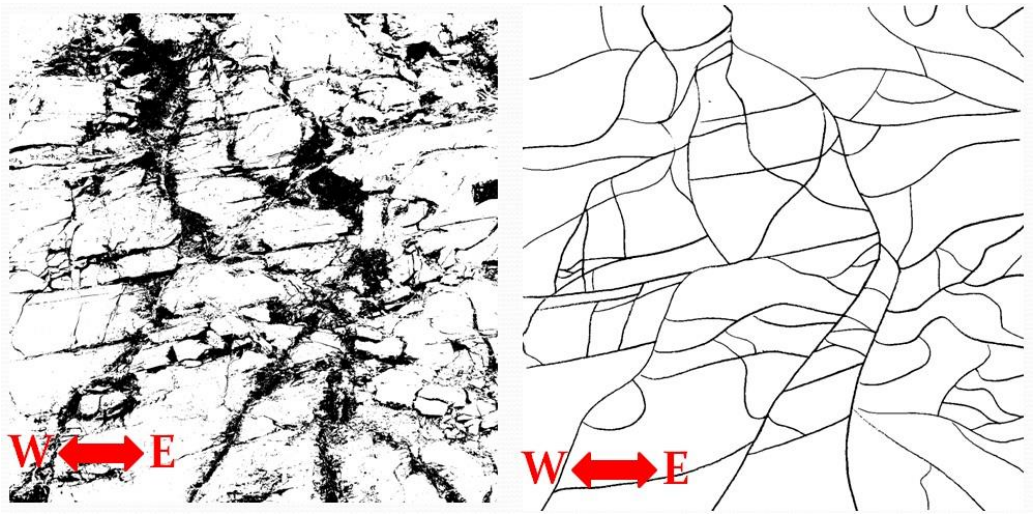

Figure 8 Design of Fracture Patterns

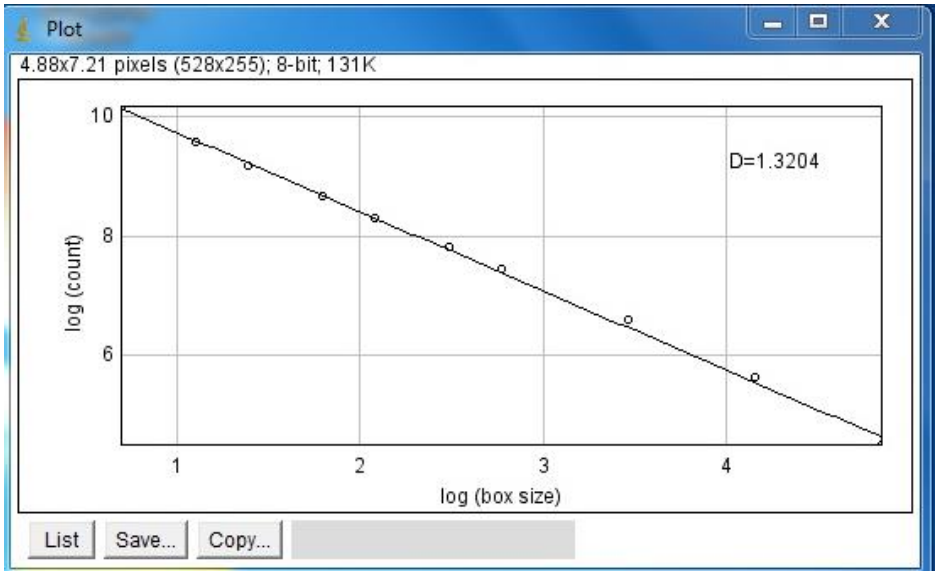

Figure 9 Fractal Dimension

In Alasehir Geothermal Field, geothermal reservoir rocks are marble, schist, quartz and gneiss. Outcrop images are taken from marble and schist outcrops obtained from the aforementioned locations. Fractal dimension is calculated using box counting method as 1,32 ± 0,03 for marble and 1,29 ± 0,04 for schist (Table 1). Similar fractal dimensions are obtained in literature for metamorphic reservoir rocks of Büyük Menderes Graben (Babadagli et al., 1997). Fractal dimension for metamorphic rocks at Germencik Field was reported as 1,411 and for metamorphic rocks at Kizildere as 1,29. Fractal dimensions calculated using satellite images for Germencik and Kizildere fields were 1,55 and 1,57 respectively.

Table 1 Fractal Dimension of Outcrop Images

Photo	FD
S-1	1,2670
S-2	1,2024
S-3	1,3152
S-4	1,2730
S-5	1,2825
S-6	1,3141
S-7	1,3381
S-8	1,3023
S-9	1,3204
S-10	1,2743
S-11	1,3420
M-1	1,3081
M-2	1,3065
M-3	1,2756
M-4	1,3121
M-5	1,3359
M-6	1,3739

5.1.2 Fracture Density

Utilizing available data as much as possible and generating more realistic fracture networks are two important factors in order to get rid of uncertainty (Kim and Schechter, 2007). Therefore, fracture density is analyzed to observe if outcrop images generate more realistic fracture network by comparing borehole mud loss data.

The fracture density is represented in three different ways. They are linear, areal and volumetric depending on the measurement or computation corresponding in terms of length, area or volume, respectively. Linear fracture density or 1-D fracture density is defined as the average number of fractures per unit length. It is measured in a direction perpendicular to the fracture plane. Result is known as fracture frequency as well. Areal fracture density or 2-D fracture density is defined as the average fracture length per unit area on a planar surface. Volumetric fracture density or 3-D fracture density is defined as the average fractured surface area per unit rock volume that is created by all fractures (Singhal, 2010).

In this study, linear fracture density is measured using outcrop images and borehole mud loss data.

5.1.2.1 Fracture Density for Outcrop Images

Fracture density from outcrop images is measured by drawing four lines perpendicular to fracture plane in X and Y direction (Figure 10) on the outcrop images. Fracture intersecting lines are then counted and divided by the line length to find fracture density with a unit of 1/m (Table 2). Other calculations are presented in Appendix B.

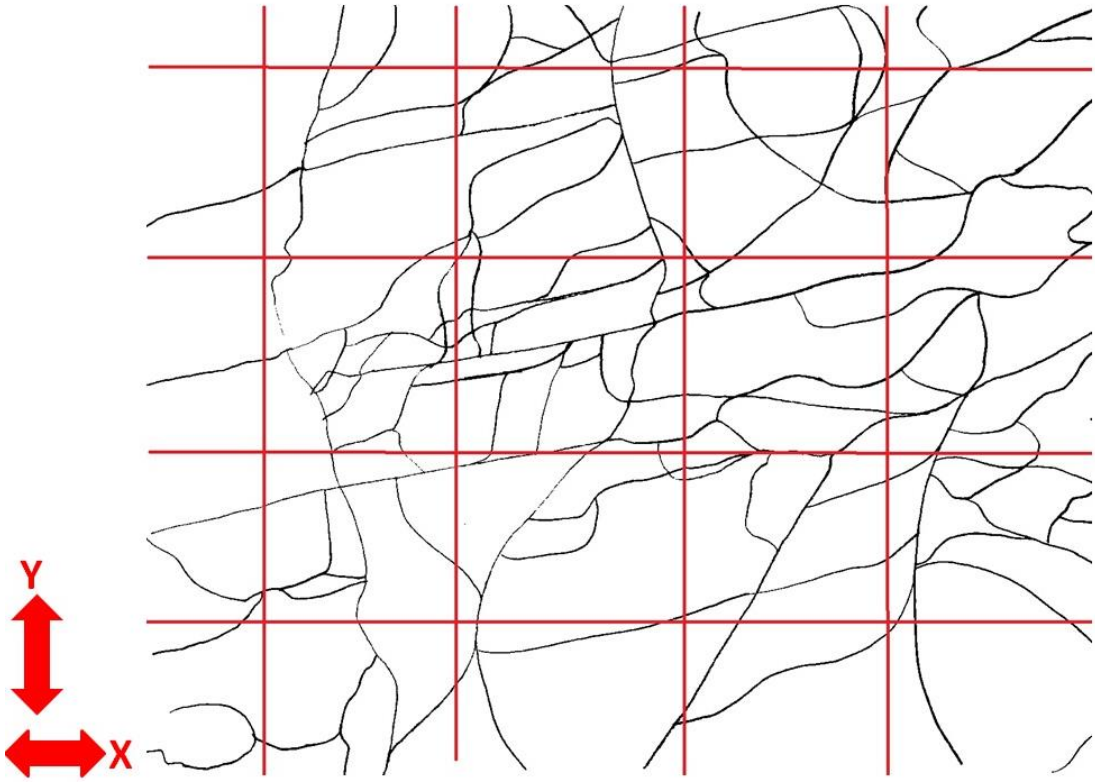

Figure 10 Fracture Density from Outcrop Image

According to Table-2, fracture density in X direction for outcrop images is 0,0934 ± 0,04 m^{-1} and fracture density in Y direction for outcrop images is 0,0898 ± 0,03 m^{-1}.

Table 2 Fracture Density from Outcrop Images

Photo	Fracture Density in X (m^{-1})					Fracture Density in Y (m^{-1})				
	1	2	3	4	Average	1	2	3	4	Average
S-1	0,1647	0,1647	0,2142	0,1318	0,1689	0,0776	0,1708	0,2019	0,1863	0,1592
S-2	0,0921	0,0921	0,0737	0,1013	0,0898	0,0690	0,0690	0,0552	0,0552	0,0621
S-3	0,0600	0,0467	0,0933	0,0600	0,0650	0,0367	0,0293	0,0342	0,0342	0,0336
S-4	0,1628	0,1848	0,2540	0,1155	0,1793	0,0796	0,1114	0,0955	0,0636	0,0875
S-5	0,1000	0,1571	0,2000	0,0714	0,1321	0,1000	0,0917	0,1000	0,0667	0,0896
S-6	0,0963	0,0889	0,0741	0,0741	0,0833	0,1143	0,0714	0,1000	0,1286	0,1036
S-7	0,1338	0,1338	0,0981	0,0981	0,1160	0,0706	0,0941	0,1059	0,0706	0,0853
S-8	0,0605	0,1210	0,1037	0,1210	0,1016	0,0843	0,0590	0,0422	0,0759	0,0653
S-9	0,1209	0,1088	0,1330	0,0967	0,1149	0,1154	0,1077	0,1000	0,1000	0,1058
S-10	0,1333	0,0533	0,0455	0,0227	0,0637	0,0727	0,0545	0,0545	0,0727	0,0636
S-11	0,0341	0,0795	0,1467	0,2000	0,1151	0,0355	0,0632	0,0671	0,0434	0,0523
M-1	0,0344	0,0402	0,0689	0,0287	0,0431	0,1146	0,1019	0,1146	0,1783	0,1274
M-2	0,0191	0,0153	0,0421	0,0115	0,0220	0,1090	0,0897	0,0641	0,0513	0,0785
M-3	0,0698	0,0349	0,0140	0,0279	0,0367	0,1154	0,0897	0,1154	0,0769	0,0994
M-4	0,0535	0,0937	0,1071	0,0268	0,0703	0,1282	0,1923	0,1026	0,1154	0,1346

5.1.2.2 Fracture Density for Boreholes

Mud loss data obtained during drilling are used to calculate fracture density. In this methodology, number of mud loss occurrences based on drilling data is divided into reservoir thickness value to find fracture density. Three wells drilled in Alasehir Geothermal Field were studied (Akin, 2013). Number of occurrences and reservoir thickness are calculated from Figure-11 considering reservoir sections. Using these data, fracture densities of three wells are calculated (Table 3). Other wells data is represented in Appendix B.

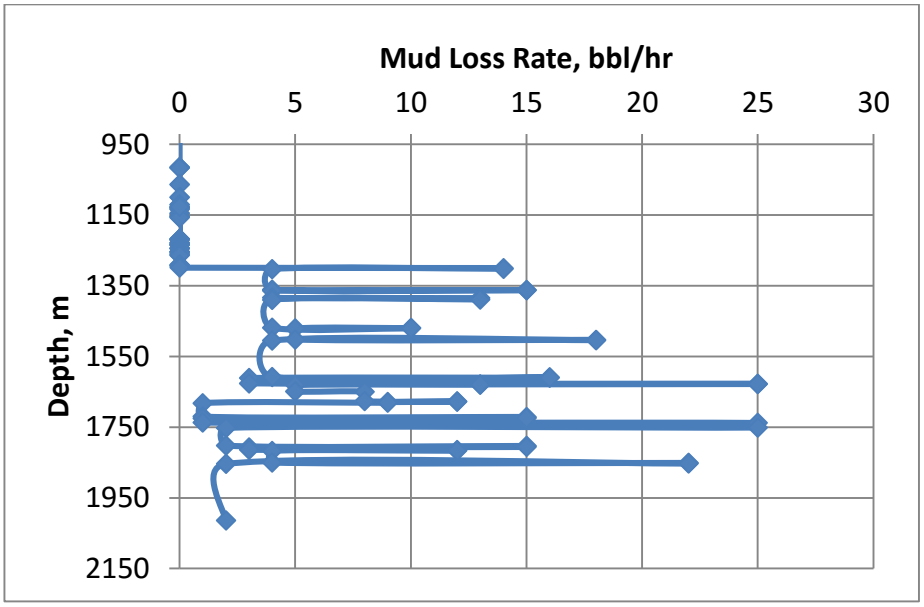

Figure 11 Mud Loss Data (Akin, 2013)

Table 3 Fracture Density from Mud Loss Data

Well	Well-1	Well-2	Well-3
Number of Occurrences	1	22	58
Reservoir Top (m)	1300	1200	1300
Reservoir Bottom (m)	1570	1604	2014
Fracture Density (m^{-1})	0,0037	0,0545	0,0812

According to Table-3, fracture density for mud loss data is 0,0465 ± 0,04 m^{-1} When outcrop and borehole fracture density quantification results are compared, it is seen that although not identical both results are close to each other. This proves that outcrop images closely reflect reservoir sections in Alasehir Geothermal Field and they can be used for reservoir characterization.

5.1.3 Porosity with FD

Porosity can be calculated with fractal dimension (FD) (Acuna et. al., 1992). In this model, it is easy to calculate porosity with FD in a specified area of the reservoir.

$$\emptyset_f(L) = \emptyset_{f0}\left(\frac{L}{L_0}\right)^{D_{fp}-E} \quad (5.2)$$

In this equation, parameters are defined that L is a side length of a region, L_0 is a side length of a region where fracture porosity is φ_{f0}, D_{fp} is a fractal dimension of fracture porosity, and E is an embedded Euclidean dimension (Kim, 2007).

Porosity is calculated using equation 5.2. Firstly, specified area is selected randomly and porosity for this area is calculated using ImageJ (Figure 12). In binarized and threshold images, fractures appear as dark and matrix appears white. After selecting randomly located small rectangular box ImageJ software automatically calculates porosity. In this method, software determines matrix area (white color) and fracture area (black color) in specified area. Then, it gives percentage of fracture area, which is porosity. FD values of each image calculated in section 5.1.1.1 are used. Euclidian dimension is taken as constant, which is 2.

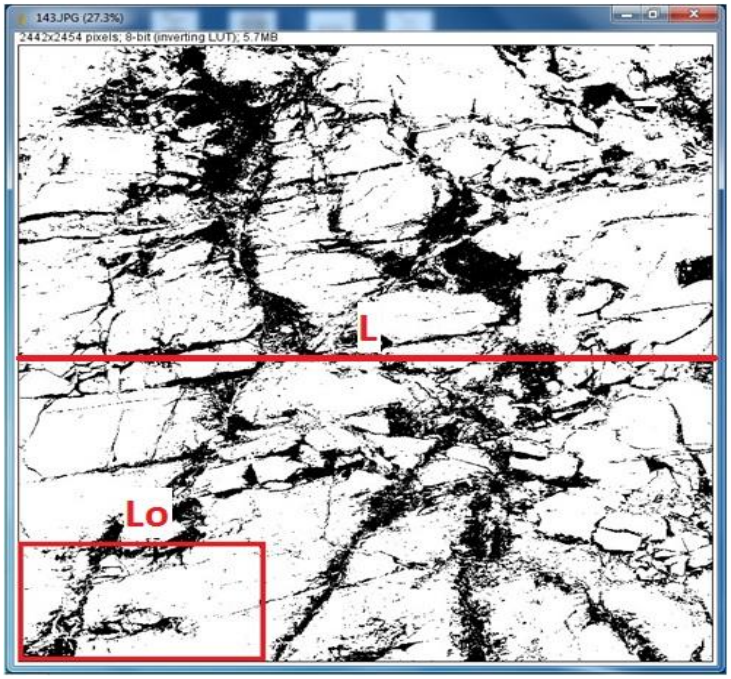

Figure 12 Porosity from ImageJ at Selected Area

Porosity is calculated and quantified as 6,6 ± 1,79 % for schist and 9,6 ± 0,98 % for marble (Table 4). However, porosity could not be calculated for M-5 and M-6 samples since they are taken with shadow. When images are threshold, fractures are not easily characterized due to shadow. For example, image for M-4 threshold and fractures seem as white color unlike others (Figure 13). Therefore, these two images' porosity values are not included in table. Rest of the calculations is represented in Appendix C.

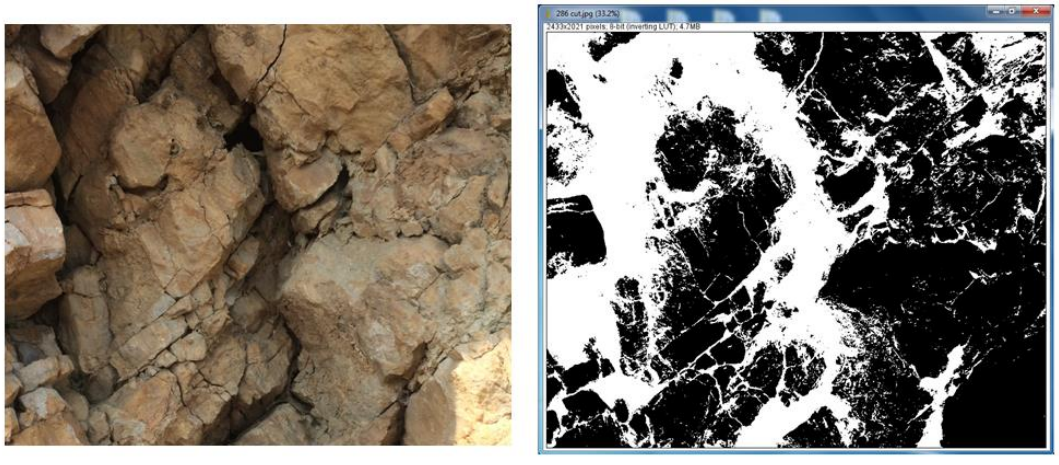

Figure 13 Threshold Image with Shadow

Table 4 Porosity calculated with FD

Photo	FD	Lo	L	Porosity @Lo	Porosity	Formation
S-1	1,2670	5,3	23,4	16,925	5,7	Schist
S-2	1,2024	4,2	27,5	22,513	5,0	
S-3	1,3152	3,4	13,5	22,480	8,7	
S-4	1,2730	4,8	15,5	16,558	7,1	
S-5	1,2825	6,5	18,6	9,920	4,7	
S-6	1,3141	9,5	33,7	14,753	6,2	
S-7	1,3381	7,9	27,6	13,141	5,7	
S-8	1,3023	8,8	31,6	14,712	6,0	
S-9	1,3204	5,9	16,8	16,311	8,0	
S-10	1,2743	4,4	11,3	20,625	10,4	
S-11	1,3420	8,1	22,0	9,651	5,0	
M-1	1,3081	5,1	22,5	24,044	8,6	Marble
M-2	1,3065	5,5	12,6	16,564	9,3	
M-3	1,2756	5,7	22,5	29,552	10,9	
M-4	1,3121	4,5	10,3	17,095	9,7	
M-5	1,3359	-	-	-	-	
M-6	1,3739	-	-	-	-	

Porosity values for marble would be higher than calculated since it is forming a karstified geothermal aquifer. In other words, if M-5 and M-6 outcrop images were used in estimation, average porosity for marble would be higher due to karstified formation.

5.1.4 Porosity from Well Test

Well test data is used to compare and confirm calculated porosity with fractal dimension. Interference testing results are used for this purpose. Interference testing is an important tool for geothermal fields in order to determine transmissivity (i.e. permeability-thickness), storativitiy (i.e. porosity-compressibility-thickness) and locate boundaries.

Essentially, interference tests are used since it is an essential and economical tool that assets the extractable heat capacity of a geothermal field and monitors changes in reservoir characteristics as the geothermal field maturates through exploitation. The existence of productive reservoir between the wells can be proved. A typical interference test is observing the pressure response. Its principle is that one producing or injecting well, called the active well is selected and pressure responses

are recorded in another well or wells, which are called observation wells. Generally, they are located a distance r from the active well (Akin, 2015).

Well testing analysis both determines the compressibility of a reservoir and provides a lumped parameter of compressibility, porosity and reservoir thickness, which is called storativitiy defined by;

$$S = \emptyset ch \tag{5.3}$$

Storativitiy unit is m/Pa or bar^{-1}. Its physical meaning is the volume of fluid stored or released per unit area of reservoir per unit pressure change (Tampubolon, 1989). It gives an idea about the aquifer's capacity to store fluid. This equation shows that the porosity and compressibility of both the rock matrix and the fluid have an equal importance on the reservoir storage capacity (Rutagarama, 2012).

Porosity can be calculated by knowing compressibility and thickness. Akin (2015) studied interference test conducted in Alasehir reservoir using were four wells. After analyzing test data, storativitiy and transmissibility values were calculated. Storativitiy of each well is reported as $1.34x10^{-6}$, $2.39x10^{-4}$, $5.61x10^{-4}$ and $6.08x10^{-4}$. If compressibility value is assumed as 5.0^{-6} bar^{-1}, and reservoir thickness are assumed as 1000 m, porosities are calculated (Table-5).

Table 5 Porosity Values from Interference Test Result

Compressibility (bar^{-1})	5,00E-06			
Thickness (m)	1000			
Wells	Well-1	Well-2	Well-3	Well-4
Storativity	1,34E-06	2,39E-04	5,61E-04	6,08E-04
Porosity (%)	0,0268	4,8	11,2	12,2

According to Table-5, porosity values are calculated and quantified as 7,05 ± 5,71 %. These values are in accord with porosity values obtained using fractal analysis. It gives an idea that porosity calculations from well test and fractal analysis are consistent. Therefore, it is possible to calculate porosity values and distributions with the fractal porosity determination method used in this study.

5.2 Thickness Estimations

Thickness of reservoir rock is important parameter for pore volume calculation. As it is stated in Chapter 4, Alasehir geothermal reservoir rocks consist of marble, schist, quartzite and gneiss. In exploration phase, gneiss and quartzite are thought as non-productive rocks due to their limited porosity and permeability compared to that of marble and schist formations. Thus, only marble and schist zone intervals are considered in reservoir thickness.

At this point, it is important to define gross thickness and net thickness. Gross thickness is thickness which contains complete Menderes metamorphic. Net thickness is the thickness, which marble and schist zones are taken into consideration. In other words, gneiss and quartzite thickness are extracted from gross thickness to find net thickness. Micaschists are not accounted for because it is known that presence of mica mineral decreases the porosity.

5.2.1 Thickness Estimation Using Drilled Wells Data

Drilling logs are used to obtain porous net thickness. First difference between a typical geothermal well and a typical oil and gas well must be identified. Normally, oil and gas wells are drilled up to possible hydrocarbon bearing zone and well completion stage is started. Generally, geothermal well targets are fault or fracture zones. That's why; geothermal wells in western Turkey are drilled to total loss depth such that observing mud loss zone indicates presence of one or more faults. If total mud loss is observed, well is drilled 50 meter more from the depth where total loss zone is observed. In addition to this, sometimes partial or limited mud loss is observed in several cases. As a conclusion bottom of reservoir may not be reached and reliable thickness information may not be obtained at the end of drilling. Therefore, drilling data may not provide sufficient information about the thickness.

Four wells (X-4, X-5, X-7 and X-8) where limited or partial mud loss was observed were selected to determine thickness by using drilling data. In these wells, true depth (TD) is selected based on geological changes. As discussed previously, marble and schist formations are possible production rocks, but quartz, gneiss and micaschist bearing formations are not. When these minerals have been observed on shale shakers, drilling stopped and assumed that TD has been reached. For example, cutting logs example of X-5 Well in Figure-14 shows that reservoir rocks starts with

quartz from 1432 m and continues up to 1490 m. Marble and schist are observed from 1490 m-1510 m according to small interval of cutting sample log example.

Similarly, X-4, X-5, X-7 and X-8 well's cutting logs are analyzed in detail to estimate gross and net thickness as shown in Appendix D. Table-6 shows that net thickness is calculated and quantified as 611 ± 154 m. Also, net to gross ratio is 50,6 ± 10,3 %.

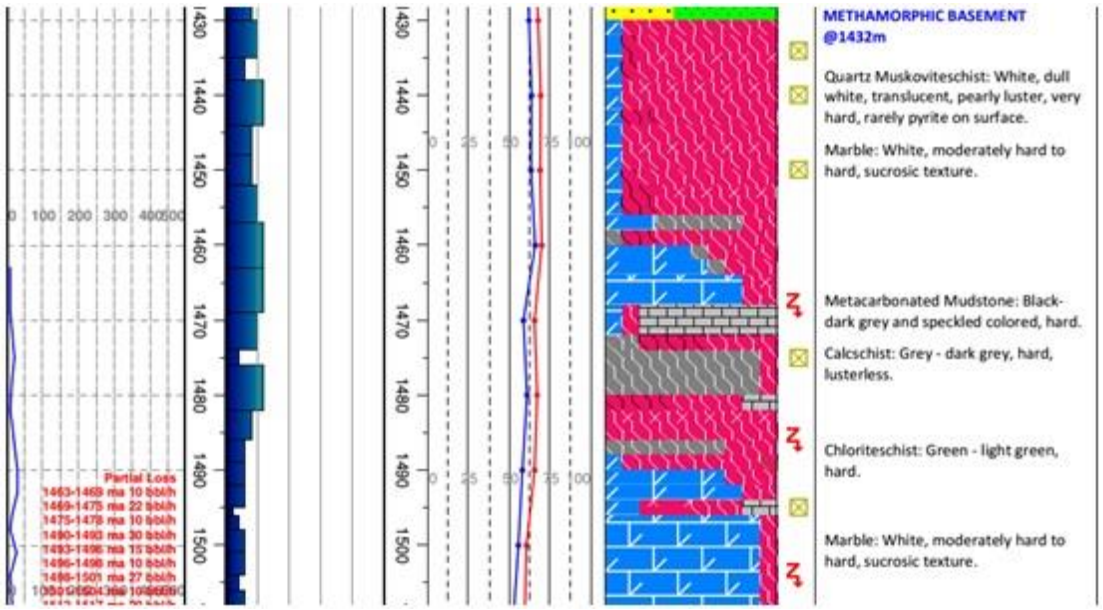

Figure 14 Cutting Sample Log

Table 6 Reservoir Thickness Determination of Wells

Wells	GROSS THICKNESS			NET THICKNESS		Percentage
	MENDERES METAMORPHICS			LOG MARBLE-SCHIST		
	Interval (m)		Thickness (m)	Interval (m)	Thickness (m)	
X-4	1440	2718	1278	1440-1480 1640-1695 2000-2210 2300-2645	650	50,9%
X-5	1432	2790	1358	1490-1630 1815-1900 2005-2050 2380-2790	680	50,1%
X-7	1717	2727	1010	1910-1930 2205-2260 2280-2405 2480-2665	385	38,1%
X-8	1783	2935	1152	1920-2210 2490-2930	730	63,4%
Average=			1200		611,25	50,6%

5.2.2 Thickness Estimation Using Seismic Data

Generally, hitting fault or fracture zones determines the drilling success or failure in geothermal drilling. Advanced seismic reflection imaging is an effective geophysical tool for accurately targeting geothermal drilling. Surface geological and geophysical studies are equally important to successfully locate new geothermal drilling targets for field development. The development of advanced seismic imaging techniques helps drilling success rates of more than 80% at some prospects. Advanced seismic imaging is a major tool to direct images of steeply dipping faults as seismic reflectors, which allows accurate planning of geothermal drill targets (Louie et.al., 2011). Although, seismic interpretation is limited to the bandwidth and frequency content of the seismic data and on the seismic velocity of the reservoir, it is still an important method for the estimation of reservoir thickness (Hanna et. al., 2011)

A seismic study conducted in 1998 (Figure 15 and 16) aiming to define graben fills top and bottom levels was used to obtain reservoir thickness (Ciftci, 2007). The

metamorphic basement rocks of the basement can be easily identified by their acoustic transparency. S-16 seismic line data is superimposed to two well's cross section: X-29, which is drilled up to 2462 meters, TVD, basement rocks started at 1578 meters and X-30, which is drilled up to 2210 meter, TVD, basement rocks started at 1544 meters. In fact, X-29 is located at eastern side of X-30. Seismic cross section between these wells shows that basement level depth is decreasing towards eastern side, resulting in shallower basement towards X-30. This can be caused by faults controlling south and north direction of the graben. When two borehole sections are superposed on seismic reflection, location of metamorphic basement on seismic profile confirms that fractured zones stay within the drawn intervals. Metamorphic basement thickness for of Alasehir geothermal field ranges from 750 m to 1750 m according to seismic profile of S-16 (Figure 16). As discussed previously, these thicknesses are gross metamorphic thicknesses based on seismic data. Using 51% net to gross ratio observed in cuttings log net thickness data provided in Table-7 has been obtained. Net thickness value is calculated and quantified as 655 ± 255 m.

Table 7 Thickness from Seismic

Case	*Gross Thickness (m)*	*Percentage*	*Net Thickness (m)*
1	750	51%	382
2	1250	51%	638
3	1750	51%	893

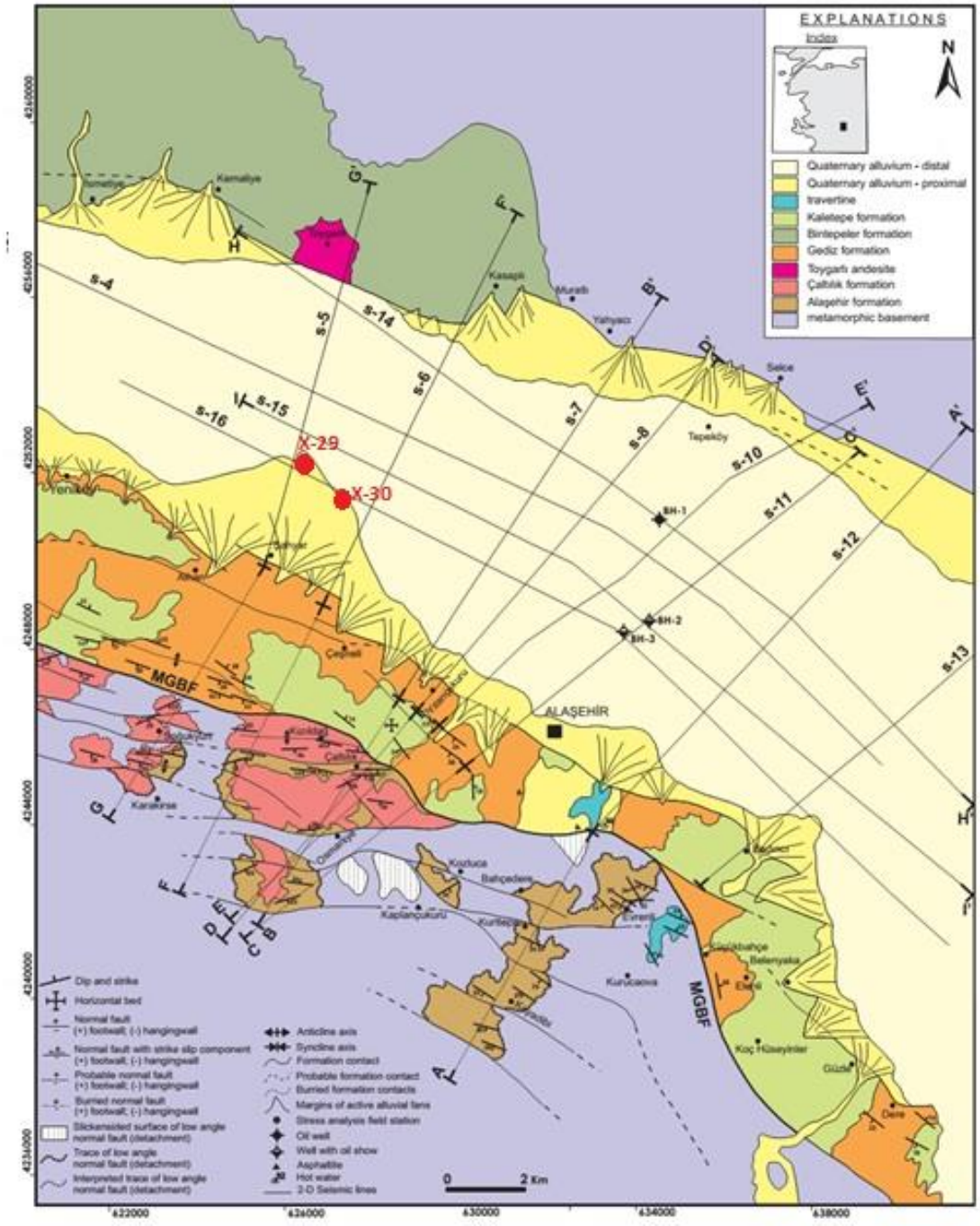

Figure 15 Seismic Profiles in Alasehir Graben (Cifci, 2007)

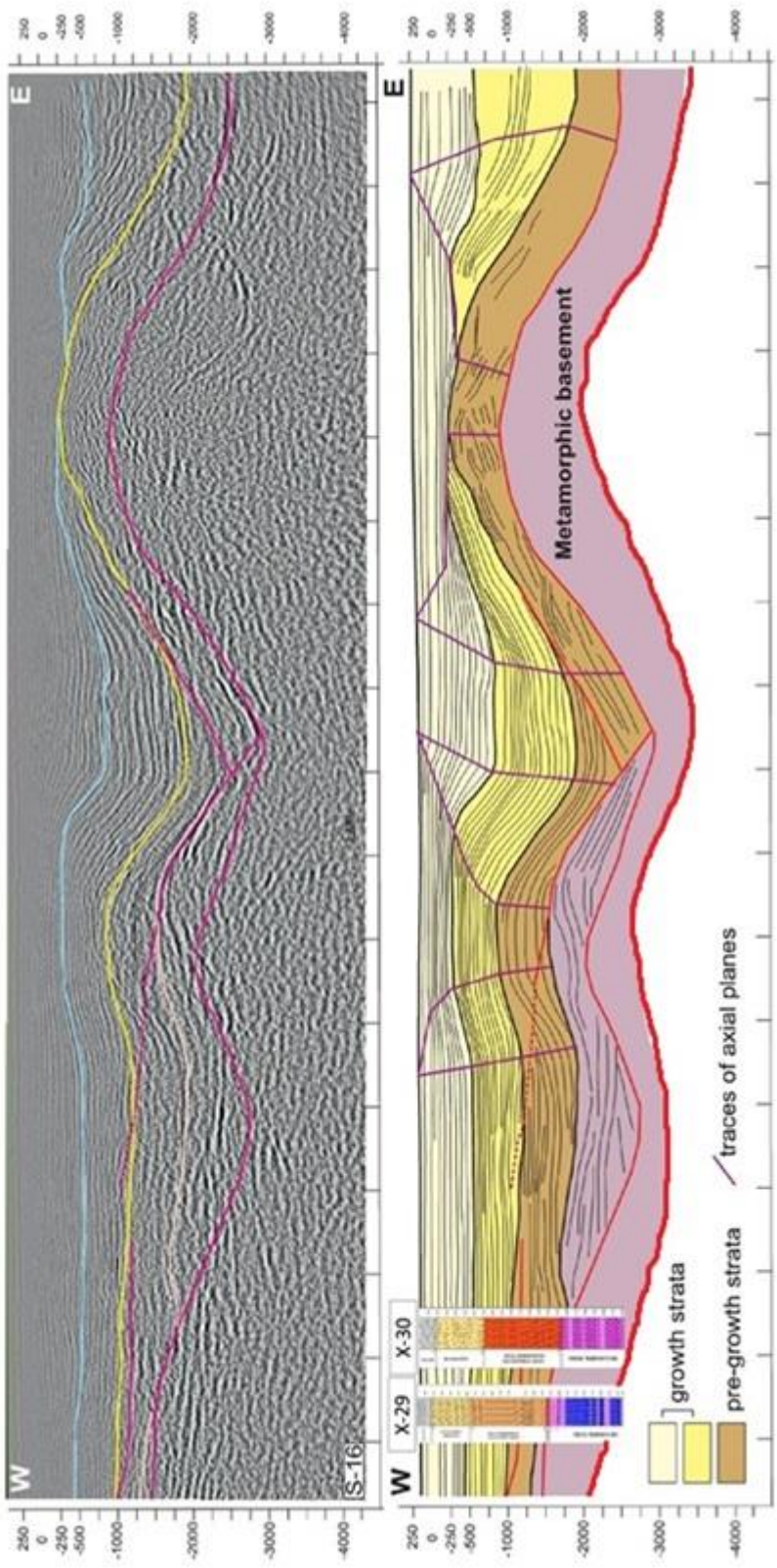

Figure 16 Seismic Profile of S-16 Superimposed with X-29 and X-30 Cross Section

5.2.3 Thickness Estimation Using Resistivity Data

Electromagnetic technique is the best tool for identifying presence of geothermal fluids in reservoir zone. This method is sensitive to fluid changes in the pore space since the resistivity of a rock changes with changing fluid conductivity (Strack, 2010). Generally, low resistivity values are seen in the resistivity data due to the combination of hydrothermal alteration with high temperature and saline fluid. The resistivity values increase at greater depths because of decreasing pore space and a change in the type of hydrothermal alteration products (clays), which is produced with geothermal fluids and the volcanic rocks interactions (Heise et.al.,2008). A study reported by Erdogan et al (2014) is used (Figure 17).

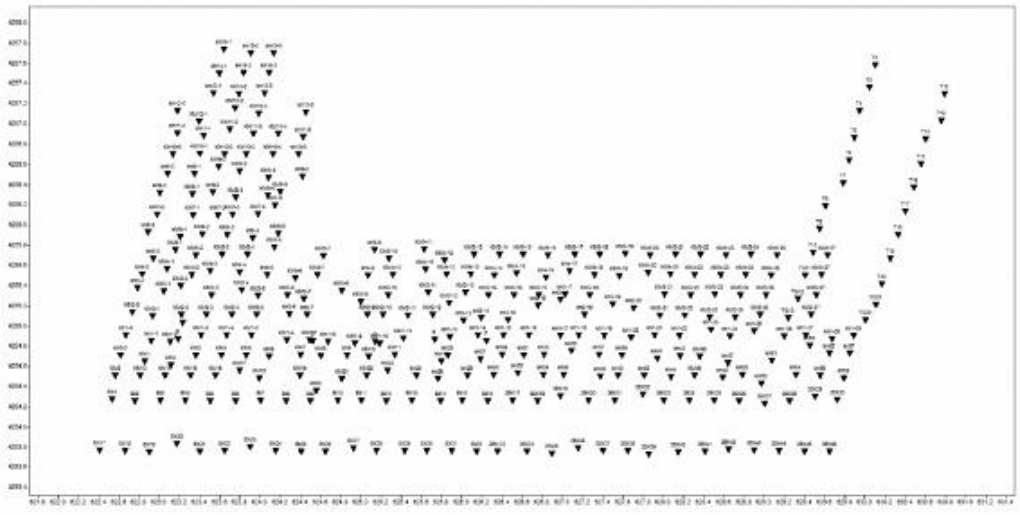

Figure 17 Site Location Map of Survey Area (Erdogan et.al., 2014)

Drilling log of an existing wellbore, which is drilled in the concession area, adjusted geologically on 2D resistivity data (Figure 18). The interpretation aim was defining the location, geometry of the major and secondary faults and the horizon boundaries, which are location, depth and the boundary between the basement metamorphic rocks below and Mio–Pliocene sediments. Resistivity values greater than 35 ohm-m indicates metamorphic basement, which are marble, schist, gneiss. Resistivity value between 6 ohm-m and 35 ohm is interpreted as Miocene-Pliocene coarse-grained sediments. Resistivity value lower than 6 ohm-m is interpreted as fine-grained sediments like claystones and sandstones. Fine-grained sedimentary graben infill has low resistivity values but they are not classified as cap rock. Both resistivity and log of drilled well overlapped, the basement cover, i.e. cap rock, has resistivity value

between 25 ohm-m and 35 ohm-m (Erdogan, et. al., 2014). Normally, resistivity values of metamorphic rocks are greater than sediments of fill. Also, resistivity values increase relatively as the depth increases in basement. There are two reasons for this increase: 1) when clay mineral content is high, it results in high resistivity. Gneiss and micaschist have comparatively higher clay content than marble and schist; 2) Lower resistivity is caused by geothermal fluids in reservoir rocks. In other words, the resistivity values increase at greater depths because of decreasing pore space. Since possible porous rocks are marble and schist, reservoir thickness can be calculated based on these two considerations. In fact, resistivity value of between 35 ohm-m and 87 ohm-m is assumed to be porous reservoir that contains geothermal fluids (Figure 19). In fact, drilled well also confirms that selected interval has is a production zone.

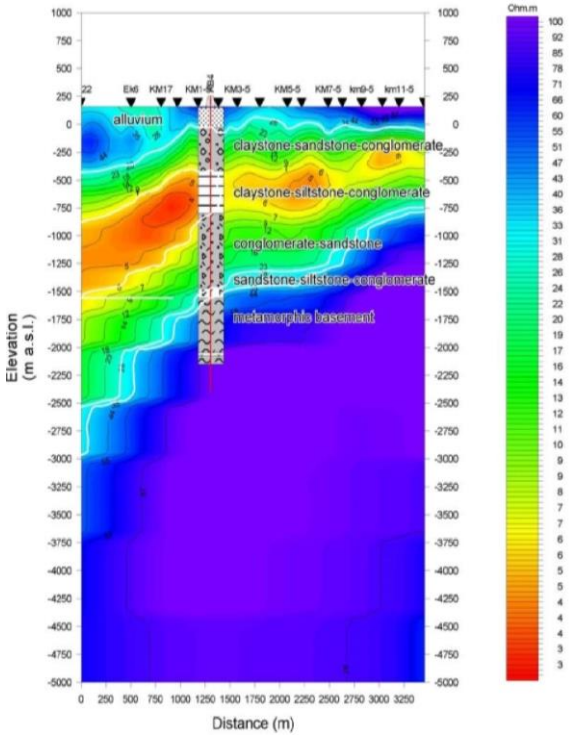

Figure 18 Borehole Section Superimposed on Resistivity Mode (Erdogan et. al., 2014)

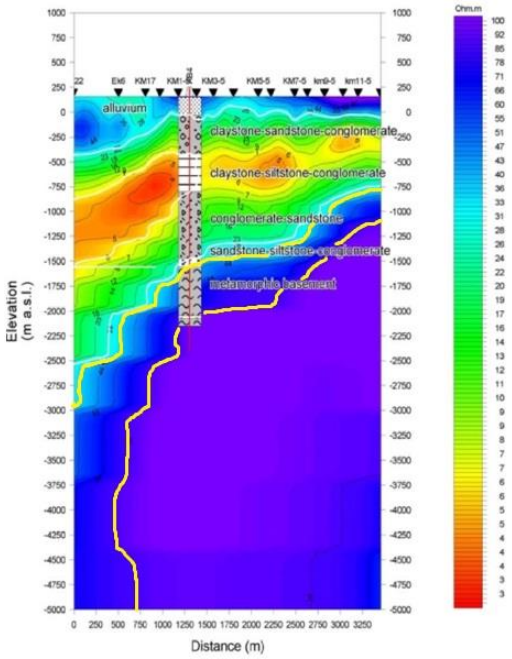

Figure 19 Porous Interval in Reservoir Basement

Using the resistivity data showing the porous section, three intervals are selected to determine thickness (Figure 19 and Figure 20). The shallowest one ranges from 800 m to 1250 m corresponding to a thickness of 450 m. The middle interval ranges from 1400 m to 2000 m corresponding to a thickness of 600 m. The deepest one ranges from 2000 m to 3000 m corresponding to a thickness of 1000 m (Table 8). Thickness values are calculated as 683 ± 284 m.

Table 8 Thickness from Resistivity Data

Cases	Thickness (m)
1	450
2	600
3	1000

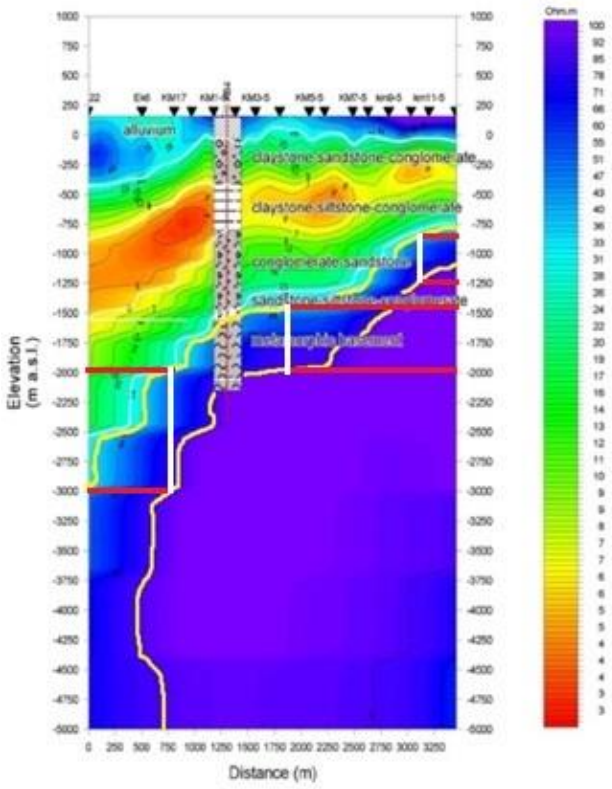

Figure 20 Three Intervals in Porous Section

5.3 Area Estimation

As Ciftci (2007) defined, Gediz Graben is divided into two locations, which are Alasehir and Salihli sub-basins. The most important geologic feature distinguishing two sub-basins is transfer fault located in Kavaklidere town with N-S direction. In this study, the area of Alasehir sub-basin is considered as the prospect area of the Alasehir Geothermal Field. Therefore, area estimations are carried out drilled wells information in Alasehir sub-basin. Although there were 39 wells in Alasehir field up to September 2015, well test data could be obtained for only 25 wells. Area edges are selected to include drilled wells location (Figure 21). Well test data is used for geothermal area determination. Table-9 shows bottom hole temperature (BHT) data of 25 wells. Using these data a contour map of reservoir temperature in Alasehir Basin is obtained by using Surfer software (Figure 22). Figure-22 also shows well locations figured out in Figure-21. The temperature profile indicates that BHT ranges from 105 ^{o}C to 250 ^{o}C.

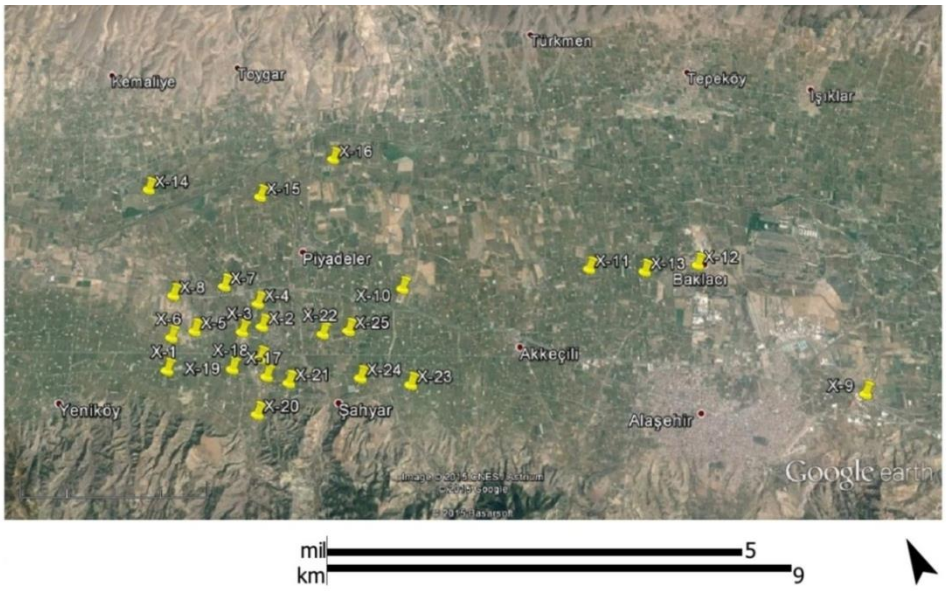

Figure 21 Area Including Drilled Wells Location

Table 9 Drilled Wells Bottom Hole Temperatures

Well	T (ºC)
X-1	194
X-2	169
X-3	191
X-4	175
X-5	201
X-6	188
X-7	208
X-8	224
X-9	106
X-10	170
X-11	220
X-12	252
X-13	253
X-14	187
X-15	180
X-16	148
X-17	188
X-18	190
X-19	198
X-20	203
X-21	185
X-22	177
X-23	158
X-24	170
X-25	160

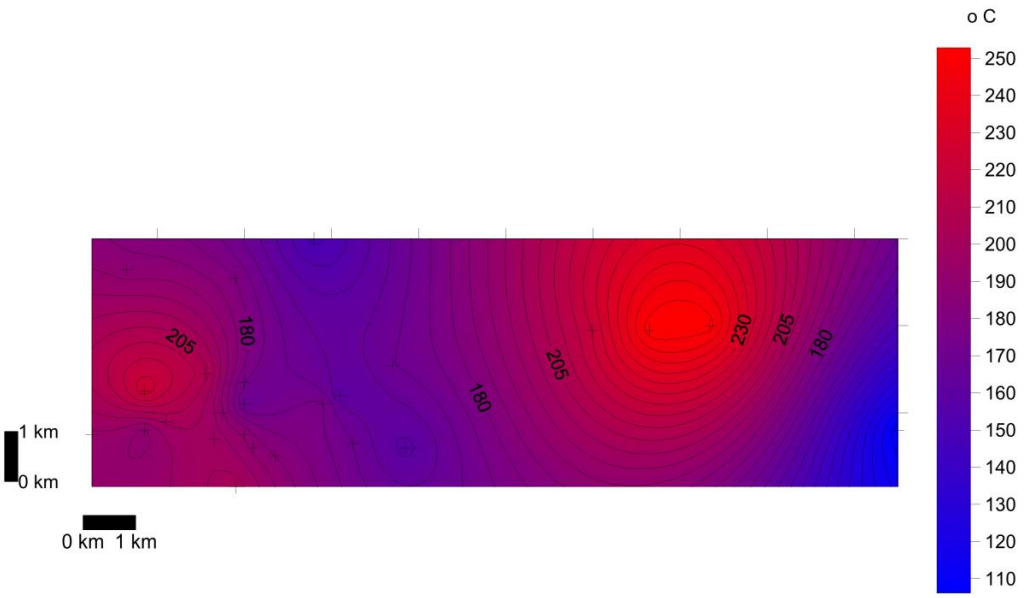

Figure 22 Temperature Contour Map

5.3.1 Proven Area

Proven area is based on drilled wells with at least 500 meters beyond the drainage of the outermost wells. It encloses an area with good permeability and demonstrated production from wells (Sarmiento and Steingrímsson, 2008). When data of 39 wells drilled in Alasehir region and 500 meters drainage radius is used, proven area is calculated as 30,6 km^2.

5.3.2 Probable Area

Probable area is considered as the area bounded by an extrapolated production temperature of average temperature of drilled wells. Since average temperature of wells is 187 ^oC, probable area corresponding to this contour line is calculated as 42,6 km^2.

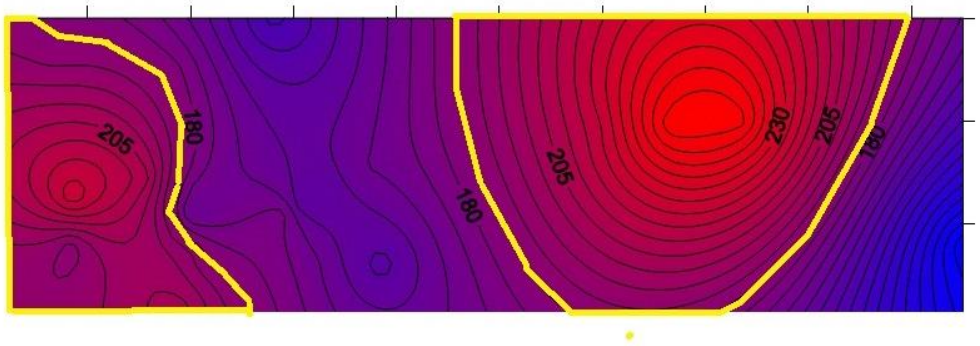

Figure 23 Probable Area with 185 ^oC

5.3.3 Possible Area

Possible area considers areas that are not yet drilled but enclosed by temperature contour map. In fact, zones with thermal surface manifestations, outflow zones, high postulated temperatures based on well test and static temperature logs can be considered within this area (Sarmiento and Steingrímsson, 2008). For Alasehir reservoir minimum measured temperature of 106 ^{o}C is selected to represent limits of possible geothermal area. Complete contour map including minimum temperature is taken into consideration to calculate maximum area. As a result, possible area is calculated as 78,9 km^2.

Table 10 Proven, Probable and Possible Areas

Proven	30615000	m^2	Drainage area with 500 m boundary for drilled 39 wells
	30,6	km^2	
Probable	42,6	km^2	Area includes average temp of 187 ^{O}C
Possible	78,9	km^2	Area calculated based on min temp of 106 ^{o}C

Proven, probable and possible areas are listed in Table-10, where calculated area for Alasehir Geothermal Field is 50 ± 25 km^2.

CHAPTER 6

MONTE CARLO SIMULATION

Monte Carlo simulation method is based on using random numbers and probability to solve problems. A deterministic model is iteratively evaluated using sets of random numbers as inputs. A certain number of input parameters in few equations are used to give a set of outputs. The same results are obtained no matter how many times the problem is recalculated. However, stochastic models use both random inputs and give different results based on the distribution functions of the input parameters. Stochastic models are applied if the model is so complex, nonlinear, or when there are a couple uncertain parameters. The simulation uses many evaluations. The deterministic model is turned into a stochastic model by random numbers (Ofwona, 2008).

In this methodology, the differential equations describing the behavior of the system are not required since simulation is directly done for the physical process. Basically, probability density functions (pdf) describe the physical system. After the pdf is described, the Monte Carlo method is simulated by random sampling from the pdf's and the desired result is obtained as average over the number of observations. Also, the statistical error, i.e. the variance, is predicted in this average (Arkan and Parlaktuna, 2005).

Monte Carlo Method is performed using @RISK Microsoft Excel spreadsheet add-in software that carries out advanced modeling and risk analysis. Risk Analysis is generally used to solve problems, make forecasts, develop strategies, or make decisions. If there is a quantified risk or determined outcomes and probabilities of occurrence, probability distribution is used to summarize risk. It is defined as a

device to present the quantified risk for a variable. Probability distributions are used for describing uncertain values in Excel worksheets and presenting results. The most common used are normal, lognormal, triangular and uniform. Each of them describes a range of possible values and their likelihood of occurrence (Palisade Corporation, 2010).

Since the main focus is determining how random variation, lack of knowledge or error affects sensitivity, performance or reliability of the system are modeled, probability distributions are used for simulating the process of sampling from actual population. After inputs distribution is selected based on closely matching the existing data, probability distribution curves or confidence intervals are obtained from simulation (Ofwona, 2008).

Calculation steps are mentioned in Arkan and Parlaktuna study in 2005. They consist of three steps;

1. Defining uncertainty of input parameters,
2. Defining output parameters,
3. Simulation.

CHAPTER 7

RESULTS AND DISCUSSIONS

7.1 Distribution Selection of Parameters

While calculating stored heat capacity, pore volume is perhaps the most important parameter. In Chapter 5, porosity, thickness and geothermal area are calculated by using fractal characterization method, drilling data, resistivity data, seismic data and bottom hole temperature profiles. As it is discussed in Chapter 2, uncertainties are identified with stochastic Monte Carlo calculations. The first step is defining distribution types.

7.1.1 Porosity

When limited fractal analysis derived porosities are analyzed a conclusion regarding the distribution of porosity can be reached. The bimodal distribution shown Figure-24 is definitely not normal. Sarmiento and Steingrímsson (2011) mentioned that a log normal distribution is the most appropriate distribution that can be used for porosity distribution. Thus, log normal distribution is selected for porosity distribution.

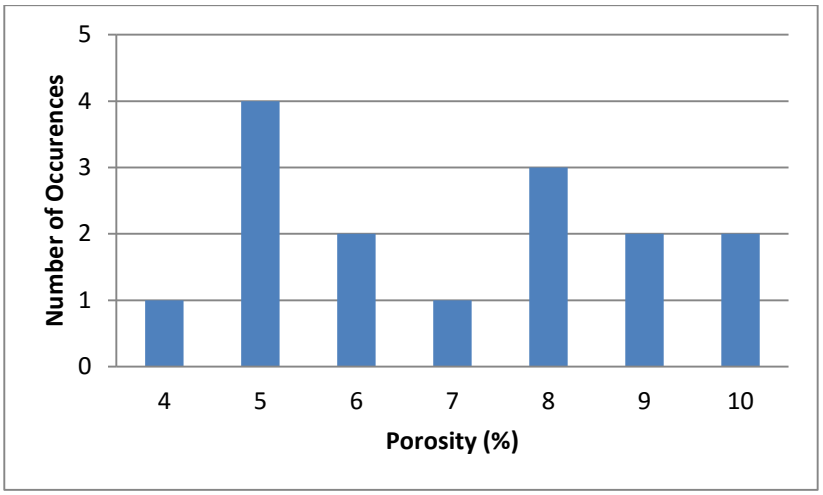

Figure 24 Porosity Distribution

7.1.2 Thickness

Sarmiento and Steingrímsson (2011) point out that the area and the thickness of the geothermal reservoir have triangular distribution because these parameters are obtained directly from drilling or well measurements. Therefore, triangular distribution is selected for thickness. In their study, proven, probable and possible definitions are stated instead of minimum, most likely and maximum values. Thus, proven value is selected from cutting sample logs corresponding to a minimum value of 385 meters. Probable value is selected as the average of net thicknesses corresponding to 600 meters. Possible value is selected as 1000 meters corresponding to maximum thickness obtained from resistivity data (Table 11).

Table 11 Thickness from different method

Method	Minimum	Average	Maximum
Cutting Logs	385	611	730
Resistivity	450	600	1000
Seismic	368	613	856

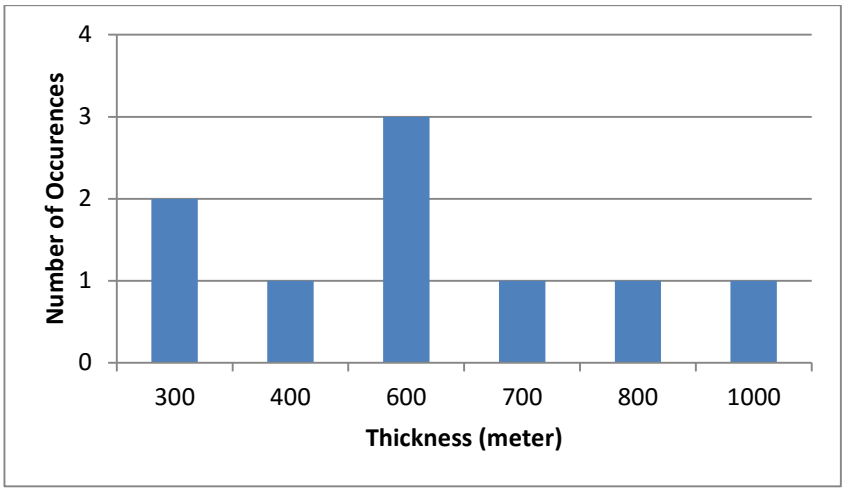

Figure 25 Thickness Distribution

7.1.3 Area

The temperature contours and electrical resistivity measurements provide good approximation of the resource area (Sarmiento and Steingrímsson, 2011). Similar to thickness distribution triangular distribution is utilized. To begin with, there are 39 wells drilled in Alasehir Geothermal Field. Proven area is calculated based on drilled wells with at least 500 meters beyond the drainage of the outermost well. Then, bottom hole static temperature values of 25 wells drilled in Alasehir are used to create temperature contour map. Average temperature of 25 wells is found to be equal to 187 ^{o}C. The area including average temperature is determined and taken as probable value. Lastly, possible area is calculated considering areas that have not been yet drilled but enclosed by temperature contour map. Since minimum temperature measured is 106 ^{o}C, possible area is calculated including the minimum value on contour map.

Table 12 Area from Contour Map

Proven	30615000	m^2
	30,6	km^2
Probable	42,6	km^2
Possible	78,9	km^2

7.2 Monte Carlo Simulation with @RISK

While applying Monte Carlo Simulation, the number of iterations was chosen as 10,000. Then the @RISK software program assigns random numbers to each variable based on the type of distribution and limits (Table 13).

Table 13 Monte Carlo Simulation Input Parameters

Porosity	Lognormal Distribution		
	Mean (%)	Standard Deviation (%)	
	7,4	2,1	
Thickness	Triangular Distribution		
	Proven (km)	Probable (km)	Possible (km)
	0,385	0,6	1
Area	Proven (km^2)	Probable (km^2)	Possible (km^2)
	30,6	42,6	78,9

Input parameters are simulated and analyzed. Firstly, the result of porosity simulation shows that it ranges from % 4,50 to % 11,25 with % 90 confidence interval (Figure 26). Then, the result of thickness simulation shows that it ranges from 0,440 km to 0,889 km with % 90 confidence interval (Figure 27). Lastly, the result of area simulation shows that it ranges from 35,98 km^2 to 69,54 km^2 with %90 confidence interval (Figure 28).

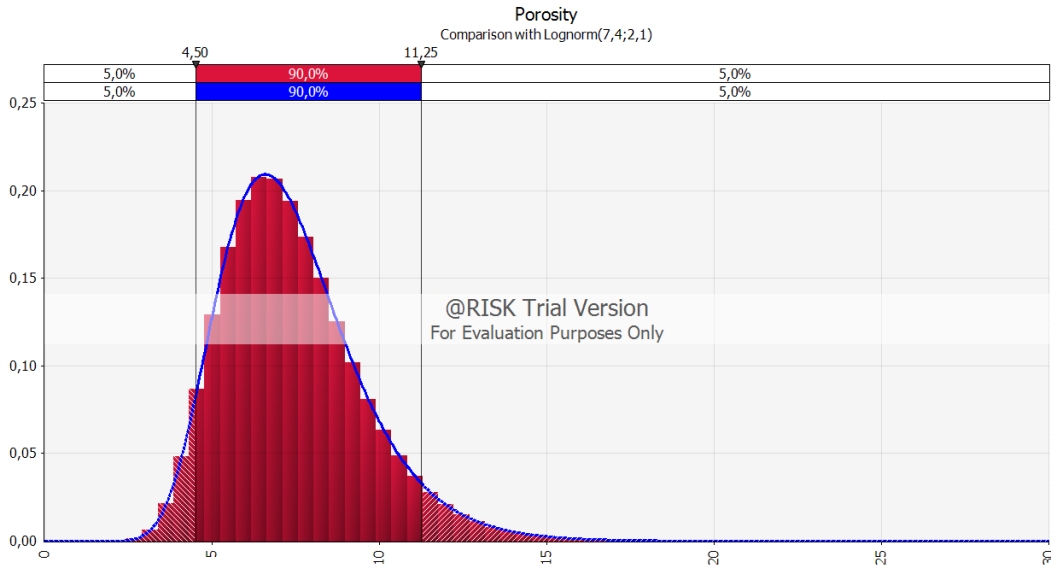

Figure 26 Porosity Lognormal Distribution with Frequency

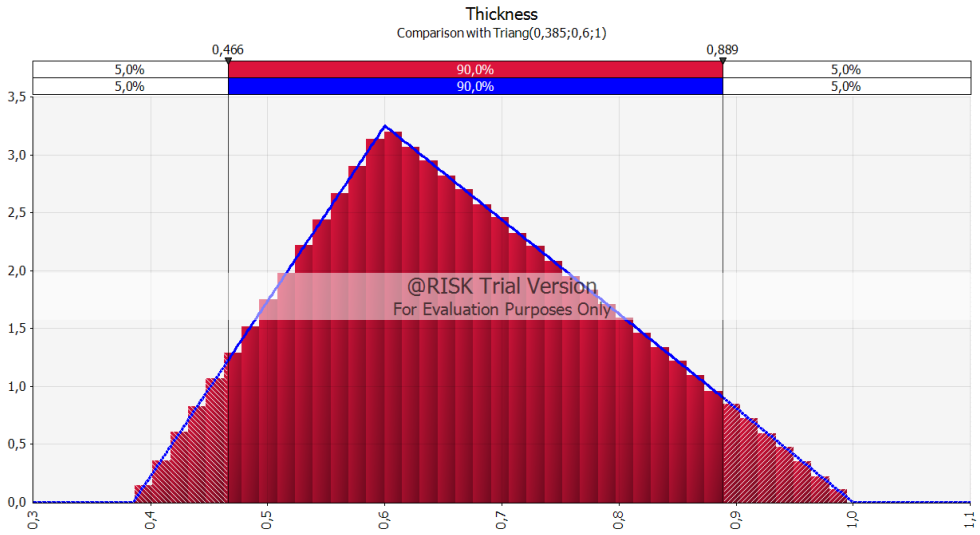

Figure 27 Thickness Triangular Distribution with Frequency

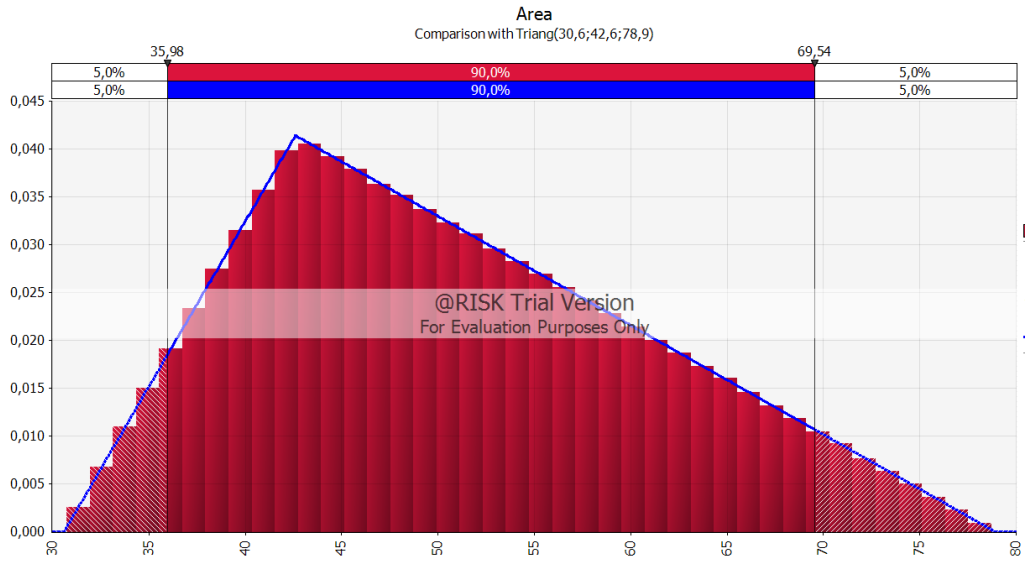

Figure 28 Area Triangular Distribution with Frequency

After input parameters and their distribution types are simulated, output result is simulated as well and it gives pore volume histogram (Figure 29). As it is seen, output result is lognormal distribution. According to histogram, pore volume ranges from 1,20 km^3 to 4,40 km^3 with %90 confidence interval. Table-14 gives detailed summary statistics for pore volume.

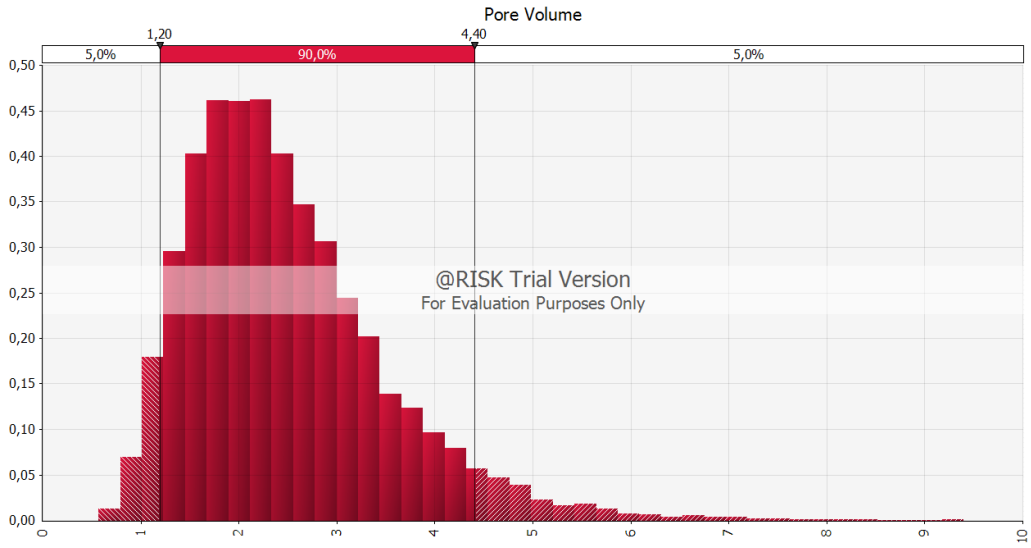

Figure 29 Monte Carlo Simulation Result (Pore Volume vs. Frequency)

Table 14 Summary Statistics for Pore Volume

Summary Statistics for Pore Volume			
Statistics		Probability	PV (km^3)
Minimum	0,569479	95%	1,1966082
Maximum	9,4019605	90%	1,3814454
Mean	2,4813671	85%	1,5263313
Std Dev	1,0097857	80%	1,6442498
Variance	1,0196672	75%	1,7575715
Skewness	1,204648	70%	1,866107
Kurtosis	5,366813	65%	1,9704763
Median	2,3010057	60%	2,0814799
Mode	1,8961156	55%	2,1859903
Left X	1,1966082	50%	2,3010057
Left P	5%	45%	2,411664
Right X	4,404848	40%	2,5413809
Right P	95%	35%	2,6824101
Diff X	3,2082399	30%	2,8257165
Diff P	90%	25%	2,9979187
#Errors	0	20%	3,1959646
Filter Min	Off	15%	3,4446782
Filter Max	Off	10%	3,8236062
#Filtered	0	5%	4,404848

Figure-30 shows probability versus Pore Volume. The minimum, mean and maximum values of the variables are listed as the result of simulation study of

@RISK in Table-15. According to simulation summary, the minimum value for Pore Volume of Alaşehir Geothermal Field is 0,57 km^3, the mean value is 2,48 km^3 and the maximum is 9,40 km^3. In terms of statically base, Pore Volume of Alasehir Geothermal Field is 1,38 km^3 with 90 % probability and 3,82 km^3 with 10 % probability.

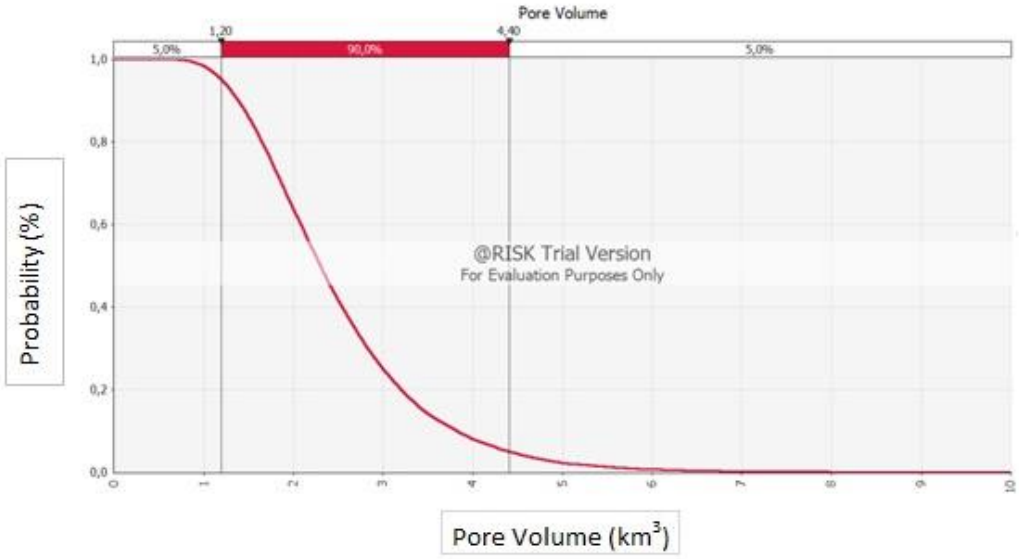

Figure 30 Probability Analysis of Pore Volume

Table 15 Simulation Summary

Simulation Summary						
Number of Simulations				1		
Number of Iterations				10000		
Number of Inputs				3		
Number of Outputs				1		
Sampling Type				Monte Carlo		
Input	**Statistics**					
Name	**Min**	**Mean**	**Max**	**P10**	**P50**	**P90**
Porosity (%)	2,03	7,40	20,81	10,17	7,12	4,98
Thickness (km)	0,39	0,66	1,00	0,84	0,65	0,50
Area (km^2)	30,69	50,70	78,83	65,66	49,29	38,21
Output	**Statistics**					
Name	**Min**	**Mean**	**Max**	**P10**	**P50**	**P90**
Pore Volume (km^3)	0,57	2,48	9,40	3,82	2,30	1,38

7.3 Sensitivity Analysis

7.3.1 Monte Carlo Simulation

Monte Carlo Simulation conducts automatically sensitivity analysis. It gives Tornado diagram to show effects of input parameters on output parameters (Figure 31). According to diagram, porosity has higher effect on pore volume following by area and thickness.

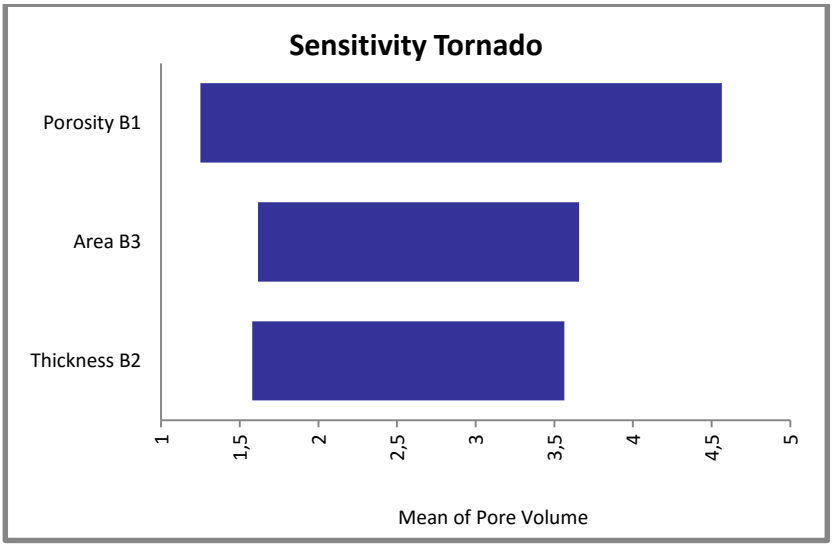

Figure 31 Tornado Sensitivity Analysis

7.3.2 Experimental Design

Experimental design (ED) is also used to identify the sensitivity of parameters on pore volume calculation. Yeten et. al. (2005) defined ED that it is an alternative method for sensitivity analysis. It determines the input parameters affect on output result. The most common experimental design techniques are full factorial design and Plackett Burman (PB) design. Difference between two techniques is scenario number to be generated. For example, there are 7 factors and 2 levels experimental design will be presented. If full factorial design is used, 128 scenarios are needed to generate. On the other hand, PB design requires only 12 scenarios. Therefore, PB design is used in order to investigate the effects of main input variables for reducing the number of experiment runs (Asrizal et. al., 2006).

7.3.2.1 Plackett-Burman Design

Plackett and Burman method is the easiest and best method to screen design and identify main effects. In this methodology, uncertainties are defined in 2 levels, which are low (-1) and high (+1). Generally, 8 and 12 runs are very efficient in PB method. In this study, 12 runs in different orders are selected. After all scenarios are analyzed, simulation is run and it generates Pareto chart showing which parameters effects on output results.

In this study, six parameters are chosen to evaluate their effects on pore volume calculation;

1. Rock types
2. Porosity
3. Top of reservoir
4. Bottom of reservoir
5. Net/Gross ratio
6. Area

The design parameters are selected from Chapter-5 based on different calculation methods where minimum and maximum values attained are used. All parameters are listed in Table-16. Pore volume is calculated using low and high values identified in Table-17.

Table 16 Reference Model Parameters Chosen for the Experimental Design

Effected Parameter	Porosity		Thickness			Area
Design Parameters	Rock Type		Top of Res.	Bottom of Res.	Net/Gross	
	Schist	Marble				
Min	4,7	8,6	1432	2718	0,38	30,6
Max	10,4	10,9	1783	2935	0,63	42,6

In PB, design parameters are represented as follow;

Factors : 6 Replicates : 1
Base runs : 12 Total runs : 12
Base blocks : 1 Total blocks : 1

Table 17 Experimental Design Simulation Run for Pore Volume

StdOrder	RunOrder	PtType	Blocks	Rock Type	Porosity	Top of Reservoir	Bottom of Reservoir	Net/Gross	Area	Pore Volume
12	1	1	1	-1	-1	-1	-1	-1	-1	0,51
8	2	1	1	-1	-1	1	1	1	-1	1,36
6	3	1	1	1	1	1	-1	1	1	2,74
11	4	1	1	-1	1	-1	-1	-1	1	2,17
3	5	1	1	-1	1	1	-1	1	-1	2,58
2	6	1	1	1	1	-1	1	-1	-1	1,90
1	7	1	1	1	-1	1	-1	-1	-1	1,29
5	8	1	1	1	1	-1	1	1	-1	2,42
4	9	1	1	1	-1	1	1	-1	1	1,60
10	10	1	1	1	-1	-1	-1	1	1	2,16
9	11	1	1	-1	-1	-1	1	1	1	1,45
7	12	1	1	-1	1	1	1	-1	1	2,53

Placket and Burman design is performed with *Minitab* software using significance at 95% confidence level. It gives Pareto Chart that shows input parameters effect on pore volume calculation (Figure 32). From this result it is seen that at least three factors are significant, which are porosity, net/gross ratio and area. The least significant factors are rock type, top of reservoir and bottom of reservoir. Red line indicates significance limit, which is 2,571.

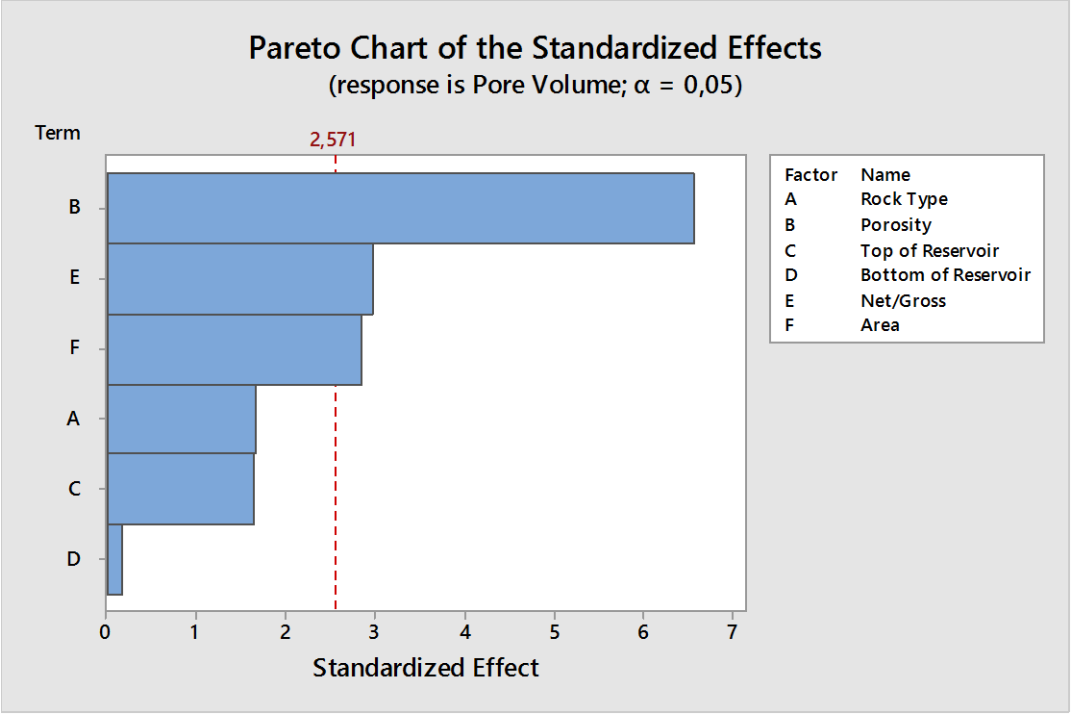

Figure 32 Pareto Chart of the Standardized Effects

Another result of PB design in Minitab software is Normal Plot of the Standardized Effects (Figure 33). It is known as a graphical technique to assesst whether factors

are normally distributed or not. If all factors are normally distributed, they fit on the line. In the normal probability plot, important effects are larger and generally away from the fitted line than unimportant effects. Unimportant parameters will be smaller and centered almost about zero.

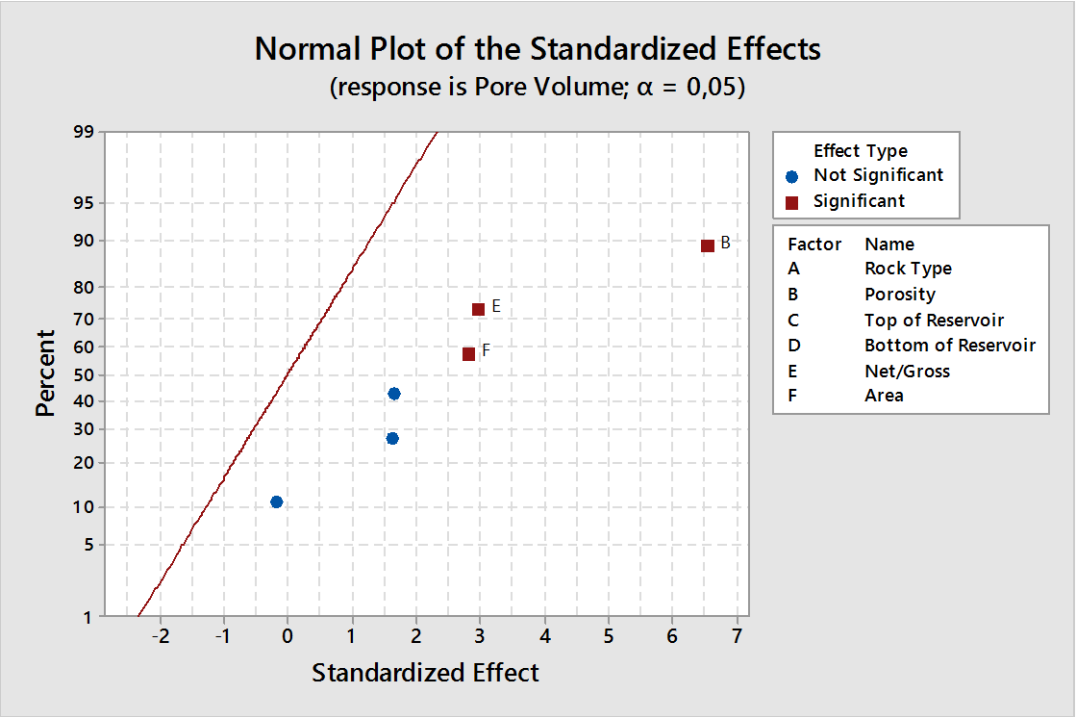

Figure 33 Normal Plot of the Standardized Effects

7.4 Error Analysis

7.4.1 Source of Error

The measured porosity, thickness and geothermal area data has some sorts of uncertainty. These uncertainties are either due to the physical phenomenon that is responsible for the physical phenomenon that is responsible for reservoir development (i.e. thickness, porosity and geothermal area) that is inherently random or errors in the predictions and estimations of the real world conditions (Ang and Tang, 1984). The inherent uncertainty is due to the nature of reservoir itself and cannot be decreased. However, it is possible to reduce the estimation and thus modeling uncertainty by use of more accurate models and/or the acquisition of more reliable and widespread data (Ang and Tang, 1984). The error in model prediction can be further subdivided into systematic and random errors. The systematic error is called the bias and it is due to factors that are not taken into account in the estimation

that are likely to affect the estimation (Duzgun, 2004). The estimations based on outcrop samples analyzed using image processing algorithms have systematic error, since they do not represent the in situ conditions of the geothermal reservoir. On the other hand, the random error is caused by lack of or limited knowledge. The sampling error that depends on the sample size is an example of such error. The use of the mean or median and the standard deviation or coefficient of variation helps the description of the errors.

When systematic errors in porosity values calculated using outcrop images are considered, it can be concluded that porosity may be somewhat different than the actual reservoir porosity. Calculated porosity can be higher than reservoir porosity due to confining pressure differences. Furthermore, outcrop rocks are exposed to weathering due to wind, rain etc, which may increase porosity. As for the random errors, images obtained from only three outcrop locations are used. The method provided in this thesis relies on accurate calculation of fractal dimension. The images used to calculate fractal dimension are processed using binarization and threshold processes that may affect the result. Therefore, porosity calculations may include some errors and they may not reflect the actual reservoir porosity.

A similar discussion can be conducted for geothermal reservoir thickness and area. For example, when thickness is calculated using drilling logs, lithological definitions of samples conducted by a geologist is considered. Percentage of minerals and lithology observation may change with a different point of view that may end up with a different interpretation. When seismic and resistivity measurements are considered the results include measurement errors as well as interpretation errors as discussed above.

Regarding the temperature measurements, temperature data is generally obtained with pressure – temperature (PT) probes. PT logging devices used in Alasehir wells is somewhat old such that temperature readings are plotted on paper and results are determined using some charts and rulers by engineers. Thus, sampling errors can be considered somewhat large.

CHAPTER 9

CONCLUSIONS

Alasehir geothermal reservoir pore volume uncertainty has been assessed by addressing geometry (top of reservoir and base of reservoir), reservoir continuity and porosity. Porosity of reservoir rocks (marble and schists) that are producing formations of Alasehir reservoir has been calculated using fractal analysis method. Thickness of the reservoir is obtained using drilling logs, seismic and resistivity data interpretations. Areal extent of the reservoir is obtained using reservoir temperature data obtained from static temperature logs of 25 previously drilled wells. Uncertainty analysis was conducted using Monte Carlo simulations. Also, Placket and Burman design is performed with Minitab software using the significance at 95% confidence level and to identify the sensitivity of parameters on pore volume calculation. The following conclusions can be drawn from the results of current study,

1. Fractal dimension calculated using box counting method is 1,32 ± 0,03 for marble and 1,29 ± 0,04 for schist which is in accord with Germencik and Kizildere geothermal fields.
2. Porosity calculated using fractal analysis is 6,6 ± 1,79 % for schist and 9,6 ± 0,98 % for marble formations.
3. Fracture density is 0,0934 ± 0,04 fractures/meter in X direction and 0,0898 ± 0,03 fractures/meter in Y direction.
4. Net thickness of the reservoir calculated using cutting sample log, seismic data and resistivity data is 611 ± 154 m, 655 ± 255 m and 683 ± 284 m respectively.
5. The geothermal extent is calculated as 50 ± 25 km^2.

6. Analysis of the stochastic results using Monte Carlo Simulation showed that Alasehir Geothermal Reservoir proven, probable and possible pore volume is 1,38 km^3, 2,30 km^3 and 3,82 km^3 respectively.
7. It has been found that porosity followed by the thickness and the area is most uncertain parameter that effect pore volume.

REFERENCES

Acuna, J., Ershaghi, I.and Yortsos, Y. C.(1992), *Fractal Analysis of Pressure Transients in the Geysers Geothermal Field*. Paper presented at Seventeenth Workshop on Geothermal Reservoir Engineering Stanford University, Stanford, California.

Akin, S. (2015). *Design and Analysis of Multi-well Interference Tests*.Paper presented at World Geothermal Congress, Melbourne.

Akin, S. (2013). *Estimating Natural-Fracture Permeability from Mud-Loss Data*. Paper presented at Thirty-Eighth Workshop on Geothermal Reservoir Engineering Stanford University, Stanford, California.

Ang, A.H. and Tang, W.H. (1984).*Probability Concepts in Engineering Planning and Design, Vol. I: Basic Principles.* John Wiley&Sons.

Arkan, S. and Parlaktuna, M. (2005).*Resource Assessment of Balçova Geothermal Field*. Paper presented at World Geothermal Congress, Antalya.

Asrizal, M., Hadi, J., Bahar, A. and Sihombing, J.M. (2006). *Uncertainty Quantification By Using Stochastic Approach In Pore Volume Calculation, Wayang Windu Geothermal Field, W. Jawa, Indonesia*. Paper presented Thirty-First Workshop on Geothermal Reservoir Engineering Stanford University, Stanford, California.

Baba, A., Simsek, C., Gunduz, O., Elci, A. and Murathan, A., (2015). *Hydrogeochemical Properties of Geothermal Fluid and Its Effect on the Environment in Gediz Graben, Western Turkey*. Paper presented at World Geothermal Congress, Melbourne.

Babadagli, T.(2000). *Evaluation of Outcrop Fracture Patterns of Geothermal Reservoirs in Southernwestern Turkey*. Paper presented at World Geothermal Congress, Antalya.

Ciftci, B. N. (2007). Geological Evolution of the Gediz Graben, SW Turkey: Temporal and Spatial Variation of the Graben. PhD dissertation, The Middle East Technical University, Ankara.

Demircioglu, D. (2009). Alasehir Grabenine Ait Sismik Kesitlerin Yapısal Yorumu. Msc dissertation. Ankara University, Ankara.

Demirmen, F. (2007). Reserves Estimation: The Challenge for the Industry. *Journal of Society of Petroleum Engineers, 59*,80-89.

Elliott, D. C. Reserve Estimates: Uncertainty and its Implications. *Journal of Canadian Petroleum Technology, 34*, 58-62

Erdogan, E., Basokur, A., Bozkurt, E., Moorkamp, M., and Avdeeva, A. (2014). *Interpretation of Kemaliye Geothermal Field Using 2D&3D MT Inversion*. Paper presented at 22nd EM Induction Workshop Weimar, Germany.

EURACHEM/CITAC (2012). *Quantifying Uncertainty in Analytical Measurement: User's Guide*.Retrieved from http://www.citac.cc/QUAM2012_P1.pdf.

Ferreira, T. and Rasband, W. (2012).*ImageJ User Guide*. Retrieved from http://imagej.nih.gov/ij/docs/guide/user-guide.pdf.

Handoko, B. T. (2010). Resource Assessment of Tompaso Geothermal Field, Indonesia(UNU-GTP Report 30). Retrieved from http://www.os.is/gogn/unu-gtp-report/UNU-GTP-2010-30.pdf.

Hanna, M. C., Gray, D., Fink, T., Mitchell, D., Jose, B., Willott, D. (2011). *Geophysical Applications – Using Geophysics for Hydrocarbon Reserves and Resources Classification and Assessment*. Retrieved from https://www.academia.edu/8357957/Geophysical_Applications_Using_Geophysics_for_Hydrocarbon_Reserves_and_Resources_Classification_and_Assessment.

Heise, W., Caldwell, T. G., Bibby H. M. and Bannister, S. C. (2008). Three-dimensional modelling of magnetotelluric data from theRotokawa geothermal field, Taupo Volcanic Zone, New Zealand. *Geophys. J. Int.*, 173,740–750.doi: 10.1111/j.1365-246X.2008.03737.x

Jafari, A. (2011). Permeability Estimation of Fracture Networks. PhD dissertation, The University of Alberta, Alberta.

Karamanderesi, İ. H. (2013). Characteristics of Geothermal Reservoirs in Turkey (IGA Academy Report 0102-2013).Retrieved from Unione Geotermica Italiana website:http://www.unionegeotermica.it/pdfiles/IGA_Academy_Report_Vol-1.pdf.

Kim, T. H. (2007). Fracture Characterization and Estimation of Fracture Porosity of Naturally Fractured Reservoirs with No Matrix Porosity Using Stochastic Fractal Model. PhD dissertation, Texas A&M University, Texas.

Kim, T. H. and Schecster, D. S., (2007), *Estimation of Fracture Porosity of Naturally Fractured Reservoirs with No Matrix Porosity Using Fractal Discrete Fracture Networks*. Paper presented at SPE Annual Technical Conference and Exhibition, California.

Kosova, R., Naco, A. and Muca, M.(2015). Uncertainty in Oil Reservoir Properties Deterministic and Stochastic Methods of Reserves Estimation. *International Journal of Science and Research, 4*, 471-474.

Louie, J. N., Pullammanappallil, S. K. and Honjas, W. (2011). *Advanced Seismic Imaging for Geothermal Development.* Paper presented at New Zealand Geothermal Workshop, Auckland, New Zealand.

The U.S. Bureau of Mines and U.S. Geological Survey. (1976). *Principles of the Mineral Resource Classification System* (No. 1450-A). Retrieved from http://pubs.usgs.gov/bul/1450a/report.pdf

Muffler, L. J. P., and Cataldi, R. (1977). *Methods for Regional Assessment of Geothermal Resources.* Paper presented at Larderello Workshop on Geothermal Resource Assessment and Reservoir Engineering, Larderello.

Muffler, P. and Cataldi, R.. (1978). Methods for regional assessment of geothermal resources. *Geothermics*, 7, 53-89.doi:10.1016/0375-6505(78)90002-0

Ofwona C. (2008). *Geothermal Resource Assessment – Case Example, Olkaria I.* Paper presented at Short Course III on Exploration for Geothermal Resources, Kenya.

Palisade Corporation. (2010). *Risk Analysis and Simulation Add-In for Microsoft-Excel.* New York, USA; Author.

Park J., Kwon S. and Sung W. (2005). Characterization of Fractured Basement Reservoir Using Statistical and Fractal Methods. *Korean J. Chem. Eng., 22(4),* 591-598.

Roy, A., Perfect, E., Dunne, W. M., and McKay, L. D. (2007). Fractal characterization of fracture networks: An improved box-counting technique. *Journal of Geophysical Research, 112*, B12201. doi:10.1029/2006JB004582.

Rutagarama, U. (2012). The role of well testing in geothermal resource assessment. Msc dissertation, The University of Iceland, Iceland.

Sarmiento, Z. F. and Steingrimsson, B. (2008). *Computer Programme for Resource Assessment and Risk Evaluation Using Monte Carlo Simulation.* Paper presented at Short Course on Geothermal Project Management and Development, Uganda.

Sarmiento, Z. F. and Steingrimsson, B. (2011). *Resource Assessment I: Introduction and Volumetric Assessment*. Paper presented at Short Course on Geothermal Drilling, Resource Development and Power Plants, El Salvador.

Singhal, B. B. S., Gupta, R. P. (2010).*Applied Hydrogeology of Fractured Rocks.*The Netherland: Kluwer Academic Publisher.

Strack, K.-M. (2010). *Advances in Electromagnetics for Reservoir Monitoring*. Paper presented at 8th International Conference & Exposition on Petroleum Geophysics, Hyderabad.

Tampubolon, T. (1989). Analysis of Well Test Data from Indonesia and Iceland (UNU-GTP Report 4). Retrieved fromhttp://www.os.is/gogn/unu-gtp-report/UNU-GTP-1989-04.pdf.

Tarcan, G., Filiz, S. and Gemici, U. (2000). *Geology and Geochemistry of the Salihli Geothermal Fields, Turkey*. Paper presented at World Geothermal Congress, Japan.

Yeten, B., Castellini, A., Guyaguler B. and Chen, W. H. (2005). *A Comparison Study on Experimental Design and Response Surface Methodologies*. Paper presented at SPE Reservoir Simulation Symposium, Houston.

Yilmazer, S., Pasvanoglu, S. and Vural, S. (2010). *The Relation of Geothermal Resources with Young Tectonics in the Gediz Graben (West Anatolia, Turkey) and Their Hydrogeochemical Analyses.* Paper presented at World Geothermal Congress, Indonesia.

APPENDIX A

FRACTAL DIMENSION ESTIMATIONS

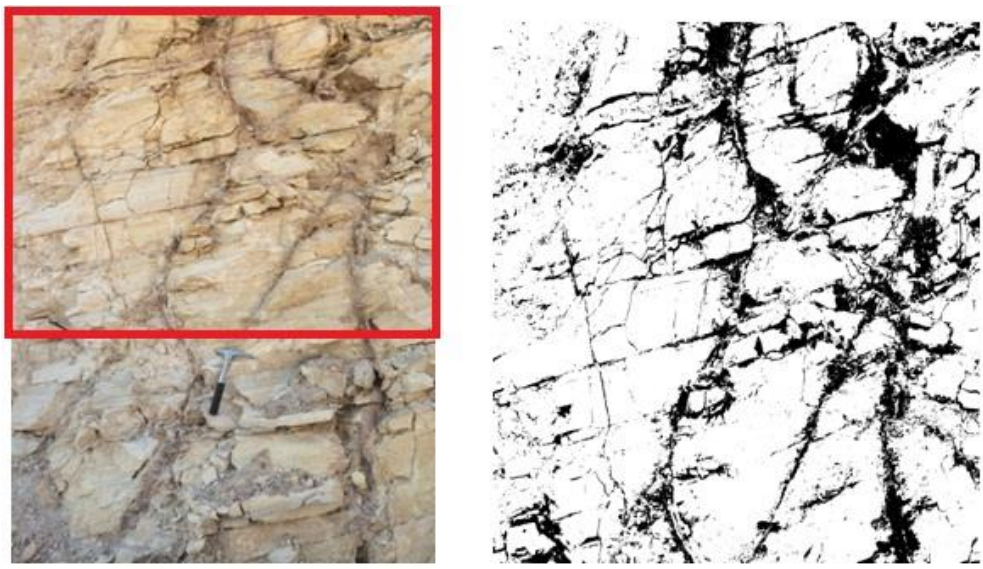

Figure 34 Threshold of S-1 Image

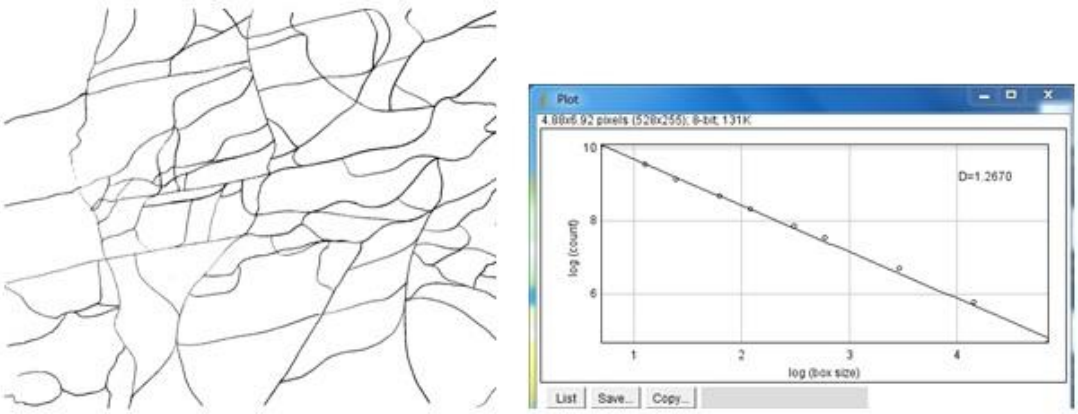

Figure 35 Fracture Pattern and FD of S-1

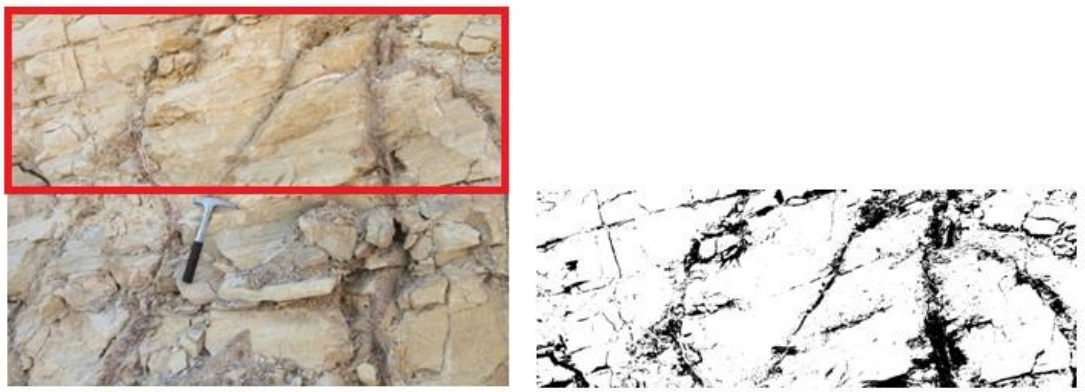

Figure 36 Threshold of S-2 Image

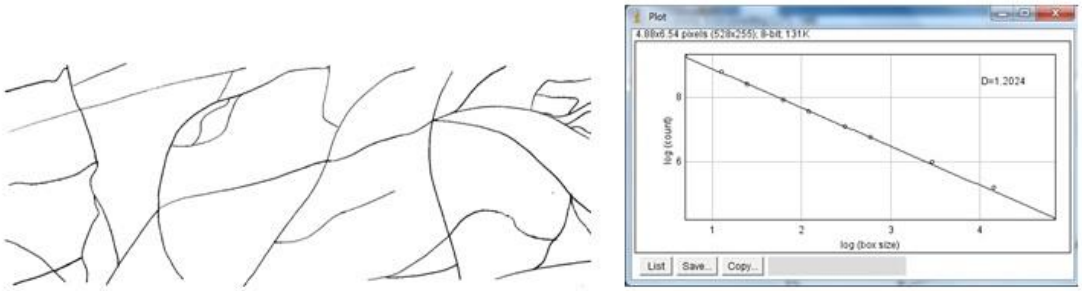

Figure 37 Fracture Pattern and FD of S-2

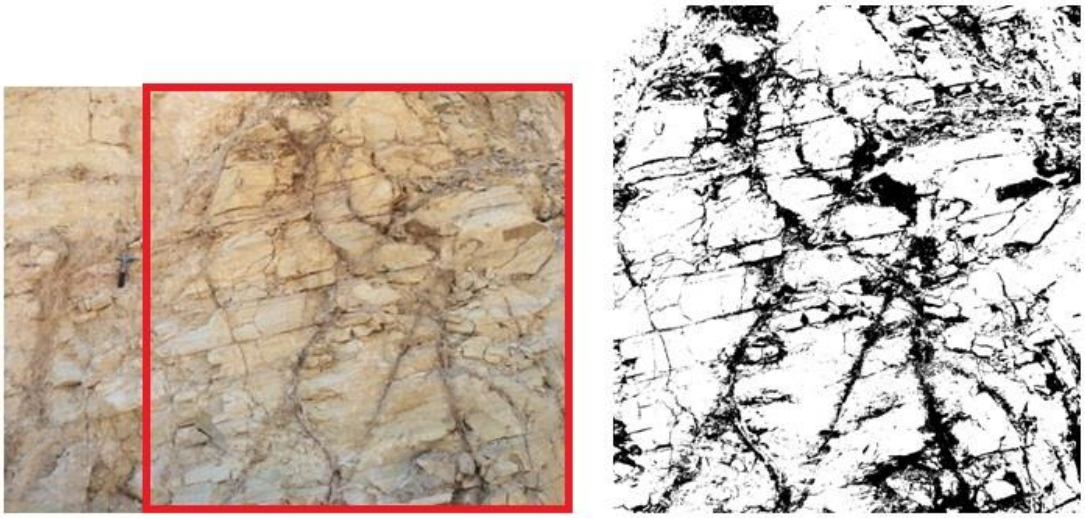

Figure 38 Threshold of S-3 Image

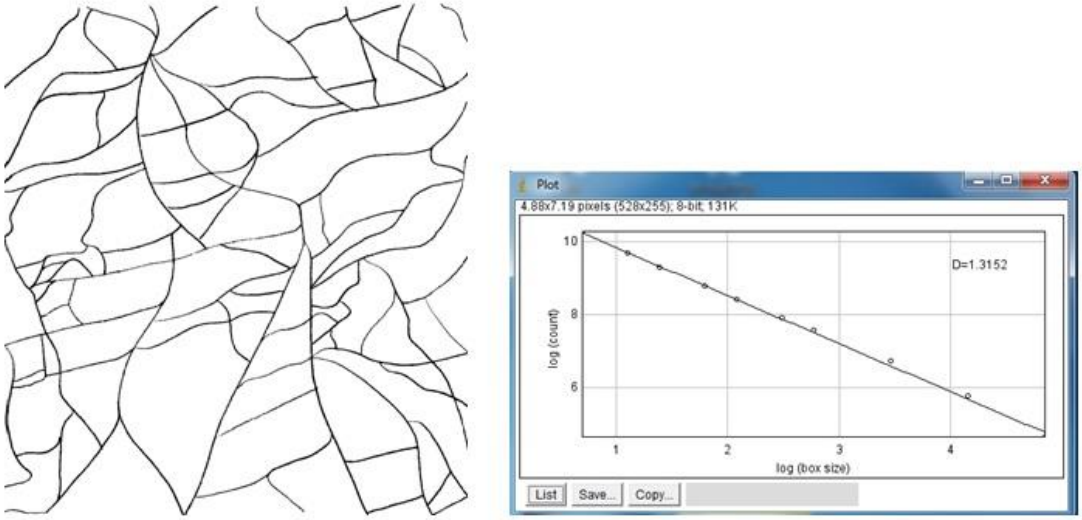

Figure 39 Fracture Pattern and FD of S-3

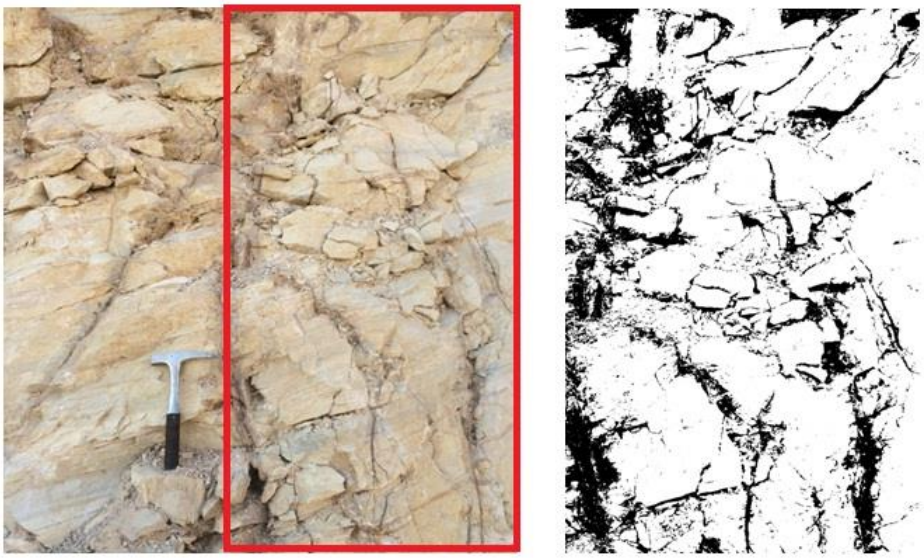

Figure 40 Threshold of S-4 Image

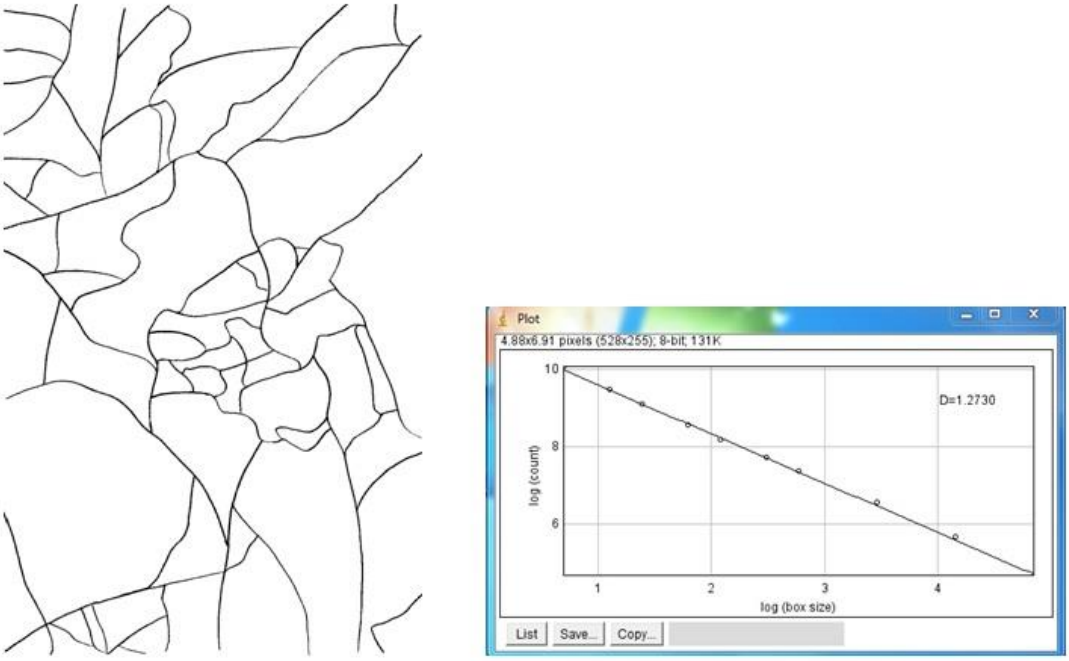

Figure 41 Fracture Pattern and FD of S-4

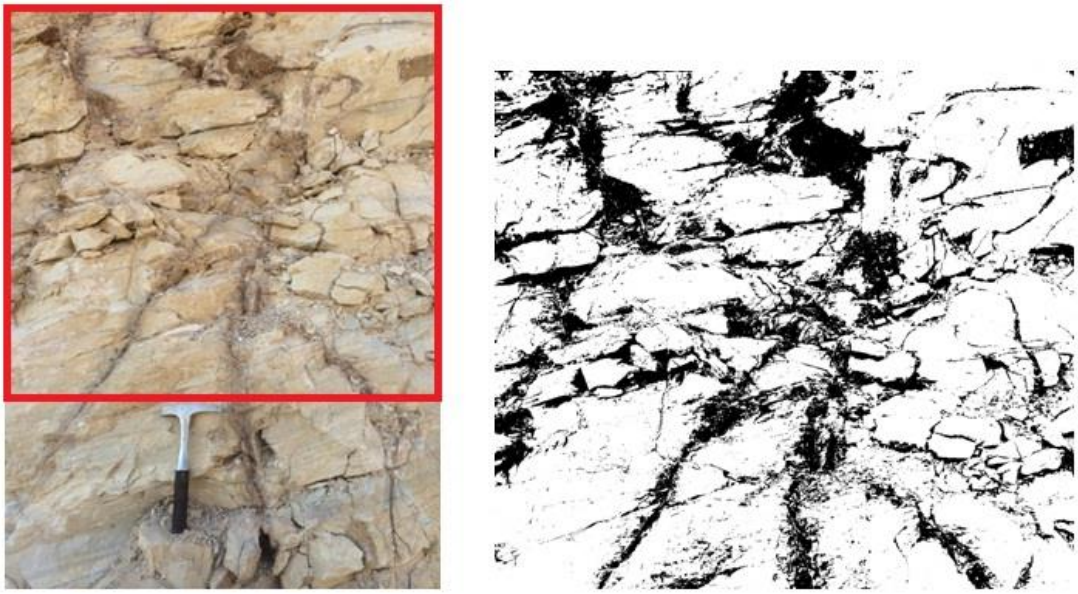

Figure 42 Threshold of S-5 Image

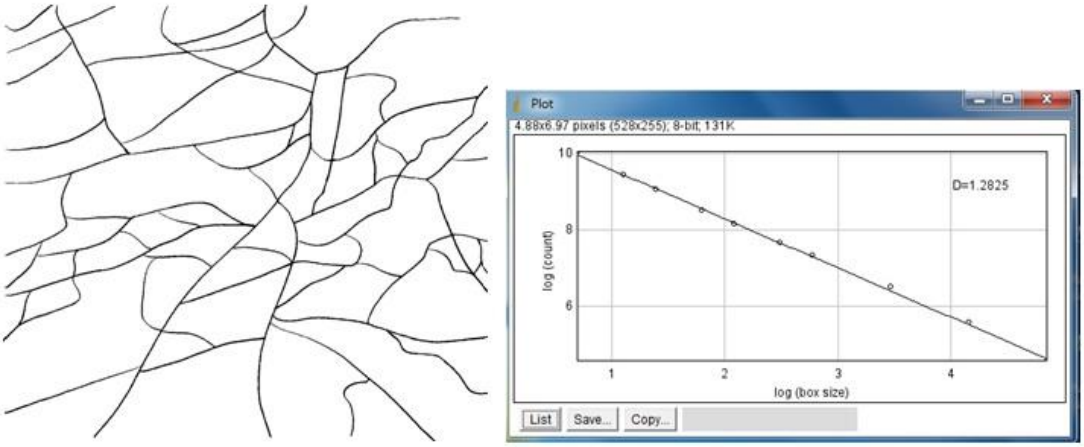

Figure 43 Fracture Pattern and FD of S-5

Figure 44 Threshold of S-6 Image

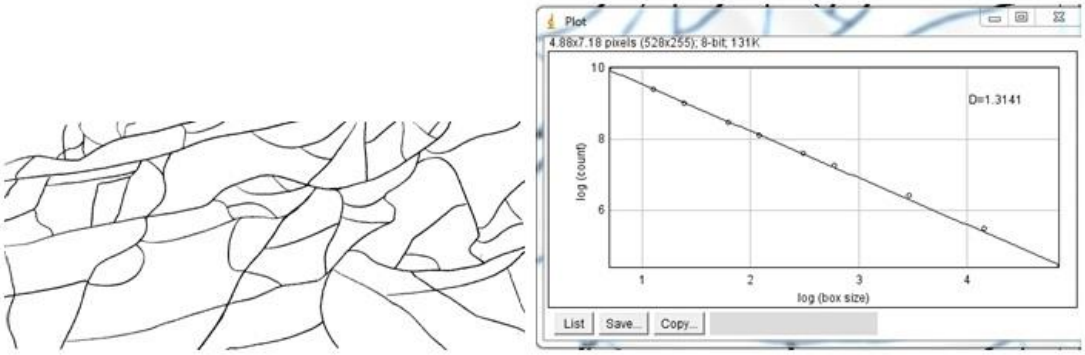

Figure 45 Fracture Pattern and FD of S-6

Figure 46 Threshold of S-7 Image

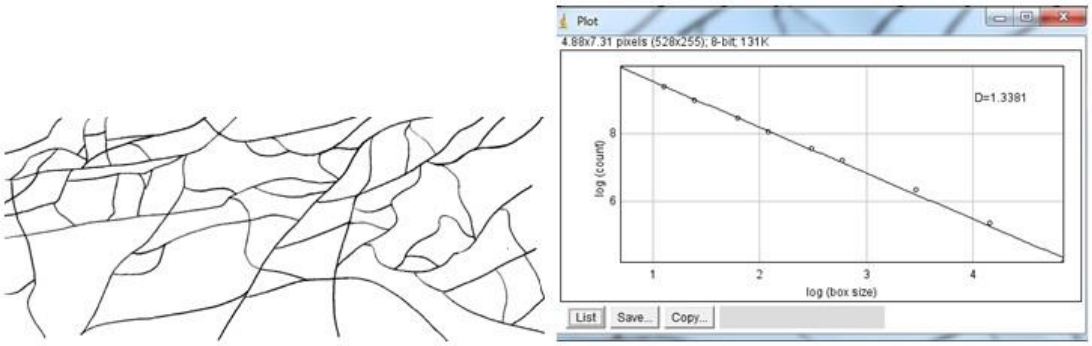

Figure 47 Fracture Pattern and FD of S-7

Figure 48 Threshold of S-8 Image

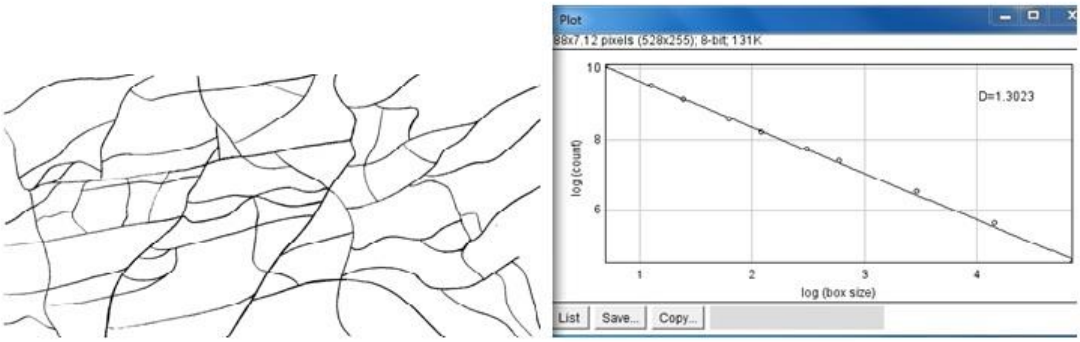

Figure 49 Fracture Pattern and FD of S-8

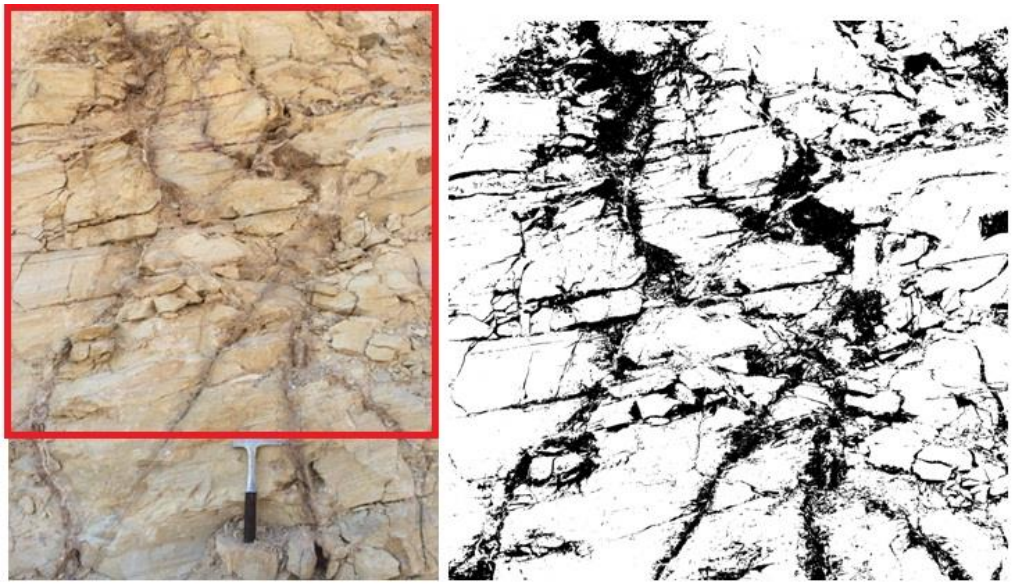

Figure 50 Threshold of S-9 Image

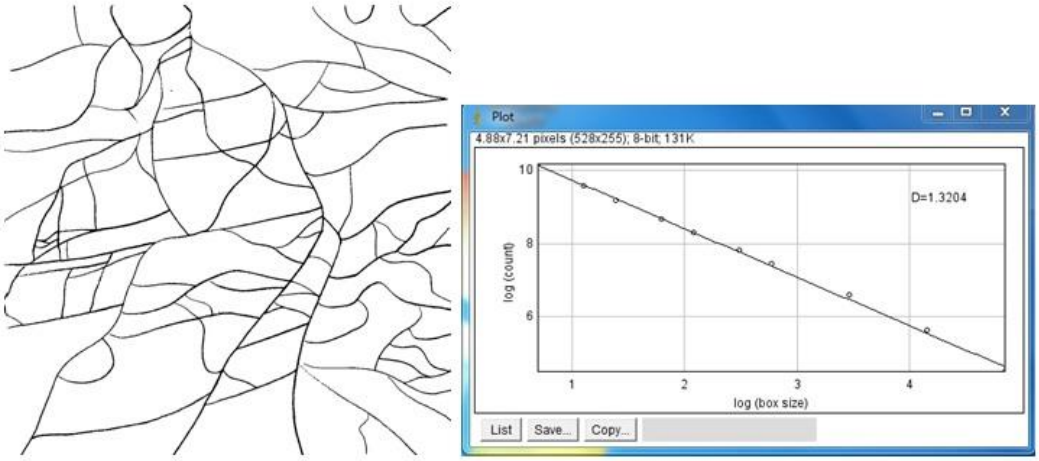

Figure 51 Fracture Pattern and FD of S-9

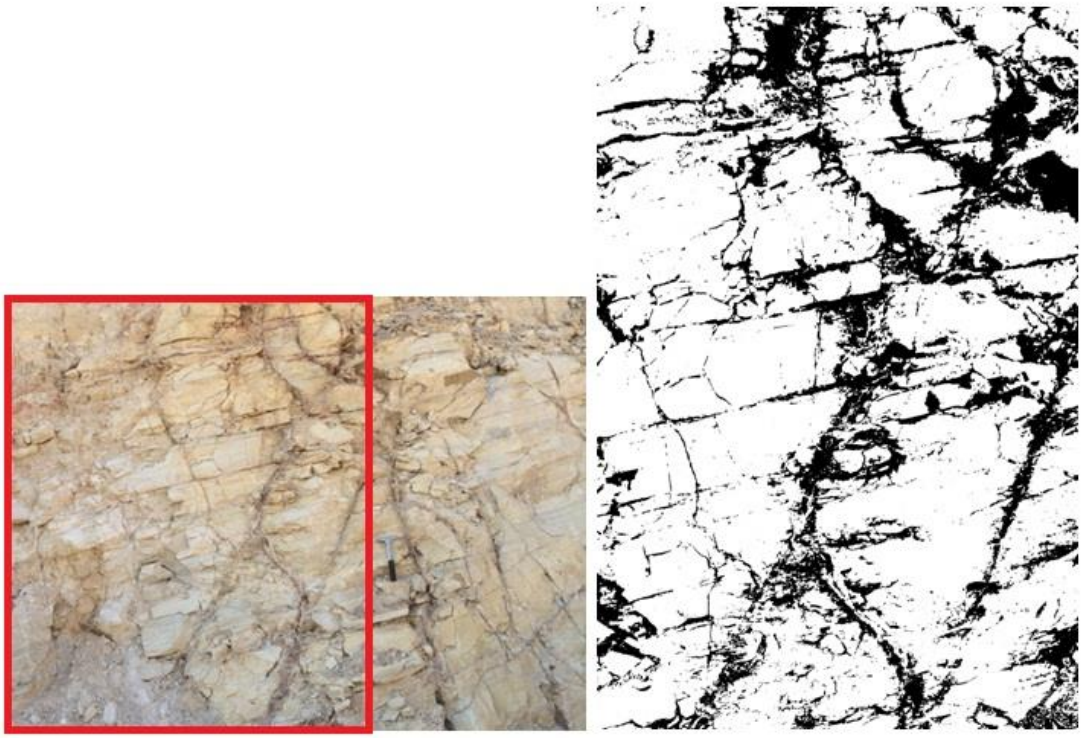

Figure 52 Threshold of S-10 Image

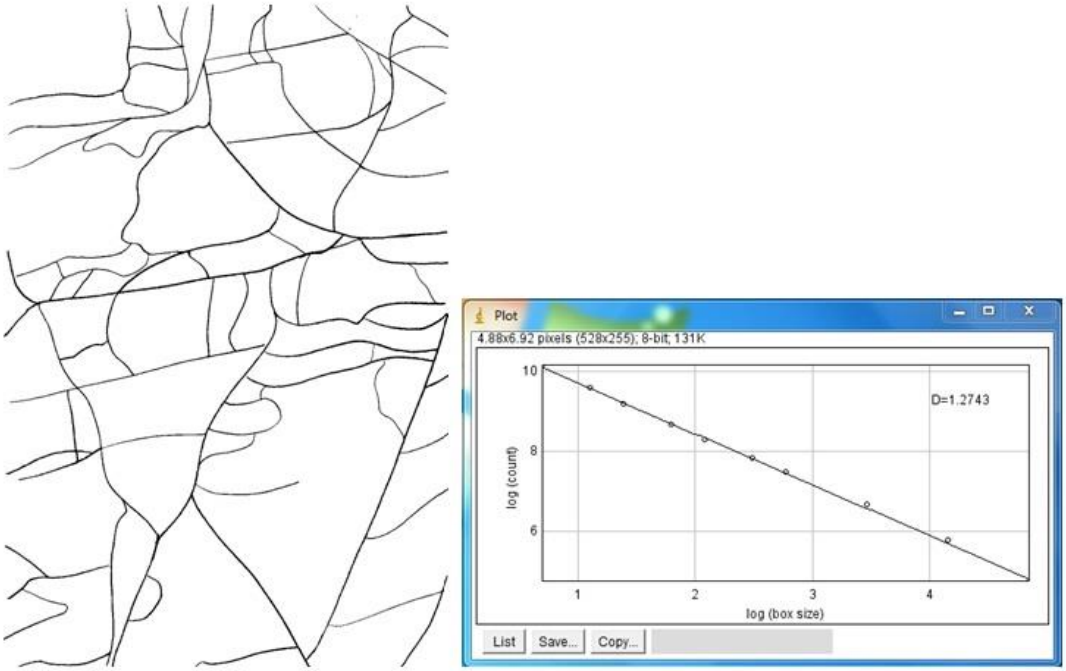

Figure 53 Fracture Pattern and FD of S-10

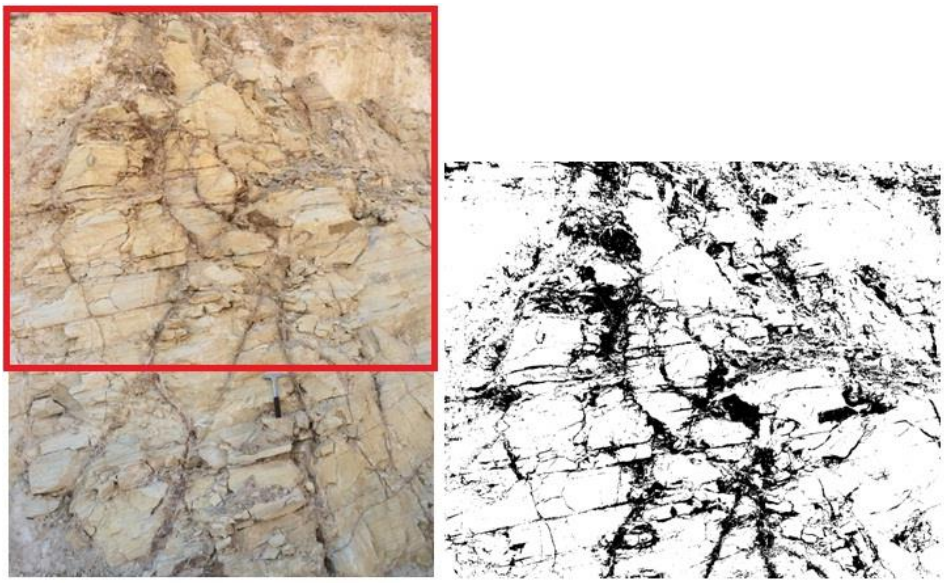

Figure 54 Threshold of S-11 Image

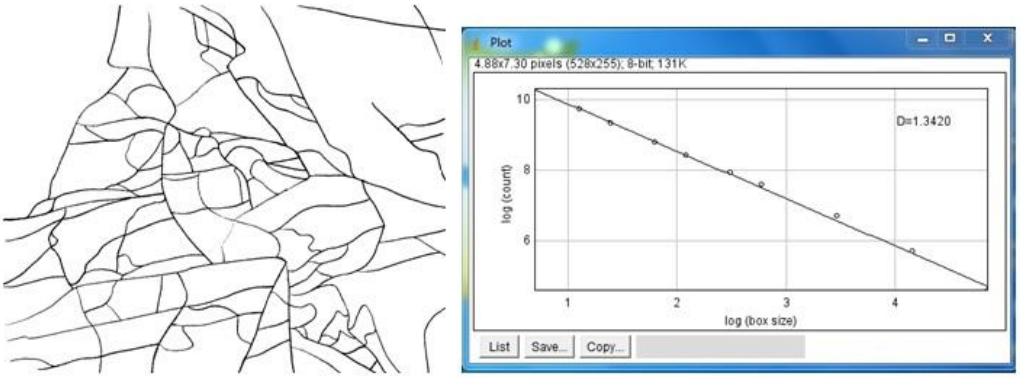

Figure 55 Fracture Pattern and FD of S-11

Figure 56 Threshold of M-1 Image

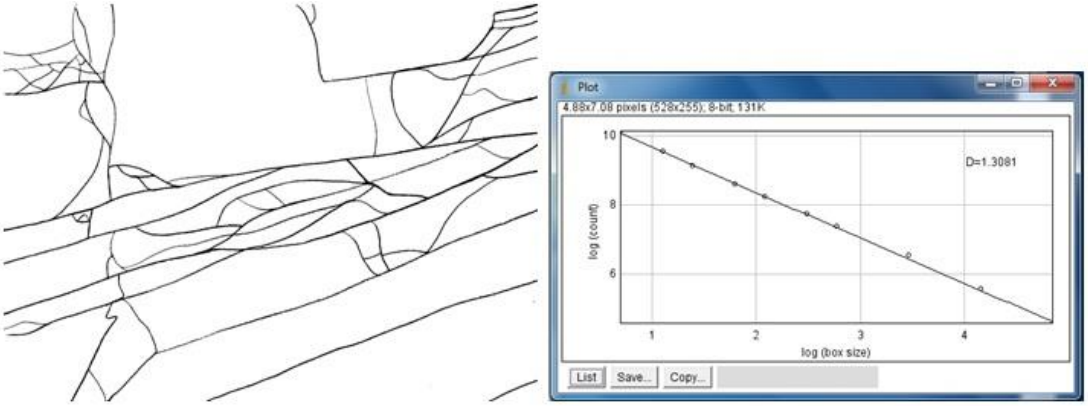

Figure 57 Fracture Pattern and FD of M-1

Figure 58 Threshold of M-2 Image

Figure 59 Fracture Pattern and FD of M-2

Figure 60 Threshold of M-3 Image

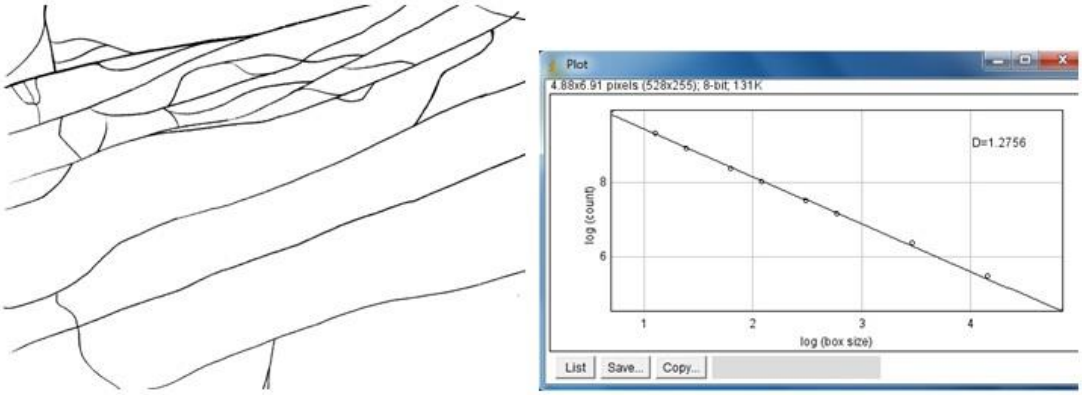

Figure 61 Fracture Pattern and FD of M-3

Figure 62 Threshold of M-4 Image

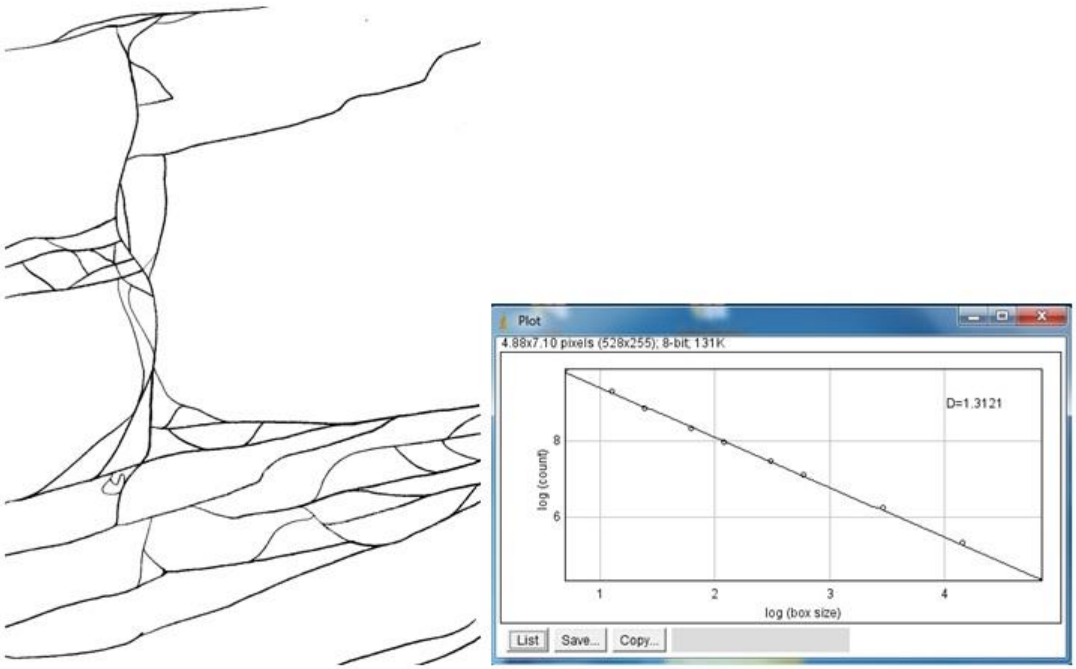

Figure 63 Fracture Pattern and FD of M-4

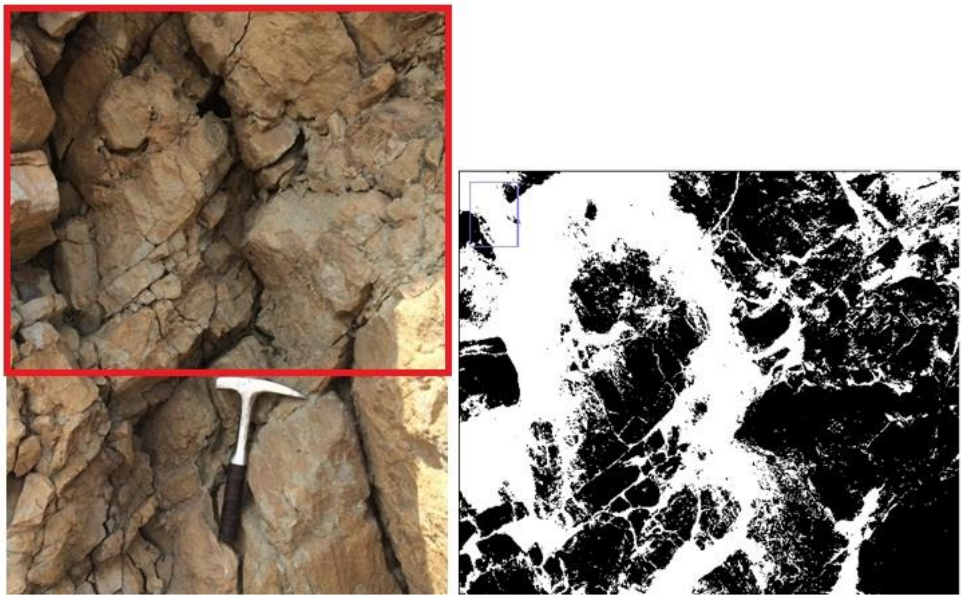

Figure 64 Threshold of M-5 Image

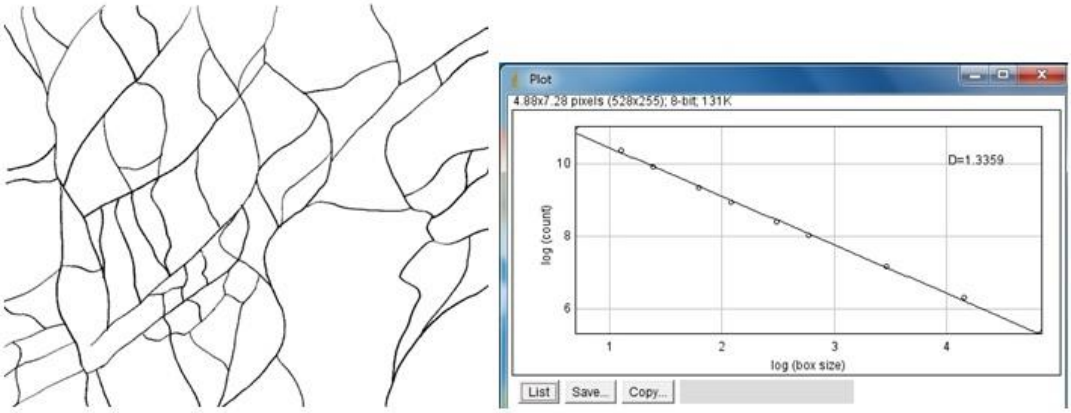

Figure 65 Fracture Pattern and FD of M-5

Figure 66 Threshold of M-6 Image

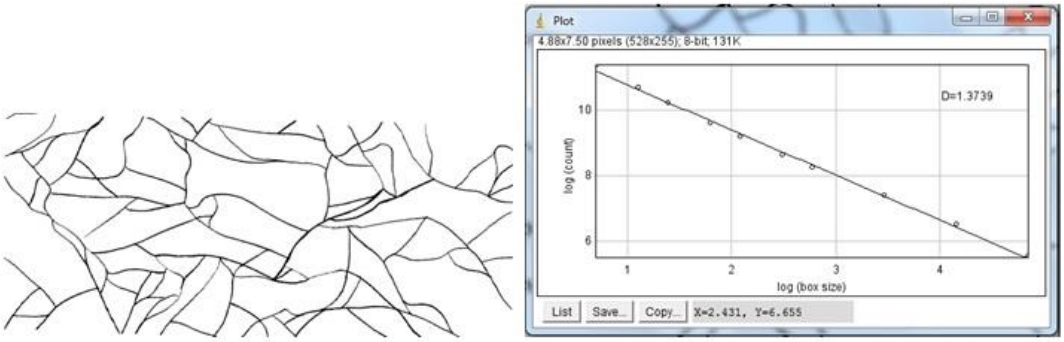

Figure 67 Fracture Pattern and FD of M-6

APPENDIX B

FRACTURE DENSITY ESTIMATIONS

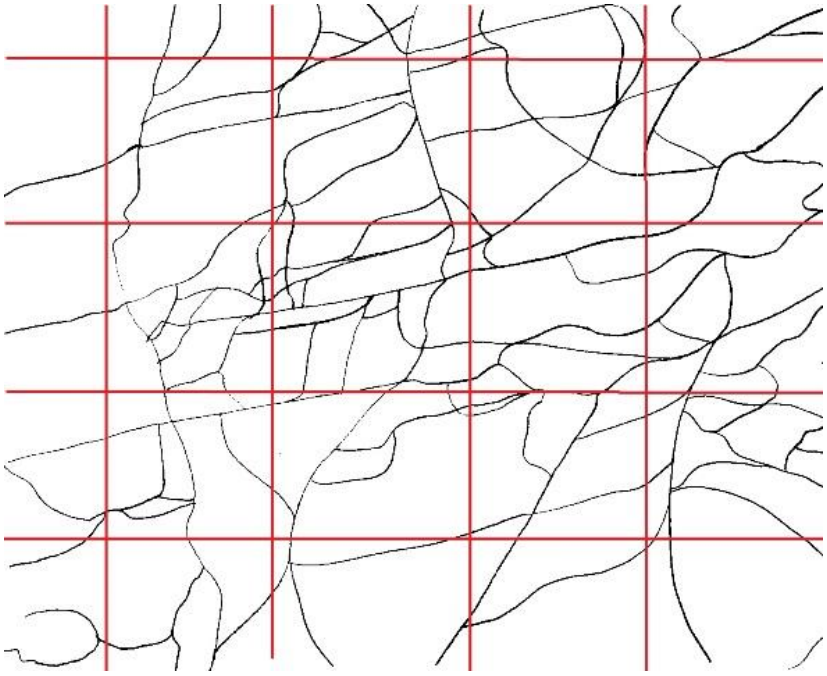

Figure 68 Fracture Density of S-1

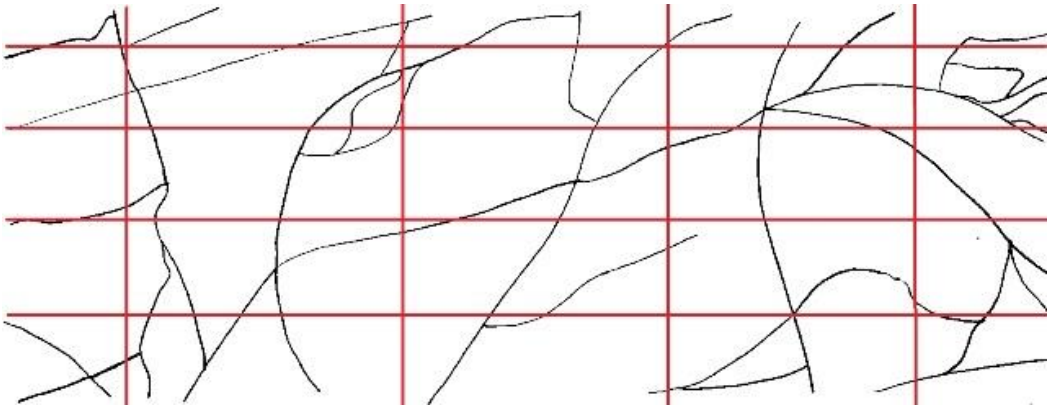

Figure 69 Fracture Density of S-2

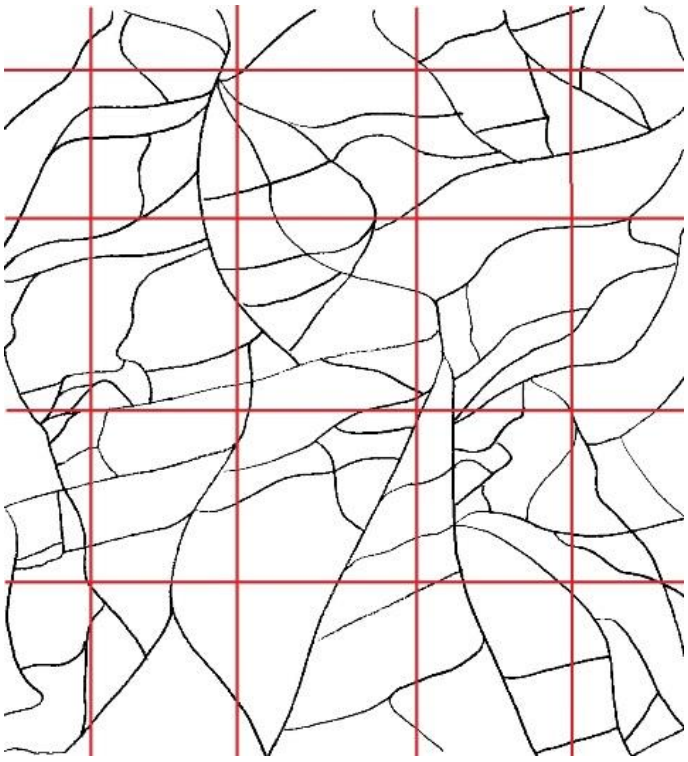

Figure 70 Fracture Density of S-3

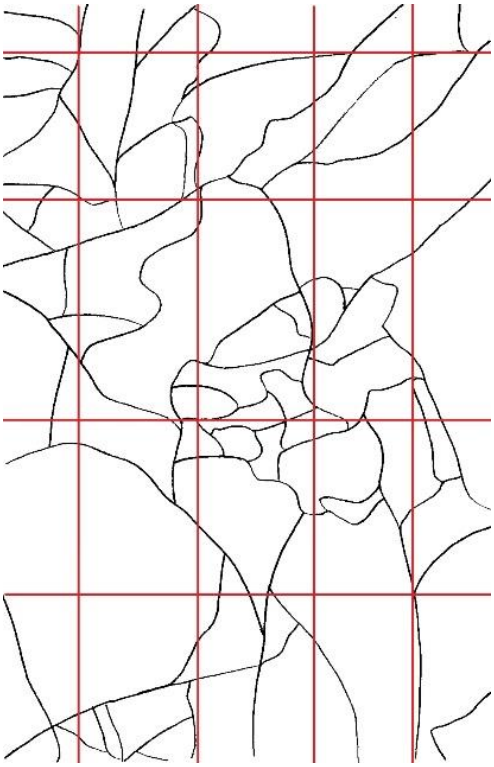

Figure 71 Fracture Density of S-4

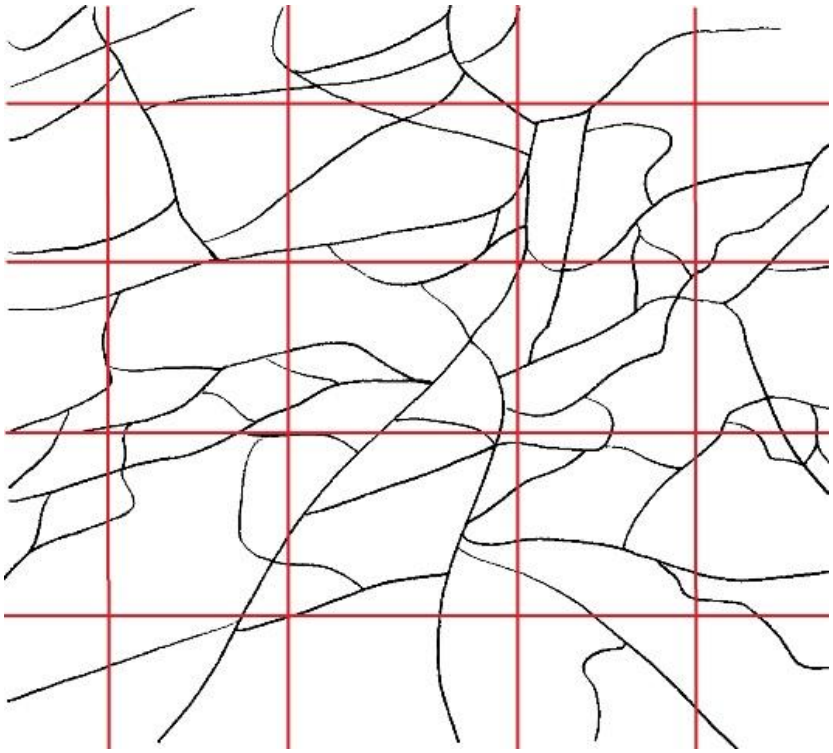

Figure 72 Fracture Density of S-5

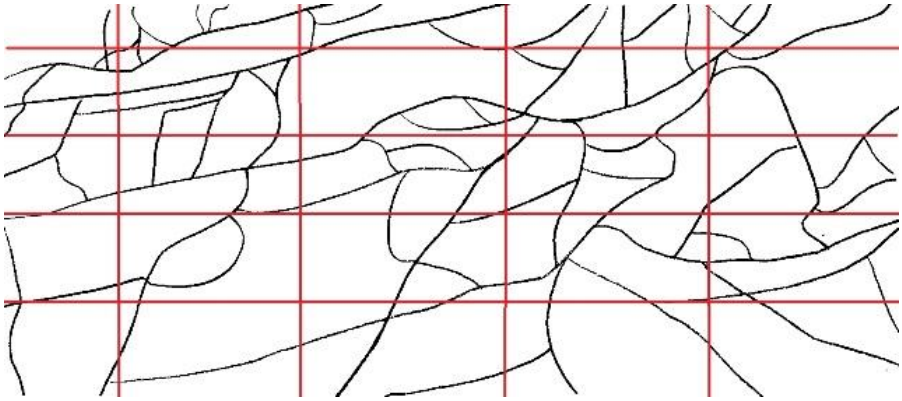

Figure 73 Fracture Density of S-6

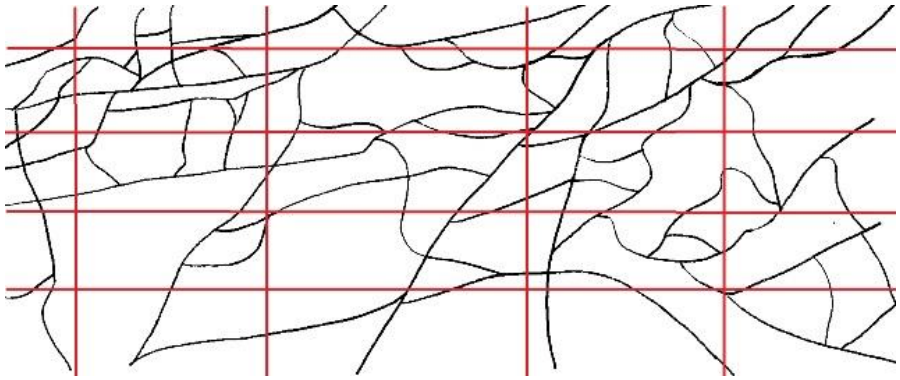

Figure 74 Fracture Density of S-7

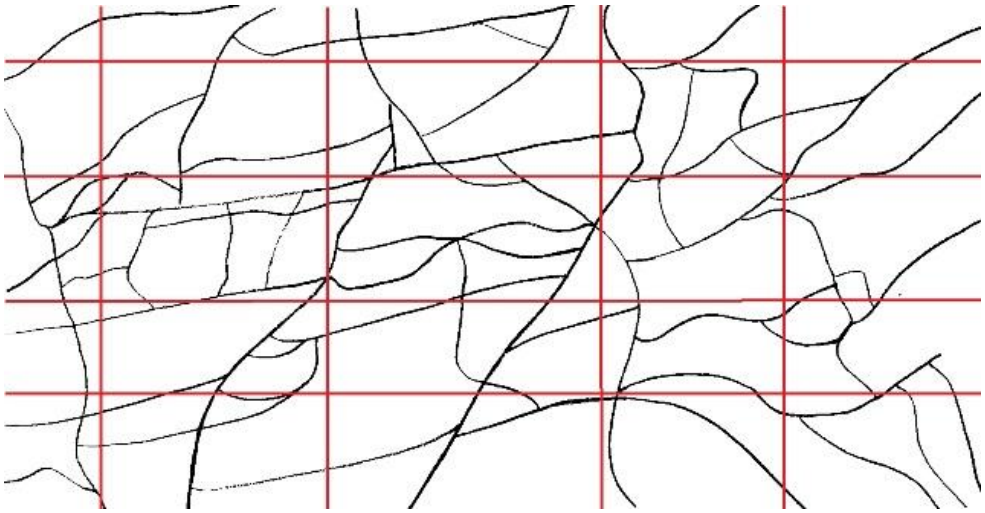

Figure 75 Fracture Density of S-8

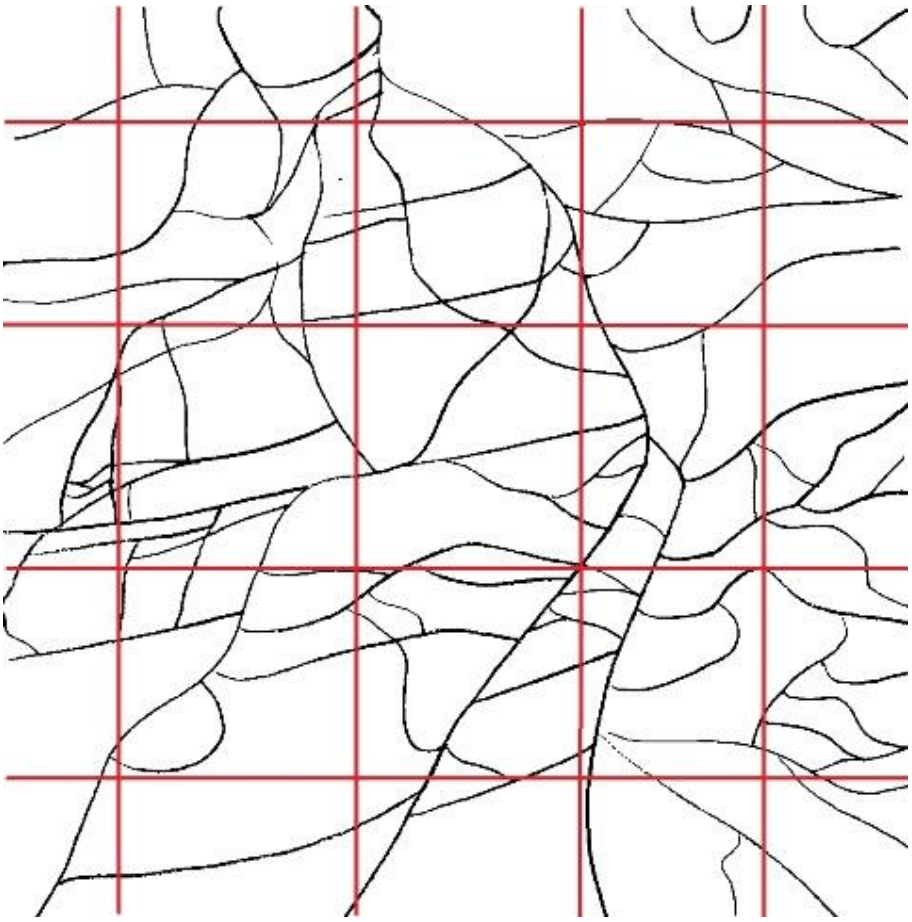

Figure 76 Fracture Density of S-9

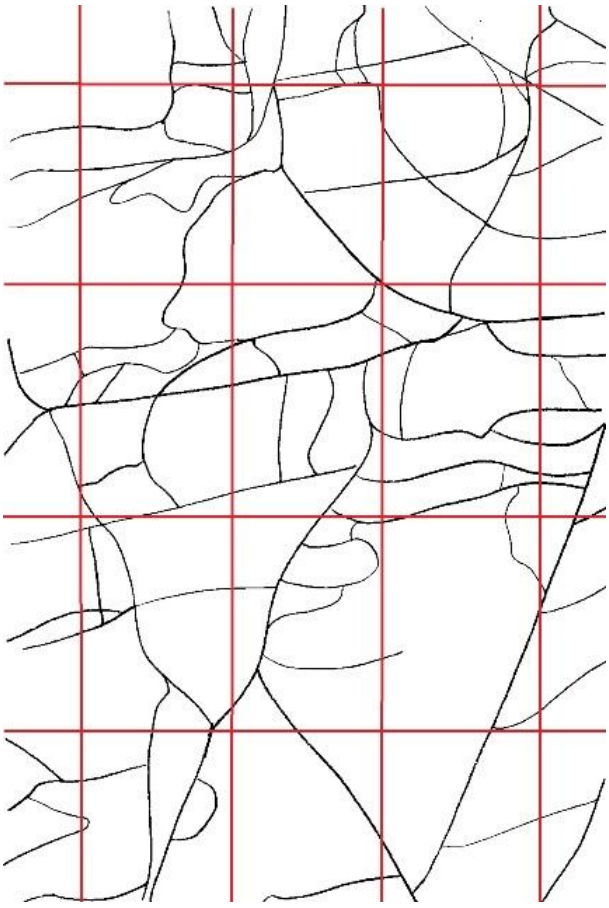

Figure 77 Fracture Density of S-10

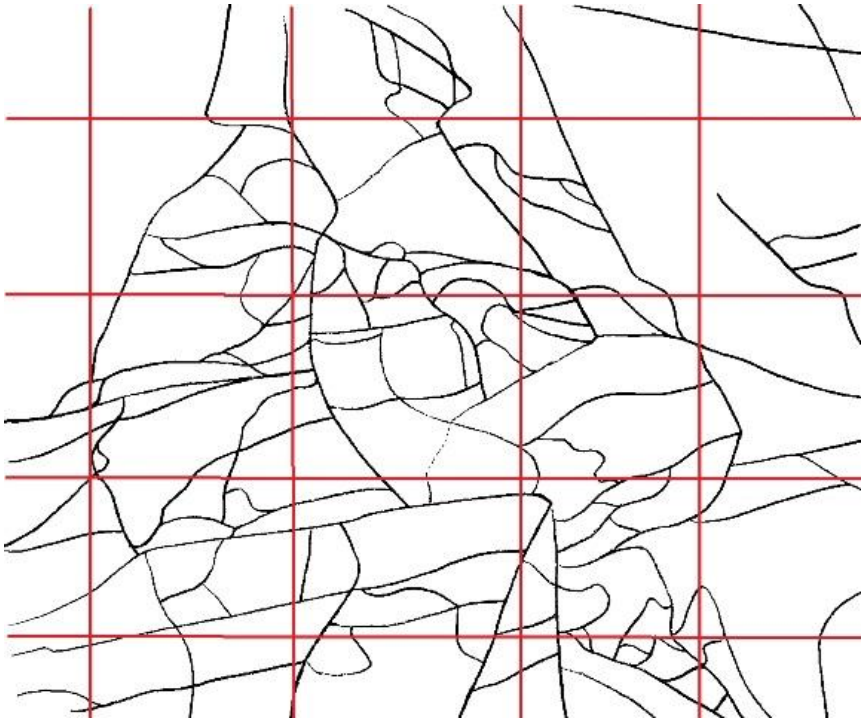

Figure 78 Fracture Density of S-11

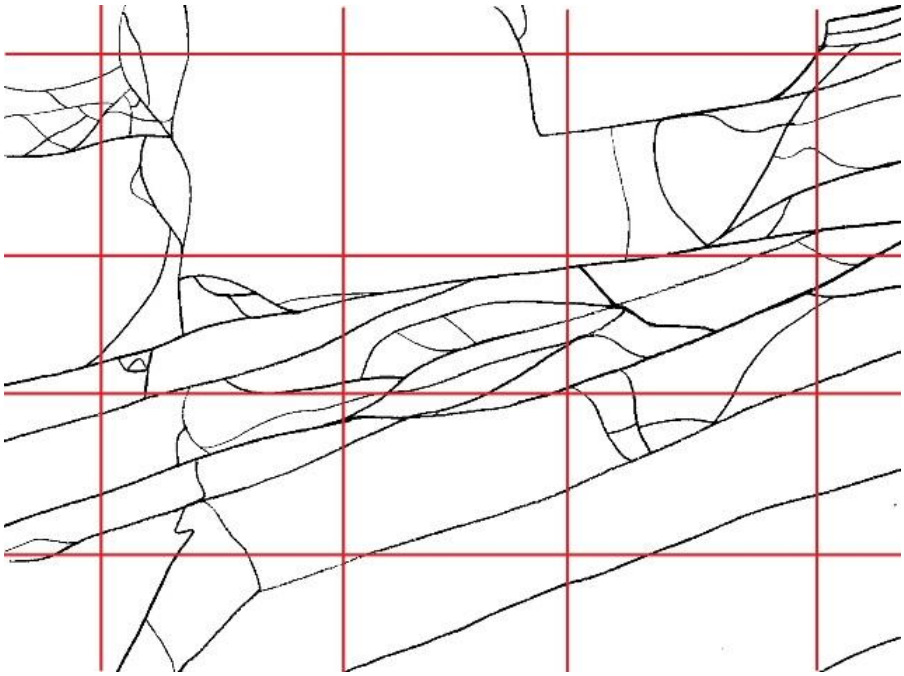

Figure 79 Fracture Density of M-1

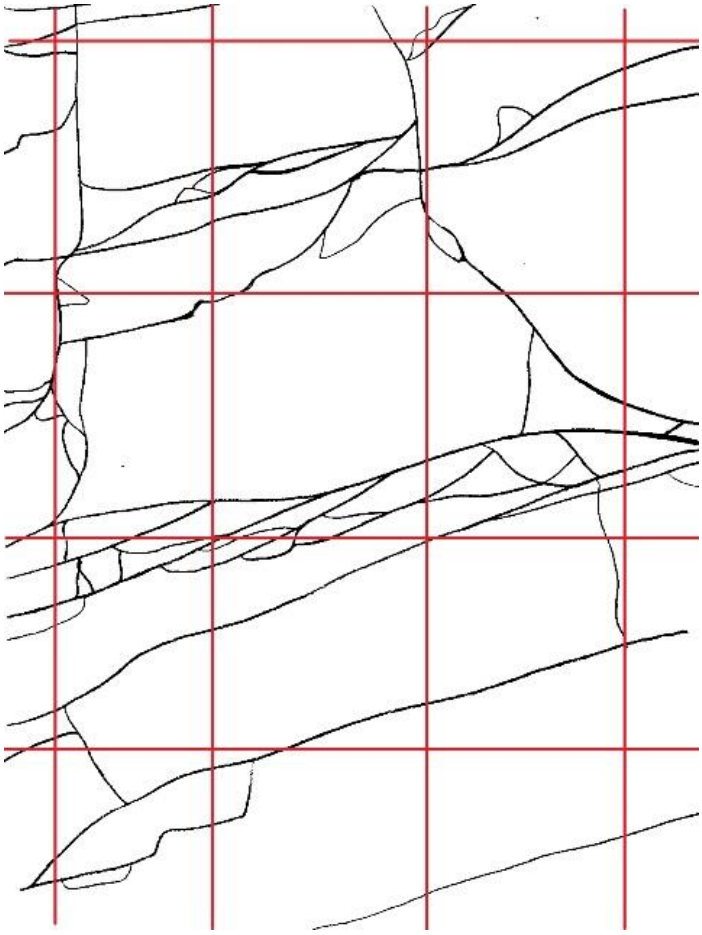

Figure 80 Fracture Density of M-2

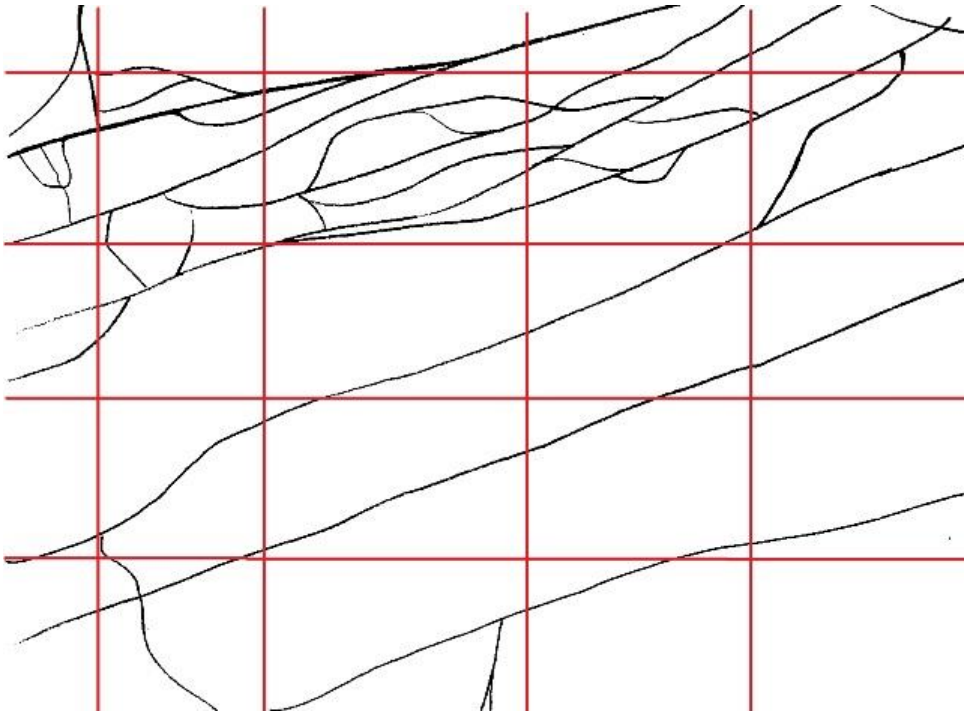

Figure 81 Fracture Density of M-3

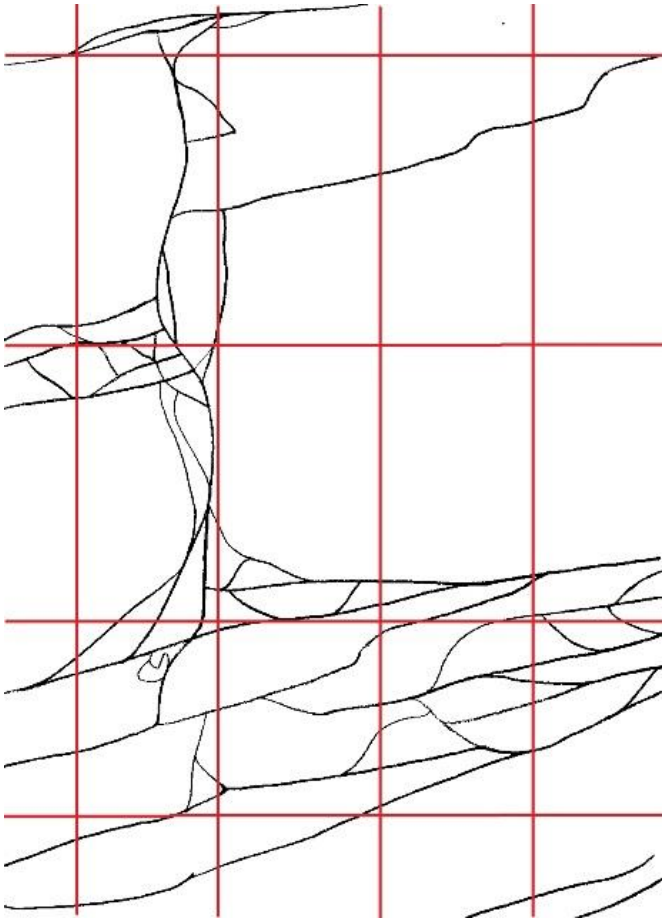

Figure B.15 Fracture Density of M-4

Table 18 Image Length and Area Calculation

Photo	Photo		Reference Material Lenght in Photo		Reference Material Length in Real		X (cm)	Y (cm)	Area (cm^2)	Area (m^2)
	X (cm)	Y (cm)	X (cm)	Y (cm)	X (cm)	Y (cm)				
S-1	9,1	5,8	1,5	2,7	10,0	30,0	60,7	64,4	3909,6	0,39
S-2	15,2	5,8	1,4	2,4	10,0	30,0	108,6	72,5	7871,4	0,79
S-3	13,5	15,0	0,9	1,1	10,0	30,0	150,0	409,1	61363,6	6,14
S-4	5,2	8,8	1,2	2,1	10,0	30,0	43,3	125,7	5447,6	0,54
S-5	9,1	8,8	1,3	2,2	10,0	30,0	70,0	120,0	8400,0	0,84
S-6	16,2	7,0	1,2	3,0	10,0	30,0	135,0	70,0	9450,0	0,95
S-7	15,7	6,8	1,4	2,4	10,0	30,0	112,1	85,0	9532,1	0,95
S-8	16,2	8,3	1,4	2,1	10,0	30,0	115,7	118,6	13720,4	1,37
S-9	9,1	9,1	1,1	2,1	10,0	30,0	82,7	130,0	10754,5	1,08
S-10	6,0	8,8	0,8	1,2	10,0	30,0	75,0	220,0	16500,0	1,65
S-11	8,8	7,6	0,5	0,9	10,0	30,0	176,0	253,3	44586,7	4,46
M-1	20,8	15,7	1,6	0,2	13,4	1	174,2	78,5	13674,7	1,37
M-2	11,7	15,6	0,6	0,1	13,4	1	261,3	156,0	40762,8	4,08
M-3	20,3	15,6	1,9	0,2	13,4	1	143,2	78,0	11167,1	1,12
M-4	11,7	15,6	2,1	0,2	13,4	1	74,7	78,0	5823,3	0,58

Table 19 Fracture Intersection Numbers in X and Y Directions

Photo	Fracture Intersection Numbers in X				Fracture Intersection Numbers in Y			
	1	2	3	4	1	2	3	4
S-1	10	10	13	8	5	11	13	12
S-2	10	10	8	11	5	5	4	4
S-3	9	7	14	9	15	12	14	14
S-4	7	8	11	5	10	14	12	8
S-5	7	11	14	5	12	11	12	8
S-6	13	12	10	10	8	5	7	9
S-7	15	15	11	11	6	8	9	6
S-8	7	14	12	14	10	7	5	9
S-9	10	9	11	8	15	14	13	13
S-10	10	4	8	4	16	12	12	16
S-11	6	14	11	15	0	16	17	11
M-1	6	7	12	5	0	8	9	14
M-2	5	4	11	3	17	14	10	8
M-3	10	5	2	4	9	7	9	6
M-4	4	7	8	2	10	15	8	9

Table 20 Fracture Density for Outcrop Images

Photo	Line Length		Fracture Density in X (m^{-1})					Fracture Density in Y (m^{-1})				
	X (cm)	Y (cm)	1	2	3	4	Average	1	2	3	4	Average
S-1	60,7	64,4	0,1647	0,1647	0,2142	0,1318	0,1689	0,0776	0,1708	0,2019	0,1863	0,1592
S-2	108,6	72,5	0,0921	0,0921	0,0737	0,1013	0,0898	0,0690	0,0690	0,0552	0,0552	0,0621
S-3	150,0	409,1	0,0600	0,0467	0,0933	0,0600	0,0650	0,0367	0,0293	0,0342	0,0342	0,0336
S-4	43,3	125,7	0,1628	0,1848	0,2540	0,1155	0,1793	0,0796	0,1114	0,0955	0,0636	0,0875
S-5	70,0	120,0	0,1000	0,1571	0,2000	0,0714	0,1321	0,1000	0,0917	0,1000	0,0667	0,0896
S-6	135,0	70,0	0,0963	0,0889	0,0741	0,0741	0,0833	0,1143	0,0714	0,1000	0,1286	0,1036
S-7	112,1	85,0	0,1338	0,1338	0,0981	0,0981	0,1160	0,0706	0,0941	0,1059	0,0706	0,0853
S-8	115,7	118,6	0,0605	0,1210	0,1037	0,1210	0,1016	0,0843	0,0590	0,0422	0,0759	0,0653
S-9	82,7	130,0	0,1209	0,1088	0,1330	0,0967	0,1149	0,1154	0,1077	0,1000	0,1000	0,1058
S-10	75,0	220,0	0,1333	0,0533	0,0455	0,0227	0,0637	0,0727	0,0545	0,0545	0,0727	0,0636
S-11	176,0	253,3	0,0341	0,0795	0,1467	0,2000	0,1151	0,0355	0,0632	0,0671	0,0434	0,0523
M-1	174,2	78,5	0,0344	0,0402	0,0689	0,0287	0,0431	0,1146	0,1019	0,1146	0,1783	0,1274
M-2	261,3	156,0	0,0191	0,0153	0,0421	0,0115	0,0220	0,1090	0,0897	0,0641	0,0513	0,0785
M-3	143,2	78,0	0,0698	0,0349	0,0140	0,0279	0,0367	0,1154	0,0897	0,1154	0,0769	0,0994
M-4	74,7	78,0	0,0535	0,0937	0,1071	0,0268	0,0703	0,1282	0,1923	0,1026	0,1154	0,1346

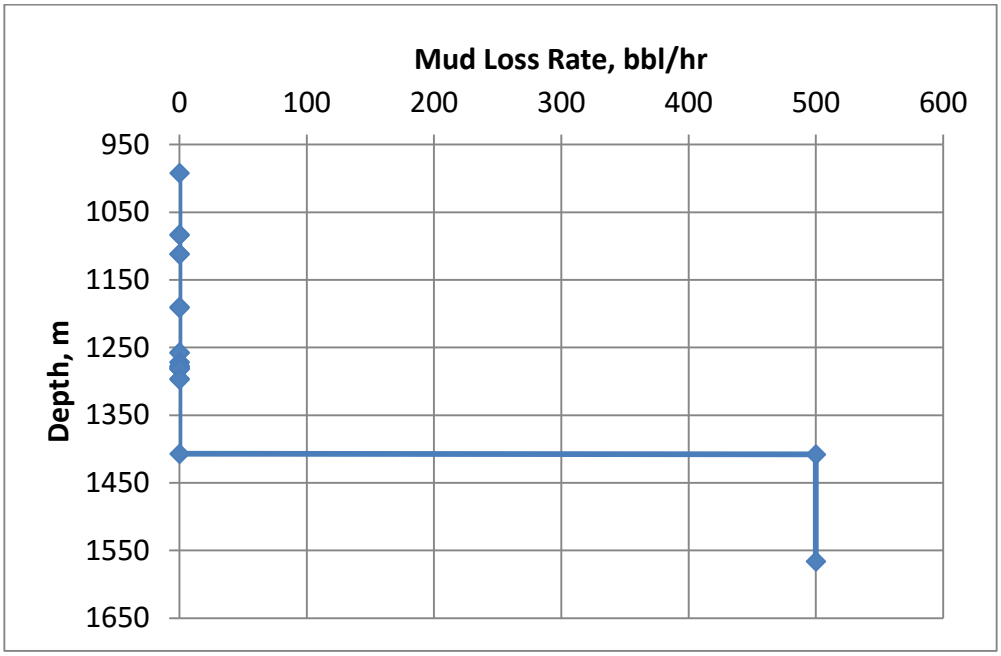

Figure 82 Mud Loss in Well-1

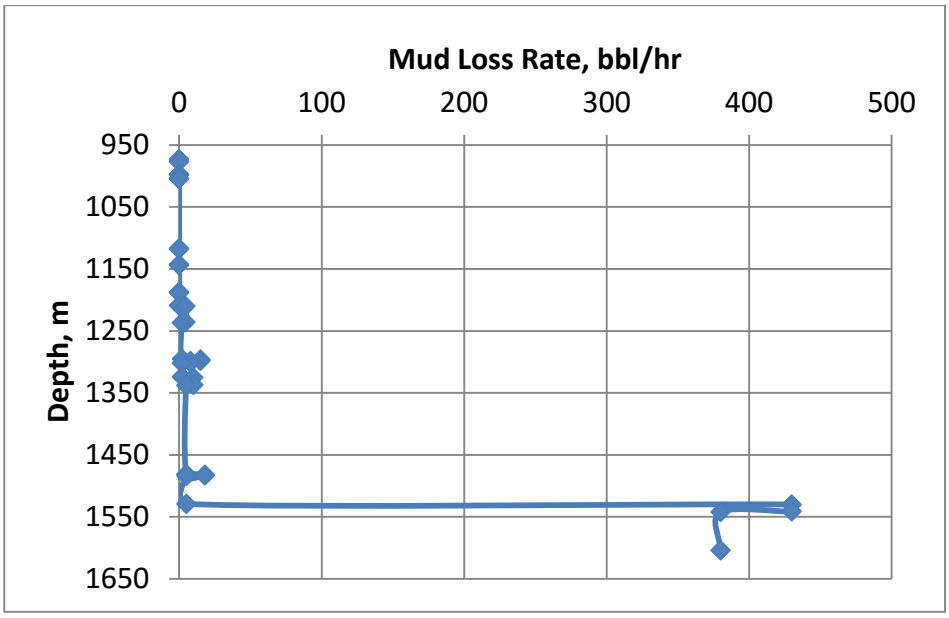

Figure 83 Mud Loss in Well-2

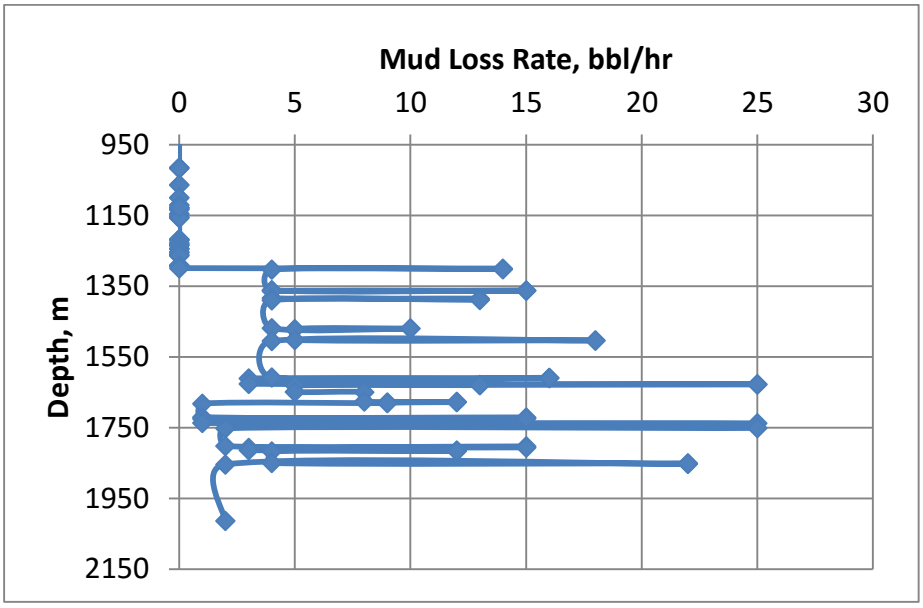

Figure 84 Mud Loss in Well-3

Table 21 Fracture Density for Borehole

Well	Well-1	Well-2	Well-3
Number of Occurrences	1	22	58
Reservoir Top (m)	1300	1200	1300
Reservoir Bottom (m)	1570	1604	2014
Fracture Density (m^{-1})	0,0037	0,0545	0,0812

APPENDIX C

POROSITY ESTIMATIONS

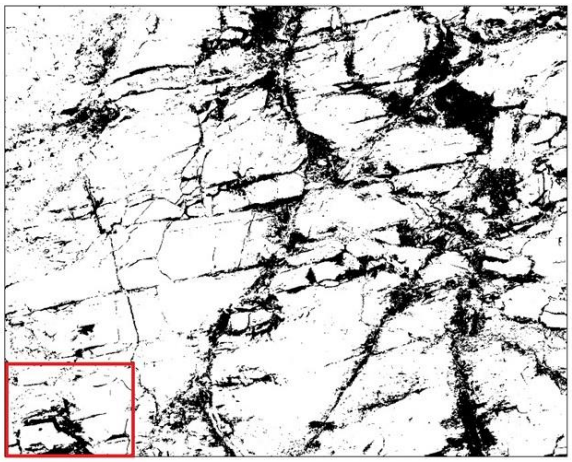

Summary

File Edit Font

Slice	Count	Total Area	Average Size	%Area	Mean	Mode	Perim.	Major	Minor	Angle
120.tif	382	37370.000	97.827	16.925	255	255	26.623	6.124	2.964	49.463

Figure 85 Porosity @Lo for S-1

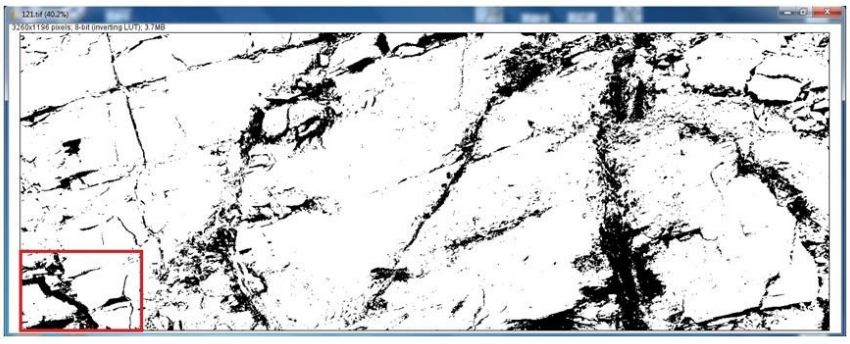

Summary

File Edit Font

Slice	Count	Total Area	Average Size	%Area	Mean	Mode	Perim.	Major	Minor	Angle
121.tif	165	34646.000	209.976	22.513	255	255	38.398	7.564	3.506	35.618

Figure 86 Porosity @Lo for S-2

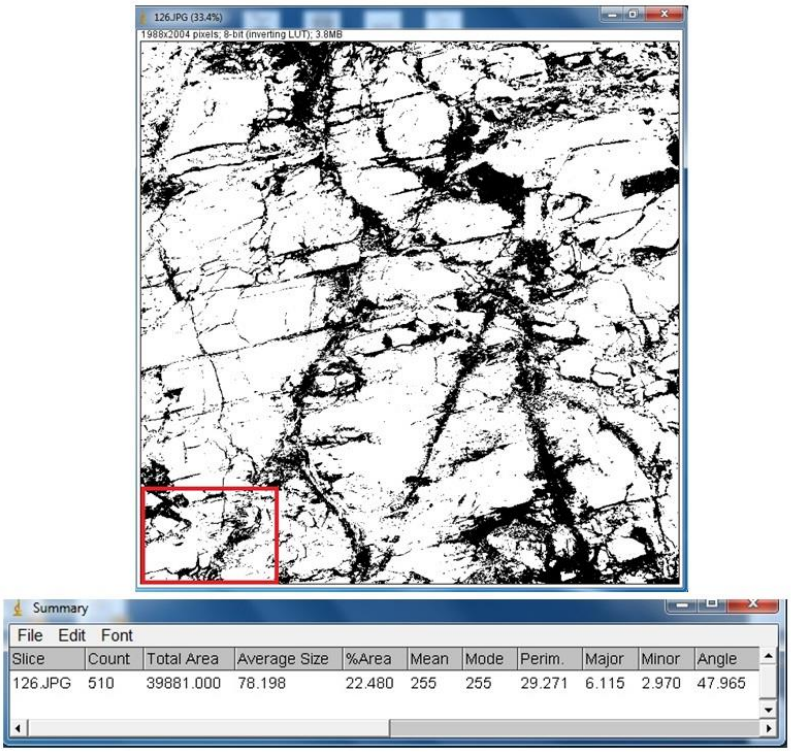

Figure 87 Porosity @Lo for S-3

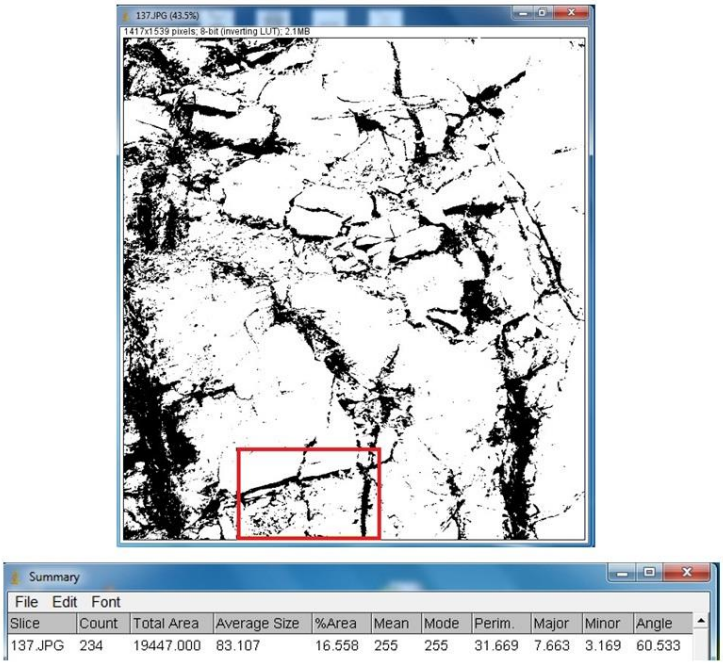

Figure 88 Porosity @Lo for S-4

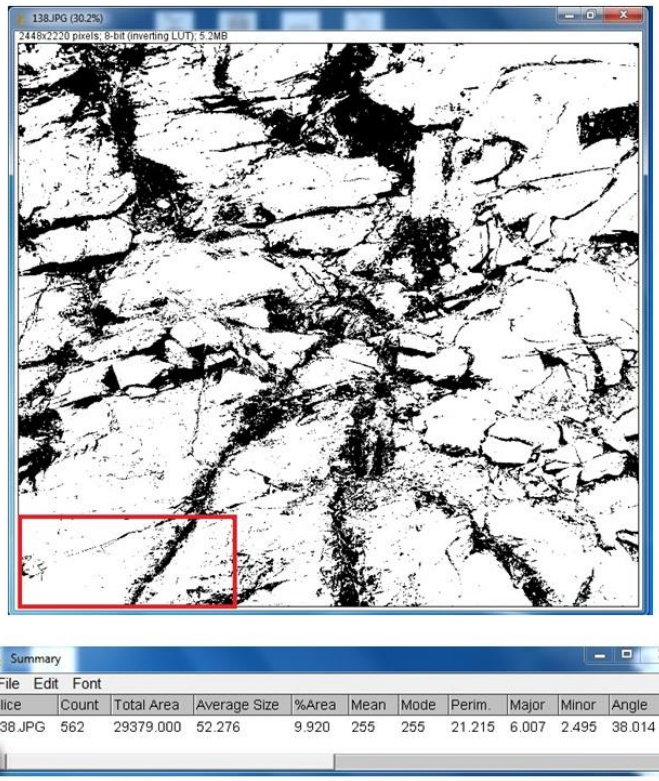

Summary

File Edit Font

Slice	Count	Total Area	Average Size	%Area	Mean	Mode	Perim.	Major	Minor	Angle
138.JPG	562	29379.000	52.276	9.920	255	255	21.215	6.007	2.495	38.014

Figure 89 Porosity @Lo for S-5

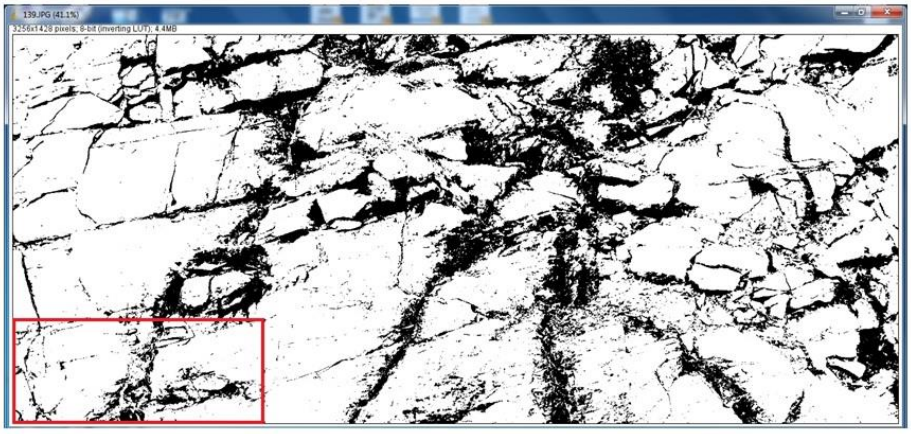

Summary

File Edit Font

Slice	Count	Total Area	Average Size	%Area	Mean	Mode	Perim.	Major	Minor	Angle
139.JPG	658	51193.000	77.801	14.753	255	255	31.814	6.918	3.049	47.903

Figure 90 Porosity @Lo for S-6

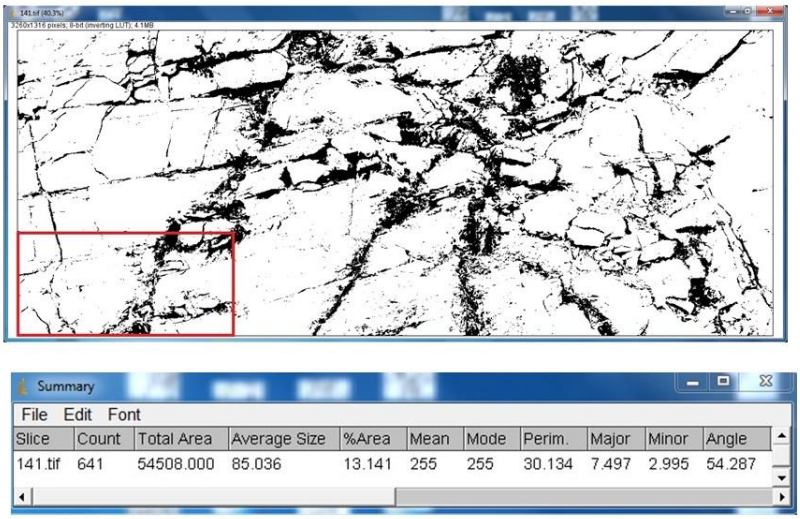

Summary

File Edit Font

Slice	Count	Total Area	Average Size	%Area	Mean	Mode	Perim.	Major	Minor	Angle
141.tif	641	54508.000	85.036	13.141	255	255	30.134	7.497	2.995	54.287

Figure 91 Porosity @Lo for S-7

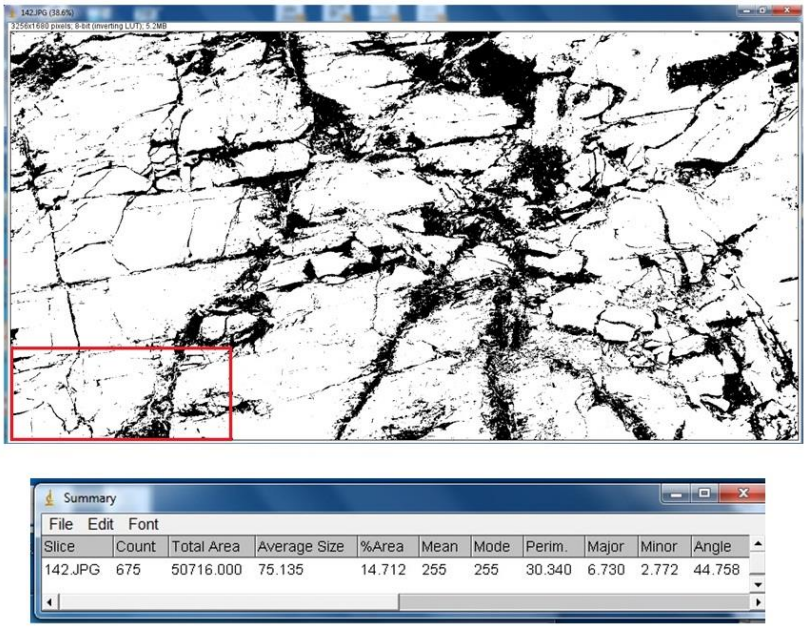

Summary

File Edit Font

Slice	Count	Total Area	Average Size	%Area	Mean	Mode	Perim.	Major	Minor	Angle
142.JPG	675	50716.000	75.135	14.712	255	255	30.340	6.730	2.772	44.758

Figure 92 Porosity @Lo for S-8

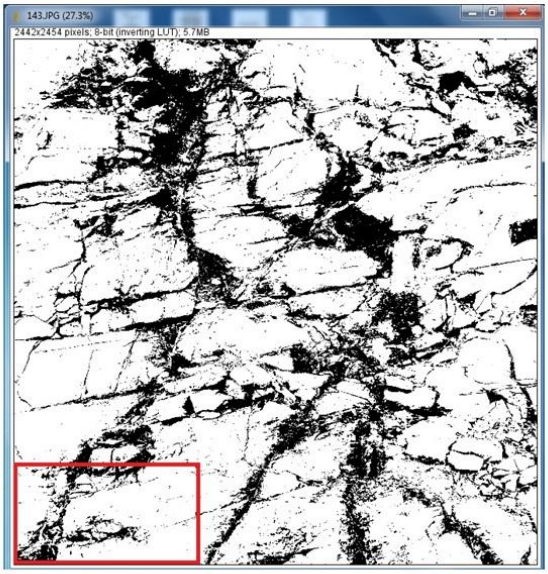

Summary

File Edit Font

Slice	Count	Total Area	Average Size	%Area	Mean	Mode	Perim.	Major	Minor	Angle
143.JPG	608	63109.000	103.798	16.311	255	255	31.157	6.024	2.754	42.715

Figure 93 Porosity @Lo for S-9

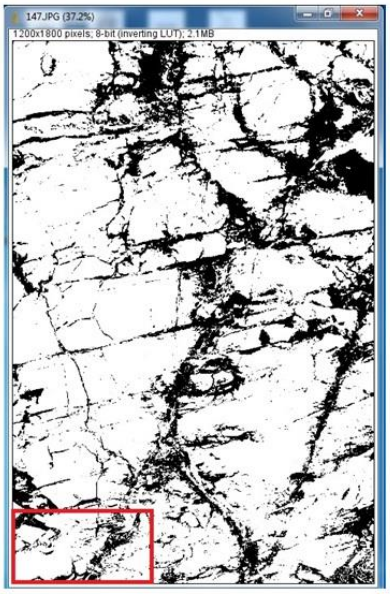

Summary

File Edit Font

Slice	Count	Total Area	Average Size	%Area	Mean	Mode	Perim.	Major	Minor	Angle
147.JPG	324	22721.000	70.127	20.625	255	255	27.884	5.934	2.754	44.271

Figure 94 Porosity @Lo for S-10

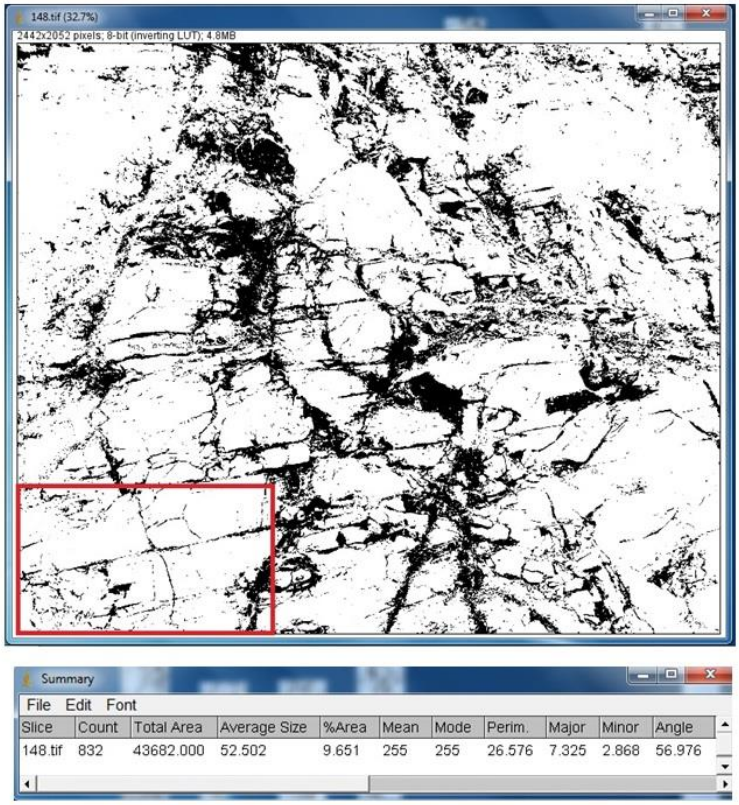

Summary

File Edit Font

Slice	Count	Total Area	Average Size	%Area	Mean	Mode	Perim.	Major	Minor	Angle
148.tif	832	43682.000	52.502	9.651	255	255	26.576	7.325	2.868	56.976

Figure 95 Porosity @Lo for S-11

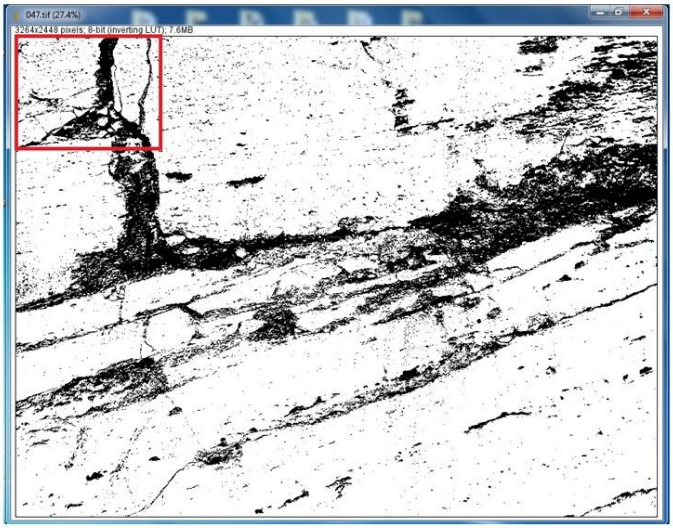

Summary

File Edit Font

Slice	Count	Total Area	Average Size	%Area	Mean	Mode	Perim.	Major	Minor	Angle
047.tif	804	102640.000	127.662	24.044	255	255	25.681	6.036	3.118	66.256

Figure 96 Porosity @Lo for M-1

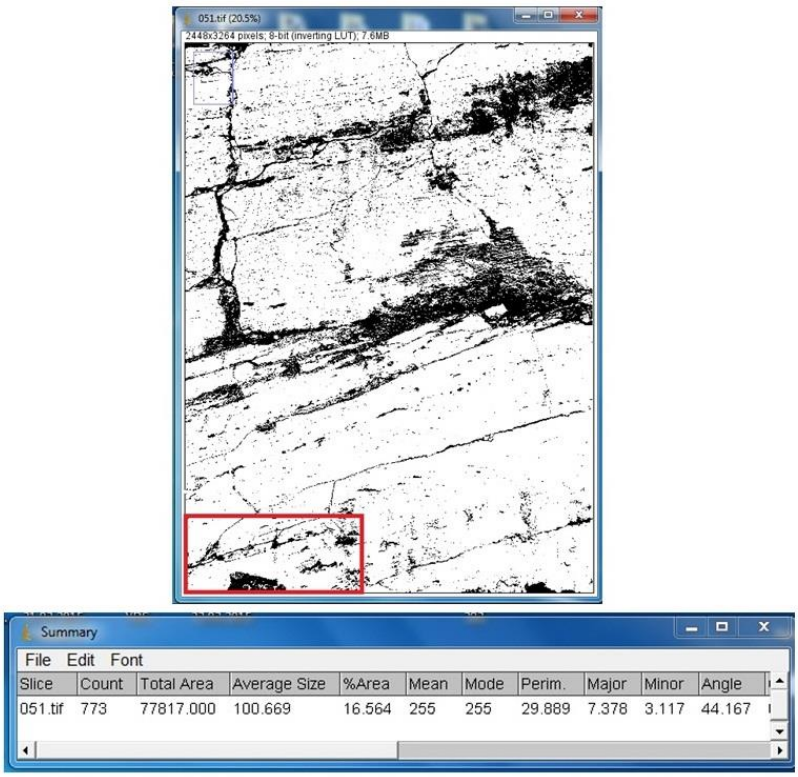

Figure 97 Porosity @Lo for M-2

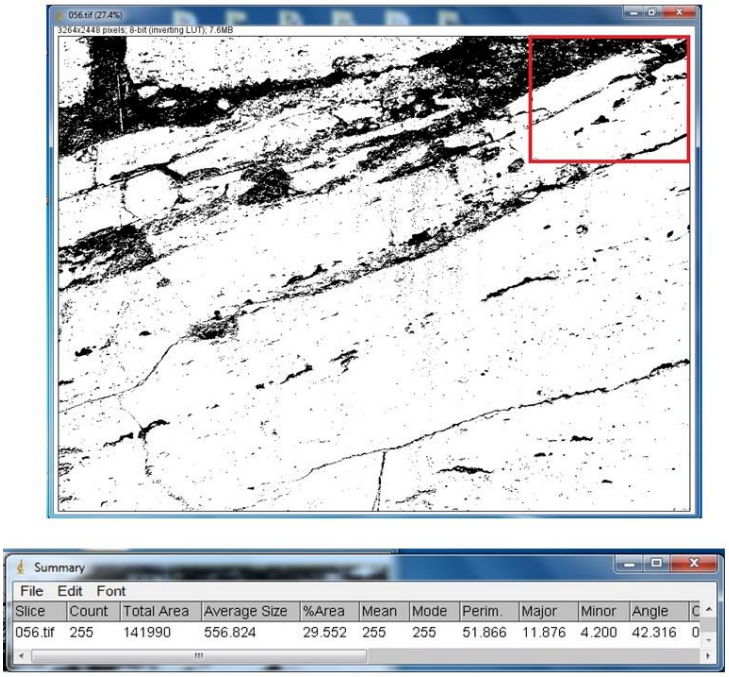

Figure 98 Porosity @Lo for M-3

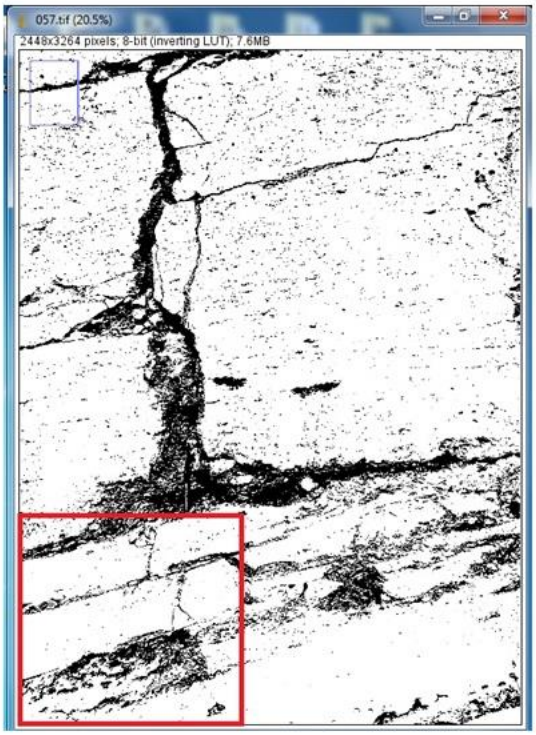

Summary

File Edit Font

Slice	Count	Total Area	Average Size	%Area	Mean	Mode	Perim.	Major	Minor	Angle
057.tif	1908	185131.000	97.029	17.095	255	255	28.350	5.895	2.607	45.527

Figure 99 Porosity @Lo for M-4

APPENDIX D

THICKNESS ESTIMATIONS FROM CUTTING SAMPLE LOGS

D.1 CUTTING SAMPLE LOG FOR X-4

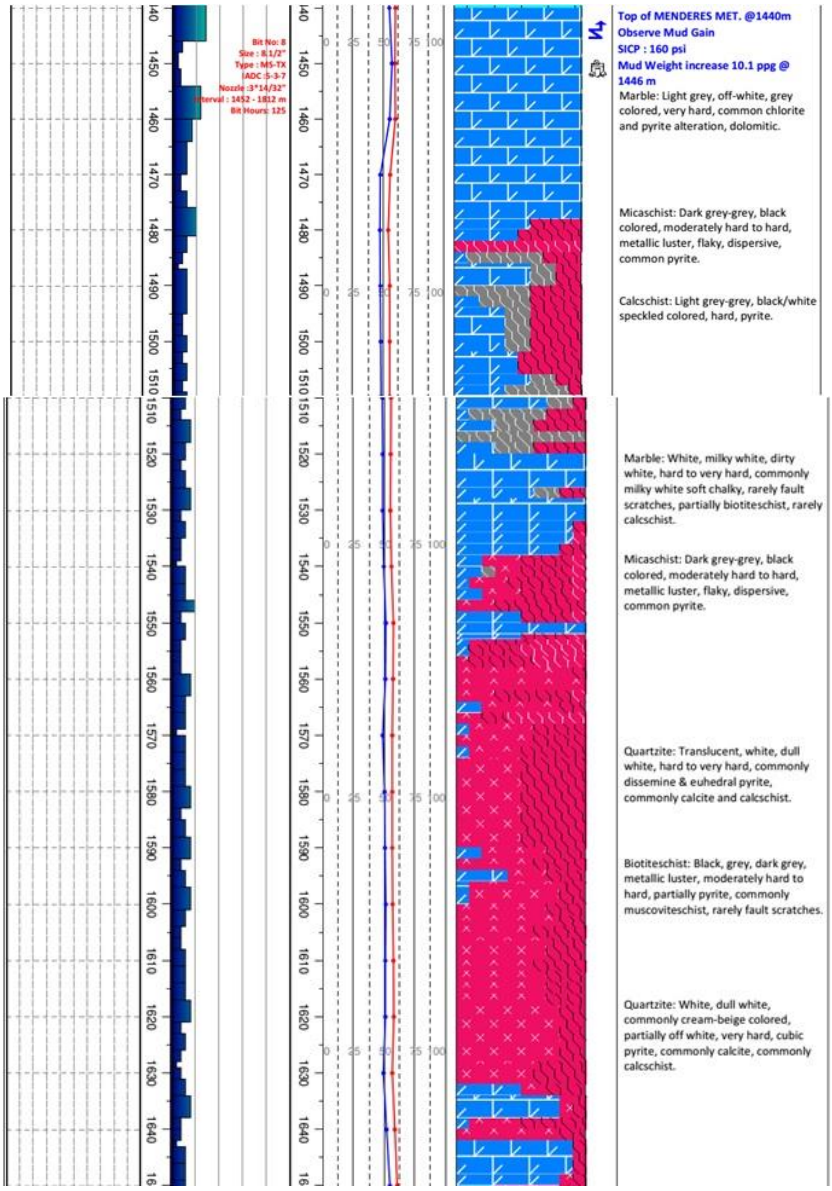

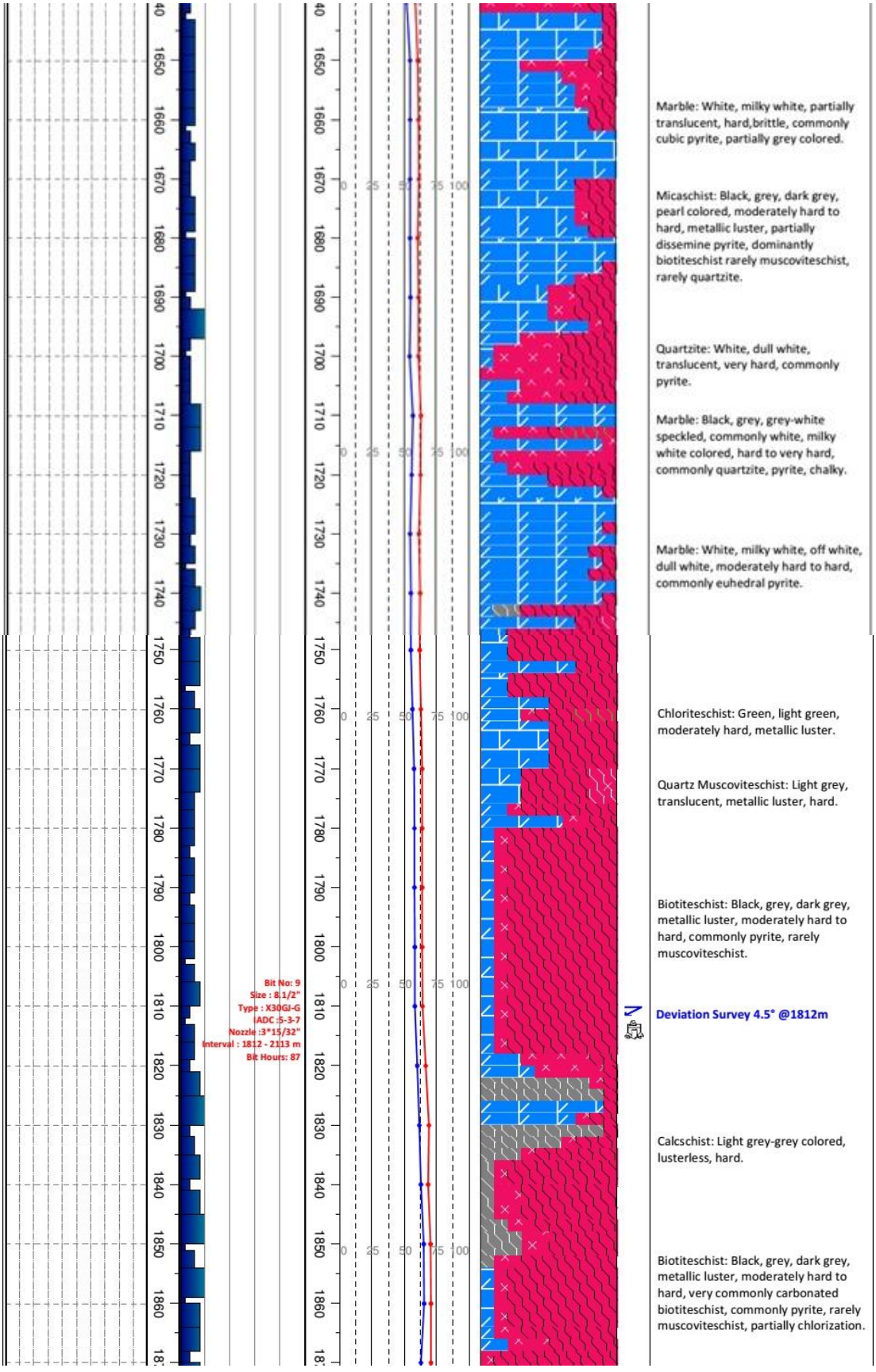
Marble: White, milky white, partially translucent, hard,brittle, commonly cubic pyrite, partially grey colored.
Micaschist: Black, grey, dark grey, pearl colored, moderately hard to hard, metallic luster, partially dissemine pyrite, dominantly biotiteschist rarely muscoviteschist, rarely quartzite.
Quartzite: White, dull white, translucent, very hard, commonly pyrite.
Marble: Black, grey, grey-white speckled, commonly white, milky white colored, hard to very hard, commonly quartzite, pyrite, chalky.
Marble: White, milky white, off white, dull white, moderately hard to hard, commonly euhedral pyrite.
Chloriteschist: Green, light green, moderately hard, metallic luster.
Quartz Muscoviteschist: Light grey, translucent, metallic luster, hard.
Biotiteschist: Black, grey, dark grey, metallic luster, moderately hard to hard, commonly pyrite, rarely muscoviteschist.
Deviation Survey 4.5° @1812m
Calcschist: Light grey-grey colored, lusterless, hard.
Biotiteschist: Black, grey, dark grey, metallic luster, moderately hard to hard, very commonly carbonated biotiteschist, commonly pyrite, rarely muscoviteschist, partially chlorization.
Bit No: 9
Size : 8.1/2"
Type : X30GJ-G
IADC :5-3-7
Nozzle :3*15/32"
Interval : 1812 - 2113 m
Bit Hours: 87
N

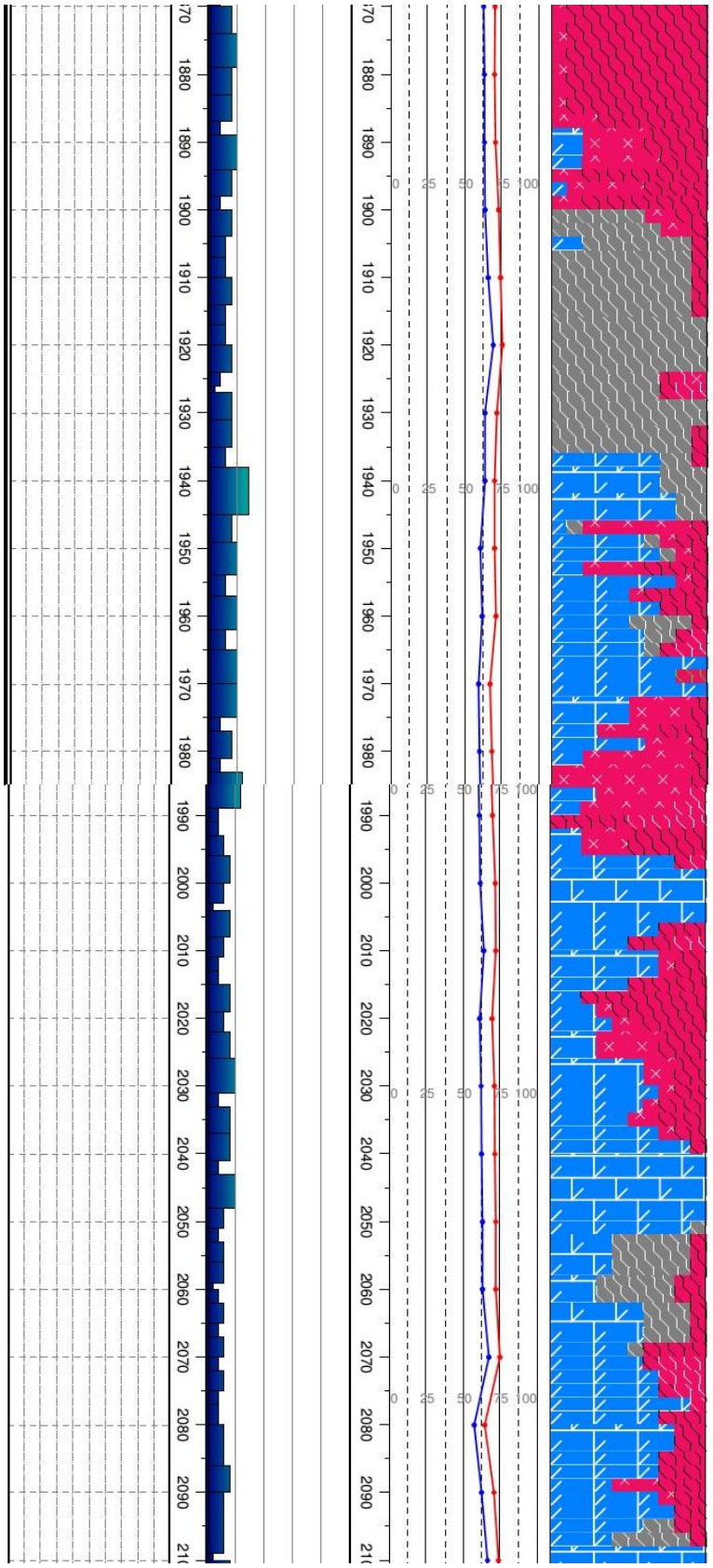
1870 1880 1890 1900 1910 1920 1930 1940 1950 1960 1970 1980 1990 2000 2010 2020 2030 2040 2050 2060 2070 2080 2090
0 25 50 75 100
Calcschist: Light grey-grey, partially grey-white speckled colored, lusterless, moderately hard to hard, nodular pyrite, partially marble.
Marble: White, matt white, moderately hard, sugar texture, pyrite.
Quartzite: White, dull white, translucent, very hard, partially chlorization.
Marble: White, matt white, dull white, partially black-white speckled colored, moderately hard, pyrite, chalky, fault scratches.
Biotiteschist: Black, dark grey colored, metallic luster, moderately hard, very commonly carbonated biotiteschist, pyrite, rarely muscoviteschist, rarely chlorization.
Calcschist: Light grey-grey, partially grey-white speckled colored, lusterless, moderately hard to hard.
Marble: Black-white speckled colored, moderately hard to hard, pyrite, chalky

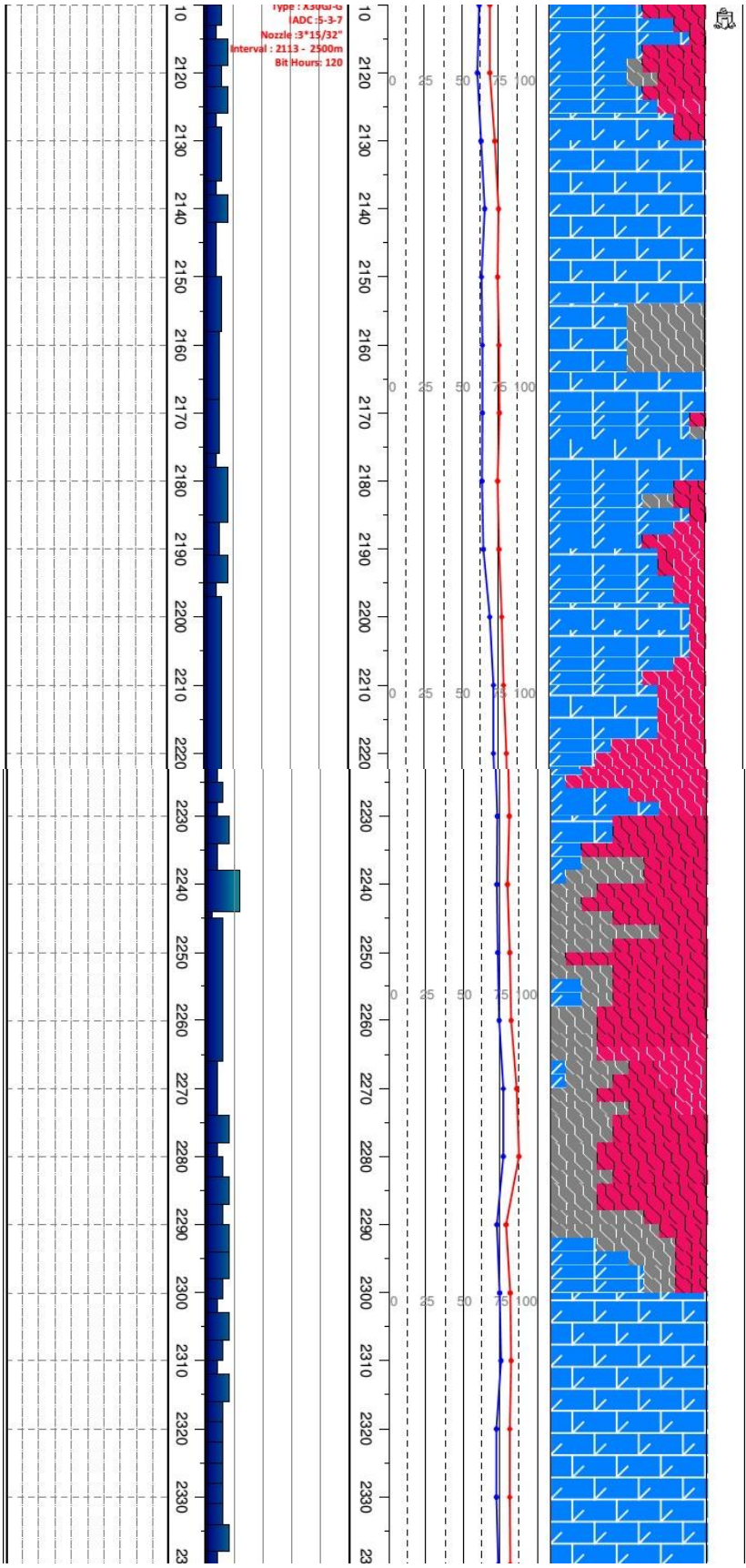

Biotiteschist: Black, dark grey colored, metallic luster, moderately hard, rarely chlorization.
Muscoviteschist: Pearly-cream colored, metallic luster, moderately hard, common pyrite.

Marble: White, moderately hard, pyrite, rarely chalky.

Calcschist: Light grey-grey, moderately hard to hard.

Marble: White-milky white, moderately hard, pyrite, rarely chalky.

Quartz Muscoviteschist: Cream-milky white-white-pearrly colored, hard.

Biotiteschist: Black, dark grey colored, metallic luster, flacky, moderately hard, common pyrite.

Calcschist (Black Marble): Black- dark grey, hard, common pyrite.

Quartz Muscoviteschist: Cream-milky, white-off white-pearly colored, hard.

Biotiteschist: Black-dark grey colored, metallic luster, flacky, moderately hard, common pyrite.

Calcschist : Dark grey-grey colored, hard, common pyrite.

Cooling Tower Breakdown & Repair @2287m

Marble: White-milky white, moderately hard, very common-common fault fillings, partly slickensides, rarely or not pyrite.

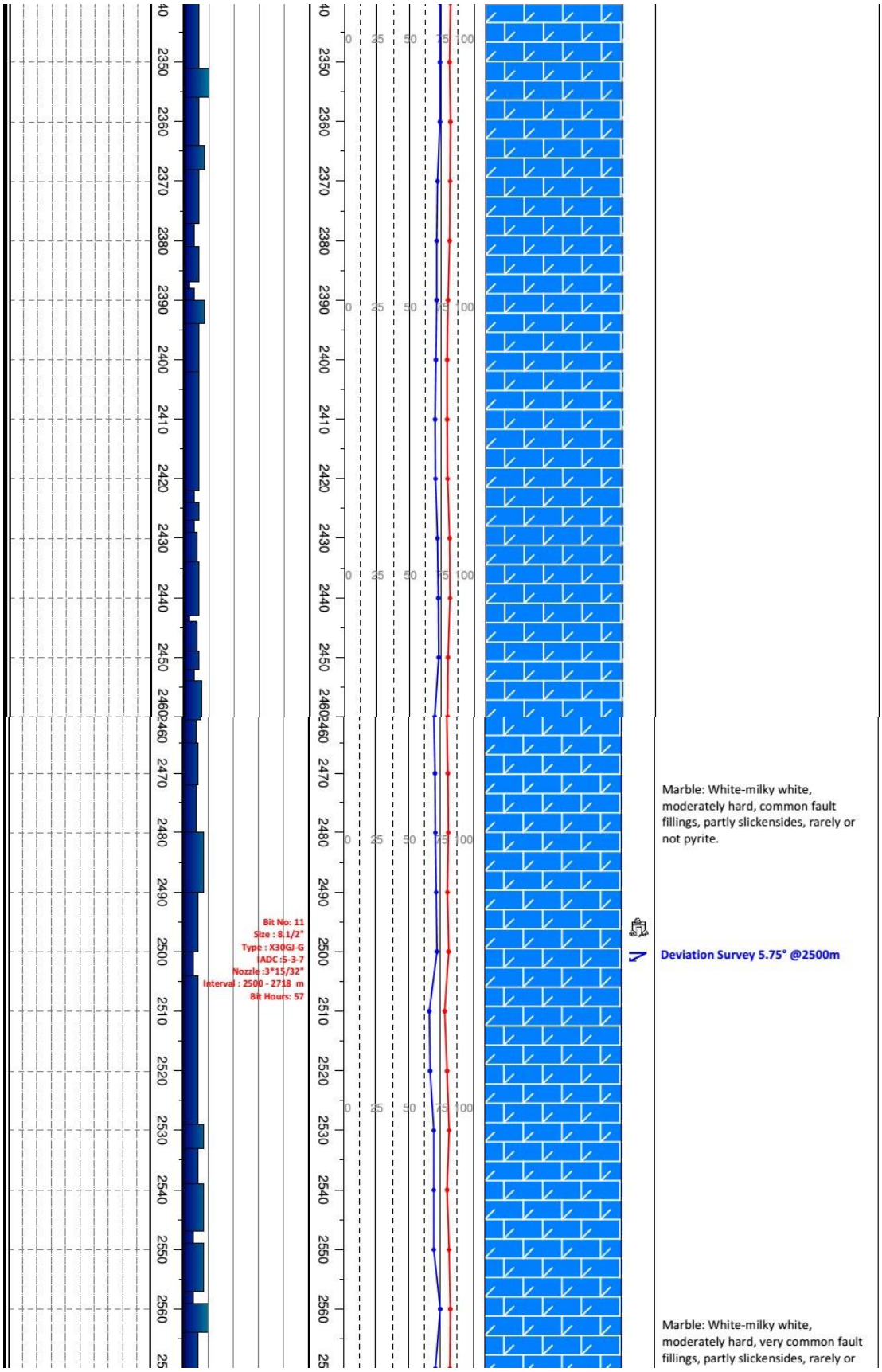
Bit No: 11
Size : 8.1/2"
Type : X30GJ-G
IADC :5-3-7
Nozzle :3*15/32"
Interval : 2500 - 2718 m
Bit Hours: 57
Marble: White-milky white, moderately hard, common fault fillings, partly slickensides, rarely or not pyrite.
Deviation Survey 5.75° @2500m
Marble: White-milky white, moderately hard, very common fault fillings, partly slickensides, rarely or

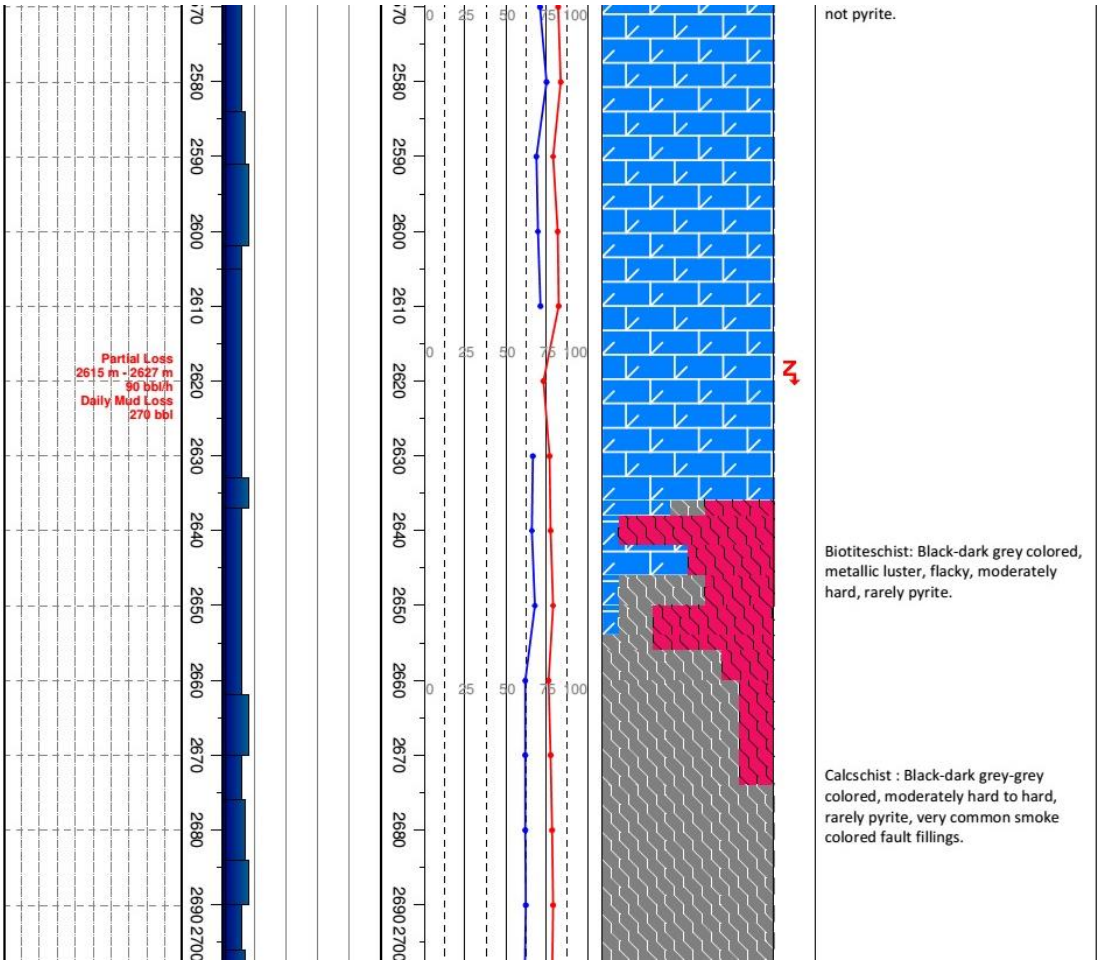

D.2 CUTTING SAMPLE LOG FOR X-5

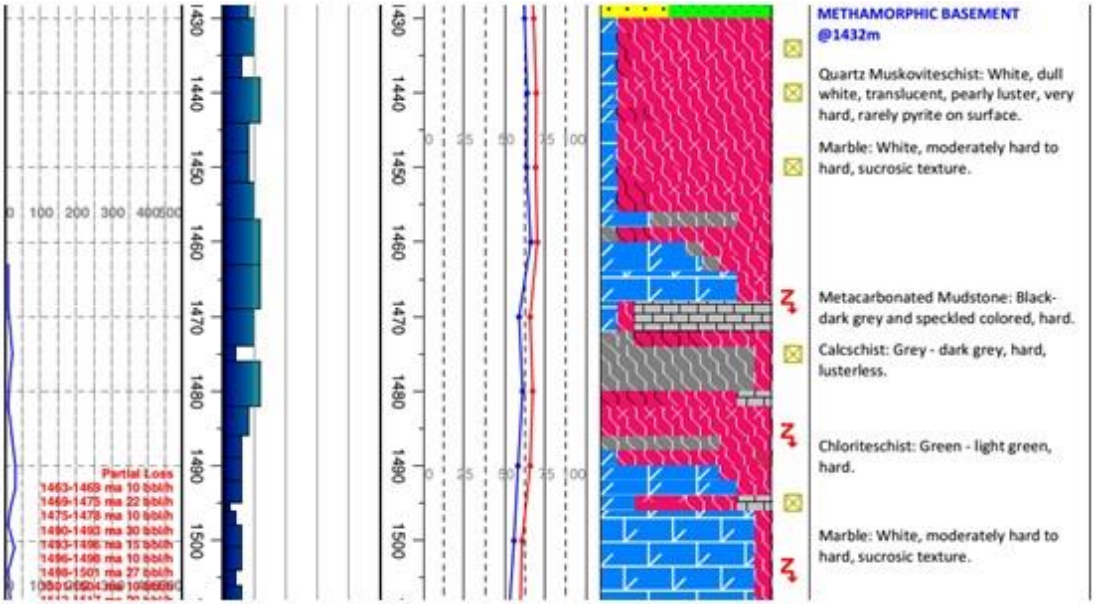

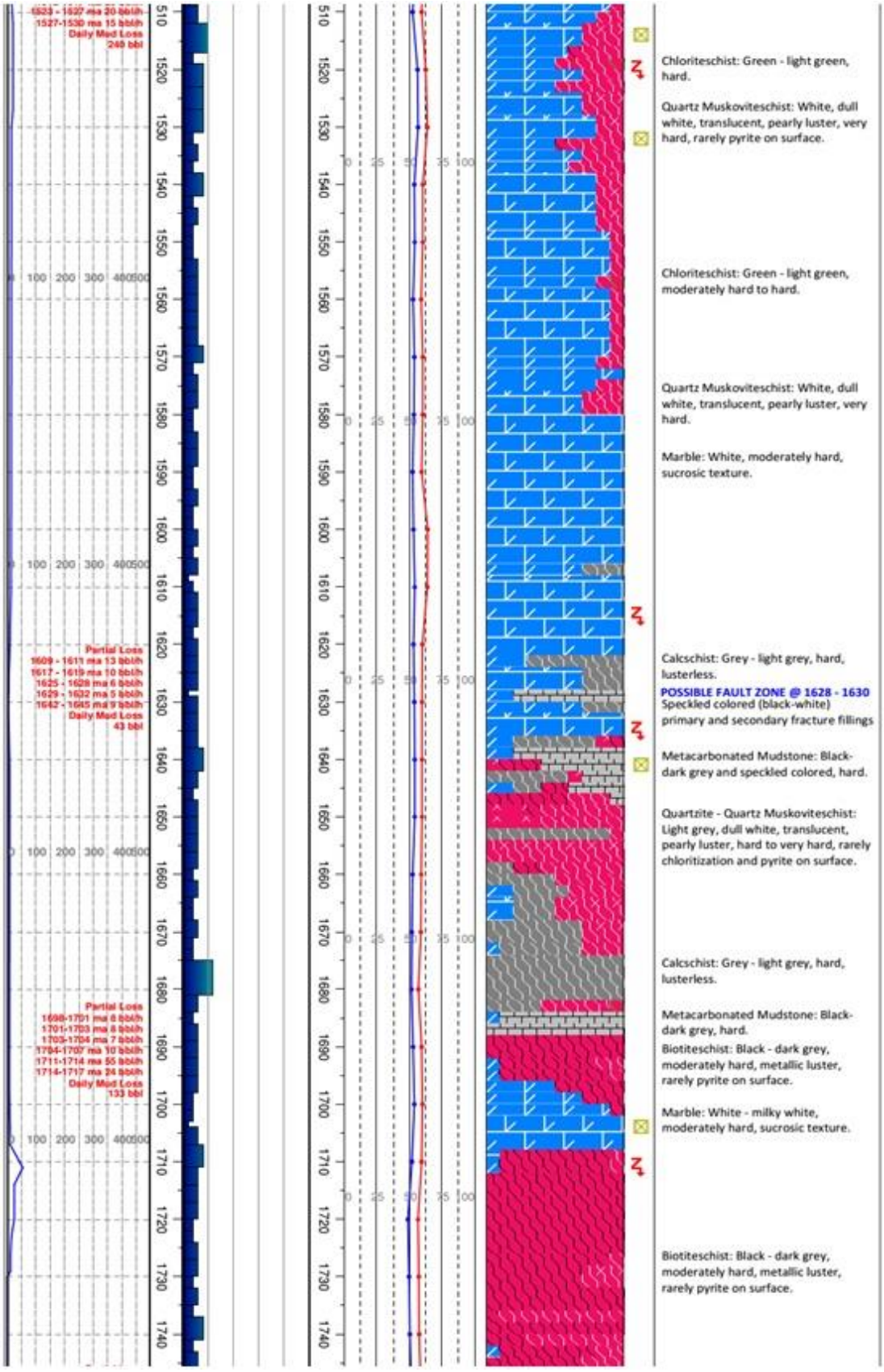
1523 - 1527 ma 20 bbl/h
1527-1530 ma 15 bbl/h
Daily Mud Loss
240 bbl
Partial Loss
1609 - 1611 ma 13 bbl/h
1617 - 1619 ma 10 bbl/h
1625 - 1628 ma 6 bbl/h
1629 - 1632 ma 5 bbl/h
1642 - 1645 md 9 bbl/h
Daily Mud Loss
43 bbl
Partial Loss
1698-1701 md 6 bbl/h
1701-1703 ma 8 bbl/h
1703-1704 ma 7 bbl/h
1704-1707 ma 10 bbl/h
1711-1714 ma 55 bbl/h
1714-1717 ma 24 bbl/h
Daily Mud Loss
133 bbl
Chloriteschist: Green - light green, hard.
Quartz Muskoviteschist: White, dull white, translucent, pearly luster, very hard, rarely pyrite on surface.
Chloriteschist: Green - light green, moderately hard to hard.
Quartz Muskoviteschist: White, dull white, translucent, pearly luster, very hard.
Marble: White, moderately hard, sucrosic texture.
Calcschist: Grey - light grey, hard, lusterless.
POSSIBLE FAULT ZONE @ 1628 - 1630
Speckled colored (black-white) primary and secondary fracture fillings
Metacarbonated Mudstone: Black-dark grey and speckled colored, hard.
Quartzite - Quartz Muskoviteschist: Light grey, dull white, translucent, pearly luster, hard to very hard, rarely chloritization and pyrite on surface.
Calcschist: Grey - light grey, hard, lusterless.
Metacarbonated Mudstone: Black-dark grey, hard.
Biotiteschist: Black - dark grey, moderately hard, metallic luster, rarely pyrite on surface.
Marble: White - milky white, moderately hard, sucrosic texture.
Biotiteschist: Black - dark grey, moderately hard, metallic luster, rarely pyrite on surface.

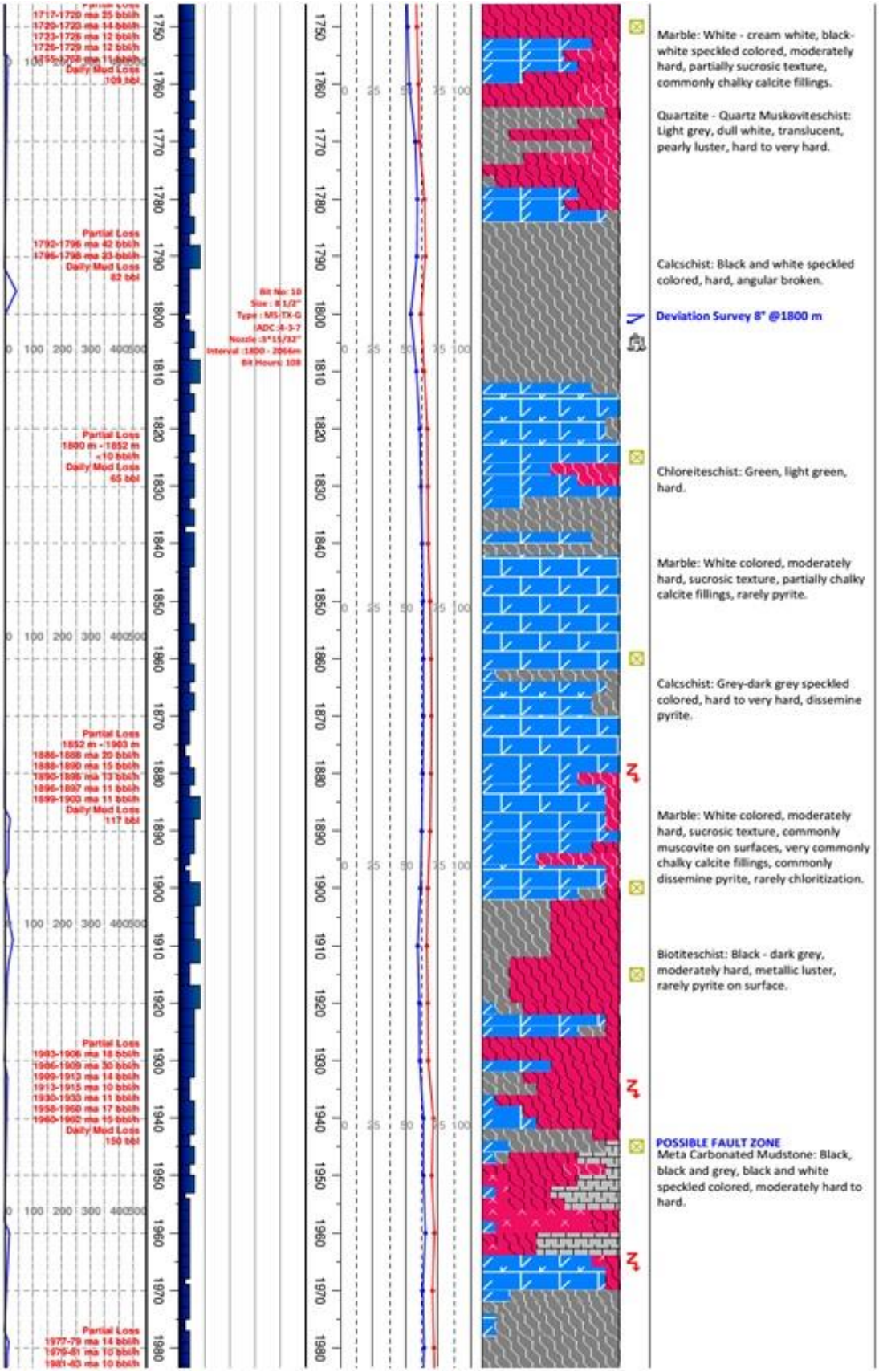
1717-1720 ma 25 bbl/h
1720-1723 ma 14 bbl/h
1723-1726 ma 12 bbl/h
1726-1729 ma 12 bbl/h
Daily Mud Loss
109 bbl
Partial Loss
1792-1796 ma 42 bbl/h
1796-1798 ma 23 bbl/h
Daily Mud Loss
82 bbl
Bit No: 10
Size : 8 1/2"
Type : MS-TX-G
IADC :8-3-7
Nozzle :3*15/32"
Interval :1800 - 2066m
Bit Hours: 108
Partial Loss
1800 m - 1852 m
~10 bbl/h
Daily Mud Loss
65 bbl
Partial Loss
1852 m - 1903 m
1886-1888 ma 20 bbl/h
1888-1890 ma 15 bbl/h
1890-1896 ma 13 bbl/h
1896-1897 ma 11 bbl/h
1899-1900 ma 11 bbl/h
Daily Mud Loss
117 bbl
Partial Loss
1903-1906 ma 18 bbl/h
1906-1909 ma 30 bbl/h
1909-1913 ma 14 bbl/h
1913-1915 ma 10 bbl/h
1930-1933 ma 11 bbl/h
1958-1960 ma 17 bbl/h
1960-1962 ma 15 bbl/h
Daily Mud Loss
150 bbl
Partial Loss
1977-79 ma 14 bbl/h
1979-81 ma 10 bbl/h
1981-83 ma 10 bbl/h
Marble: White - cream white, black-white speckled colored, moderately hard, partially sucrosic texture, commonly chalky calcite fillings.
Quartzite - Quartz Muskoviteschist: Light grey, dull white, translucent, pearly luster, hard to very hard.
Calcschist: Black and white speckled colored, hard, angular broken.
Deviation Survey 8° @1800 m
Chloreiteschist: Green, light green, hard.
Marble: White colored, moderately hard, sucrosic texture, partially chalky calcite fillings, rarely pyrite.
Calcschist: Grey-dark grey speckled colored, hard to very hard, dissemine pyrite.
Marble: White colored, moderately hard, sucrosic texture, commonly muscovite on surfaces, very commonly chalky calcite fillings, commonly dissemine pyrite, rarely chloritization.
Biotiteschist: Black - dark grey, moderately hard, metallic luster, rarely pyrite on surface.
POSSIBLE FAULT ZONE
Meta Carbonated Mudstone: Black, black and grey, black and white speckled colored, moderately hard to hard.

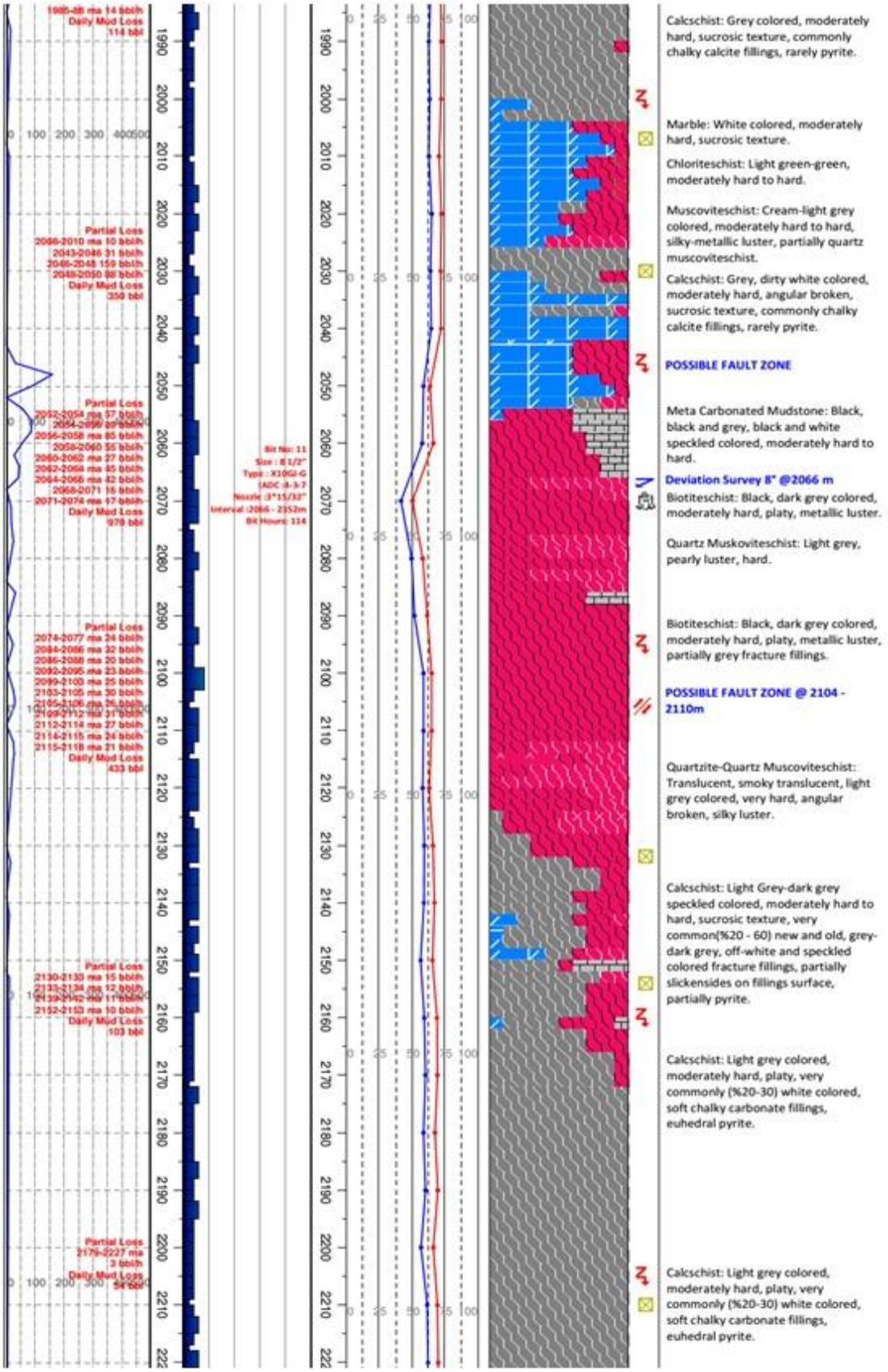
1985-88 ma 14 bbl/h
Daily Mud Loss
114 bbl
Partial Loss
2008-2010 ma 10 bbl/h
2043-2046 31 bbl/h
2046-2048 159 bbl/h
2048-2050 88 bbl/h
Daily Mud Loss
359 bbl
Partial Loss
2052-2054 ma 57 bbl/h
2054-2056 ma 65 bbl/h
2056-2058 ma 65 bbl/h
2058-2060 55 bbl/h
2060-2062 ma 27 bbl/h
2062-2064 ma 45 bbl/h
2064-2066 ma 42 bbl/h
2068-2071 16 bbl/h
2071-2074 ma 47 bbl/h
Daily Mud Loss
970 bbl
Partial Loss
2074-2077 ma 24 bbl/h
2084-2086 ma 32 bbl/h
2086-2088 ma 20 bbl/h
2092-2095 ma 23 bbl/h
2099-2103 ma 25 bbl/h
2103-2105 ma 30 bbl/h
2105-2106 ma 26 bbl/h
2109-2112 ma 31 bbl/h
2112-2114 ma 27 bbl/h
2114-2115 ma 24 bbl/h
2115-2118 ma 21 bbl/h
Daily Mud Loss
433 bbl
Partial Loss
2130-2133 ma 15 bbl/h
2133-2134 ma 12 bbl/h
2139-2142 ma 11 bbl/h
2152-2153 ma 10 bbl/h
Daily Mud Loss
103 bbl
Partial Loss
2179-2227 ma
3 bbl/h
Daily Mud Loss
Bit No: 11
Size : 8 1/2"
Type : X10GJ-G
IADC :8-3-7
Nozzle :3*15/32"
Interval :2066 - 2352m
Bit Hours: 114
Calcschist: Grey colored, moderately hard, sucrosic texture, commonly chalky calcite fillings, rarely pyrite.
Marble: White colored, moderately hard, sucrosic texture.
Chloriteschist: Light green-green, moderately hard to hard.
Muscoviteschist: Cream-light grey colored, moderately hard to hard, silky-metallic luster, partially quartz muscoviteschist.
Calcschist: Grey, dirty white colored, moderately hard, angular broken, sucrosic texture, commonly chalky calcite fillings, rarely pyrite.
POSSIBLE FAULT ZONE
Meta Carbonated Mudstone: Black, black and grey, black and white speckled colored, moderately hard to hard.
Deviation Survey 8° @2066 m
Biotiteschist: Black, dark grey colored, moderately hard, platy, metallic luster.
Quartz Muskoviteschist: Light grey, pearly luster, hard.
Biotiteschist: Black, dark grey colored, moderately hard, platy, metallic luster, partially grey fracture fillings.
POSSIBLE FAULT ZONE @ 2104 - 2110m
Quartzite-Quartz Muscoviteschist: Translucent, smoky translucent, light grey colored, very hard, angular broken, silky luster.
Calcschist: Light Grey-dark grey speckled colored, moderately hard to hard, sucrosic texture, very common(%20 - 60) new and old, grey-dark grey, off-white and speckled colored fracture fillings, partially slickensides on fillings surface, partially pyrite.
Calcschist: Light grey colored, moderately hard, platy, very commonly (%20-30) white colored, soft chalky carbonate fillings, euhedral pyrite.
Calcschist: Light grey colored, moderately hard, platy, very commonly (%20-30) white colored, soft chalky carbonate fillings, euhedral pyrite.

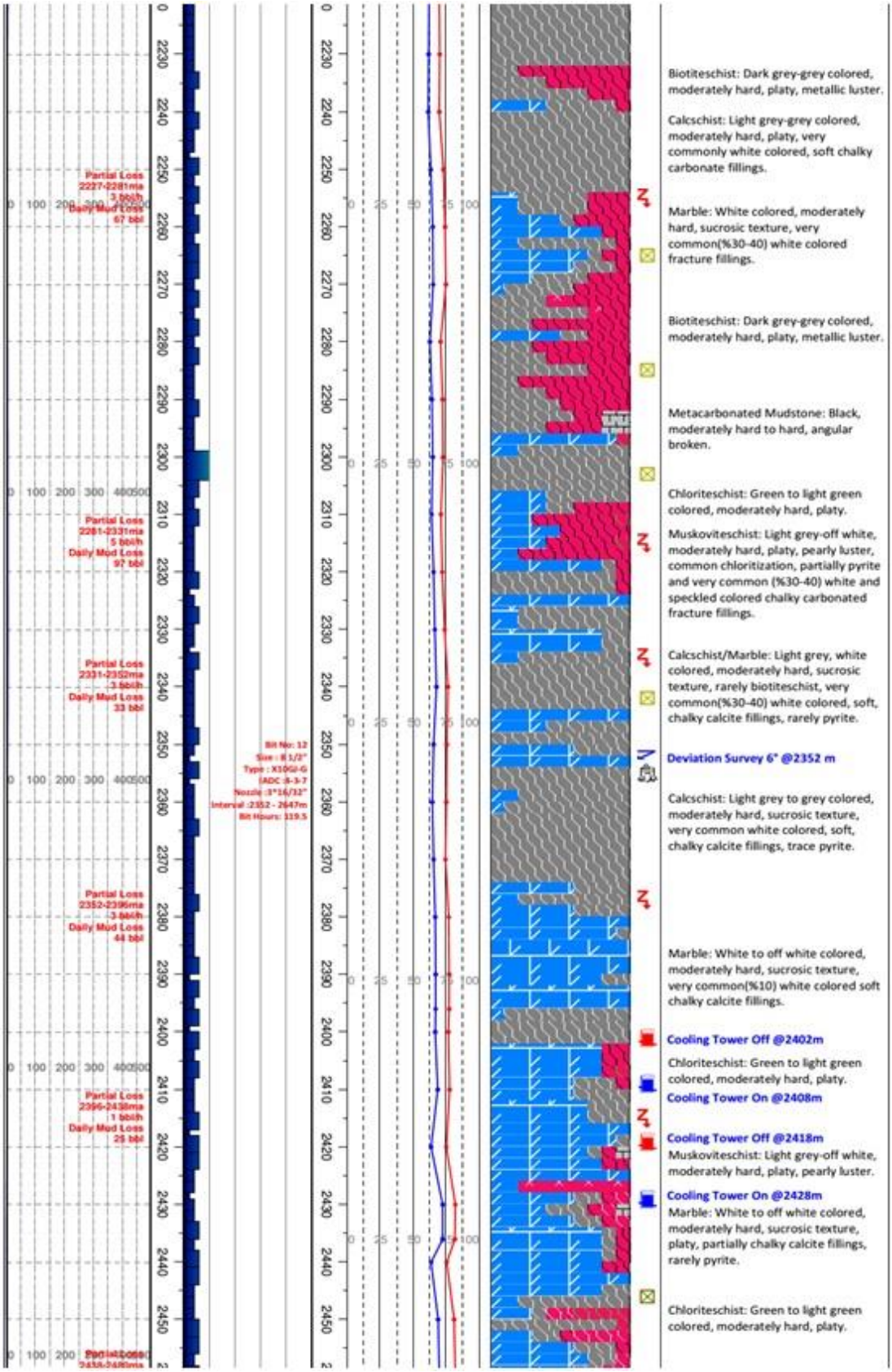
Partial Loss
2227-2281ma
3 bbl/h
Daily Mud Loss
67 bbl
Partial Loss
2281-2331ma
5 bbl/h
Daily Mud Loss
97 bbl
Partial Loss
2331-2352ma
3 bbl/h
Daily Mud Loss
33 bbl
Bit No: 12
Size : 8 1/2"
Type : X10GI-G
IADC :4-3-7
Nozzle :3*16/32"
Interval :2352 - 2647m
Bit Hours: 119.5
Partial Loss
2352-2396ma
3 bbl/h
Daily Mud Loss
44 bbl
Partial Loss
2396-2438ma
1 bbl/h
Daily Mud Loss
25 bbl
Biotiteschist: Dark grey-grey colored, moderately hard, platy, metallic luster.
Calcschist: Light grey-grey colored, moderately hard, platy, very commonly white colored, soft chalky carbonate fillings.
Marble: White colored, moderately hard, sucrosic texture, very common(%30-40) white colored fracture fillings.
Biotiteschist: Dark grey-grey colored, moderately hard, platy, metallic luster.
Metacarbonated Mudstone: Black, moderately hard to hard, angular broken.
Chloriteschist: Green to light green colored, moderately hard, platy.
Muskoviteschist: Light grey-off white, moderately hard, platy, pearly luster, common chloritization, partially pyrite and very common (%30-40) white and speckled colored chalky carbonated fracture fillings.
Calcschist/Marble: Light grey, white colored, moderately hard, sucrosic texture, rarely biotiteschist, very common(%30-40) white colored, soft, chalky calcite fillings, rarely pyrite.
Deviation Survey 6° @2352 m
Calcschist: Light grey to grey colored, moderately hard, sucrosic texture, very common white colored, soft, chalky calcite fillings, trace pyrite.
Marble: White to off white colored, moderately hard, sucrosic texture, very common(%10) white colored soft chalky calcite fillings.
Cooling Tower Off @2402m
Chloriteschist: Green to light green colored, moderately hard, platy.
Cooling Tower On @2408m
Cooling Tower Off @2418m
Muskoviteschist: Light grey-off white, moderately hard, platy, pearly luster.
Cooling Tower On @2428m
Marble: White to off white colored, moderately hard, sucrosic texture, platy, partially chalky calcite fillings, rarely pyrite.
Chloriteschist: Green to light green colored, moderately hard, platy.

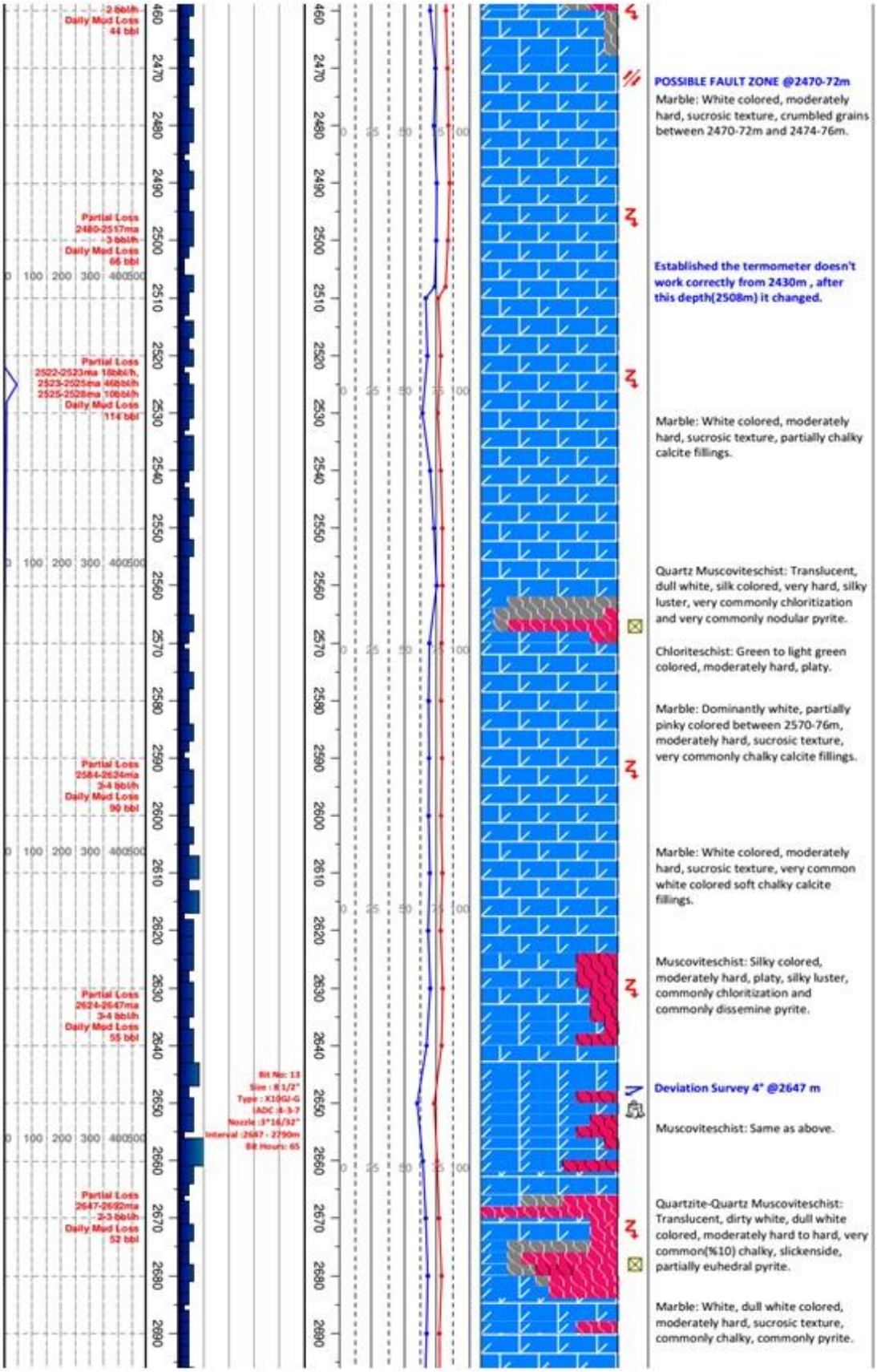
2 bbl/h
Daily Mud Loss
44 bbl
Partial Loss
2480-2517ma
+3 bbl/h
Daily Mud Loss
66 bbl
Partial Loss
2522-2523ma 18bbl/h,
2523-2525ma 46bbl/h
2525-2528ma 10bbl/h
Daily Mud Loss
114 bbl
Partial Loss
2584-2624ma
3-4 bbl/h
Daily Mud Loss
90 bbl
Partial Loss
2624-2647ma
3-4 bbl/h
Daily Mud Loss
55 bbl
Bit No: 13
Size : 8 1/2"
Type : K10GJ-G
IADC :8-3-7
Nozzle :3*16/32"
Interval :2647 - 2790m
Bit Hours: 65
Partial Loss
2647-2692ma
2-3 bbl/h
Daily Mud Loss
52 bbl
POSSIBLE FAULT ZONE @2470-72m
Marble: White colored, moderately hard, sucrosic texture, crumbled grains between 2470-72m and 2474-76m.
Established the termometer doesn't work correctly from 2430m , after this depth(2508m) it changed.
Marble: White colored, moderately hard, sucrosic texture, partially chalky calcite fillings.
Quartz Muscoviteschist: Translucent, dull white, silk colored, very hard, silky luster, very commonly chloritization and very commonly nodular pyrite.
Chloriteschist: Green to light green colored, moderately hard, platy.
Marble: Dominantly white, partially pinky colored between 2570-76m, moderately hard, sucrosic texture, very commonly chalky calcite fillings.
Marble: White colored, moderately hard, sucrosic texture, very common white colored soft chalky calcite fillings.
Muscoviteschist: Silky colored, moderately hard, platy, silky luster, commonly chloritization and commonly dissemine pyrite.
Deviation Survey 4° @2647 m
Muscoviteschist: Same as above.
Quartzite-Quartz Muscoviteschist: Translucent, dirty white, dull white colored, moderately hard to hard, very common(%10) chalky, slickenside, partially euhedral pyrite.
Marble: White, dull white colored, moderately hard, sucrosic texture, commonly chalky, commonly pyrite.

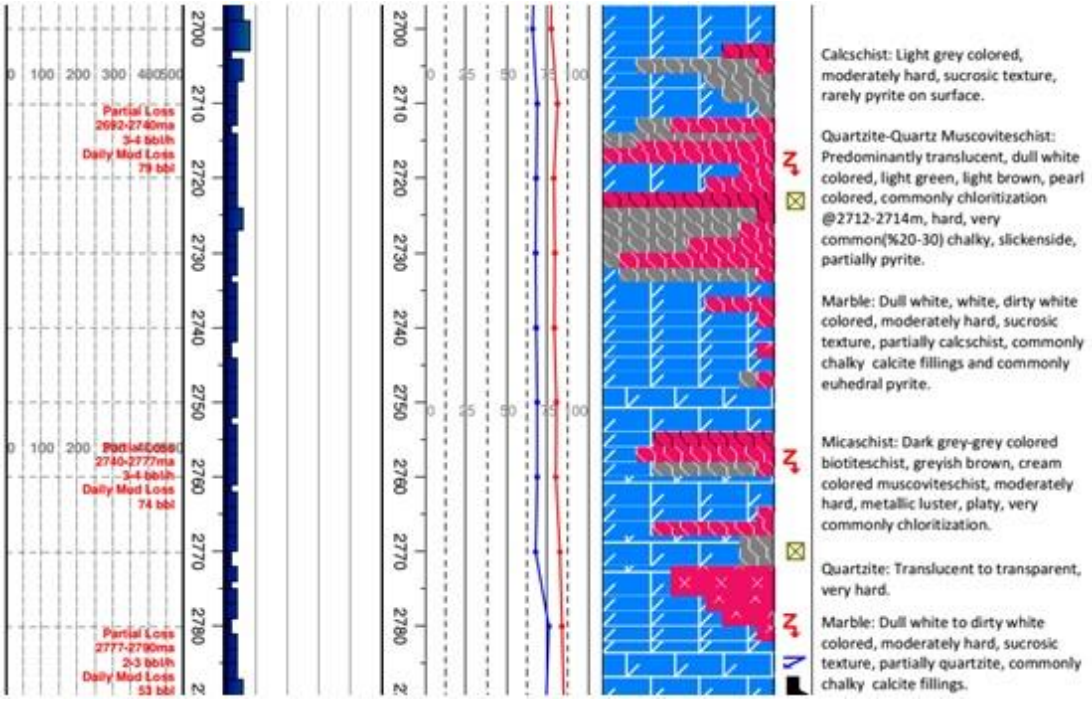

D.3 CUTTING SAMPLE LOG FOR X-7

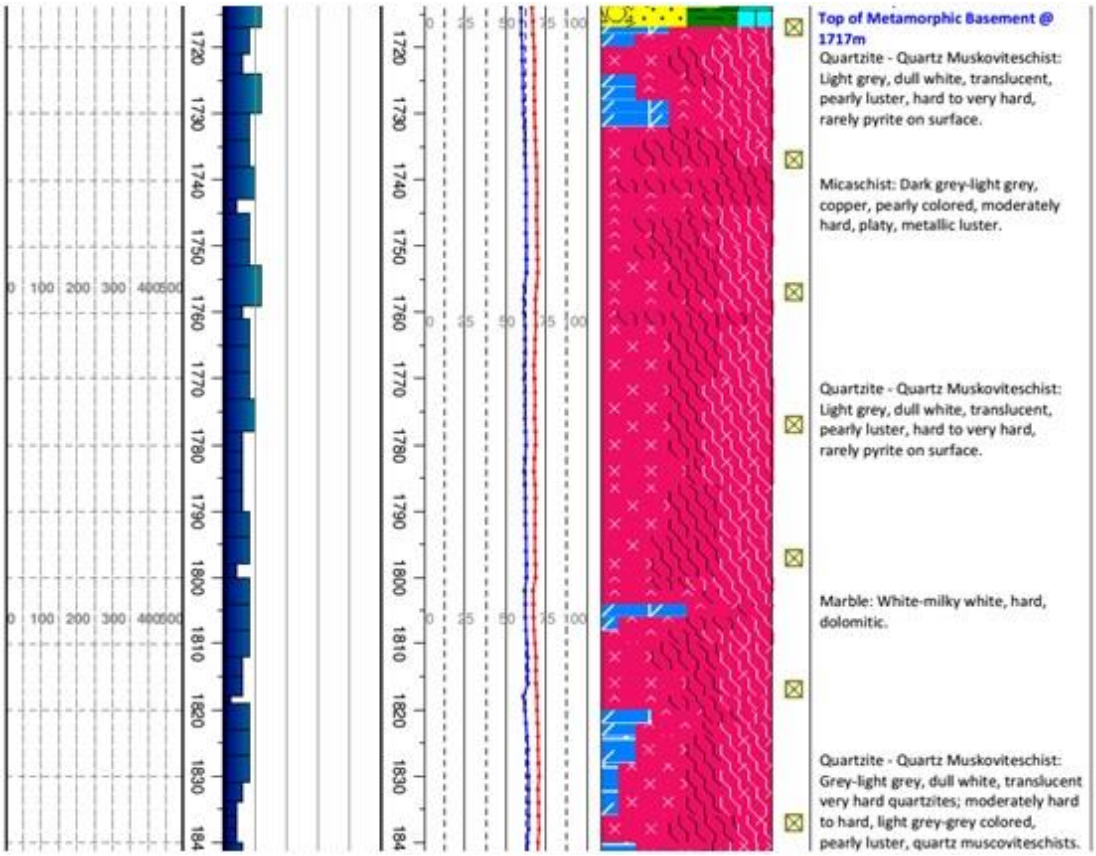

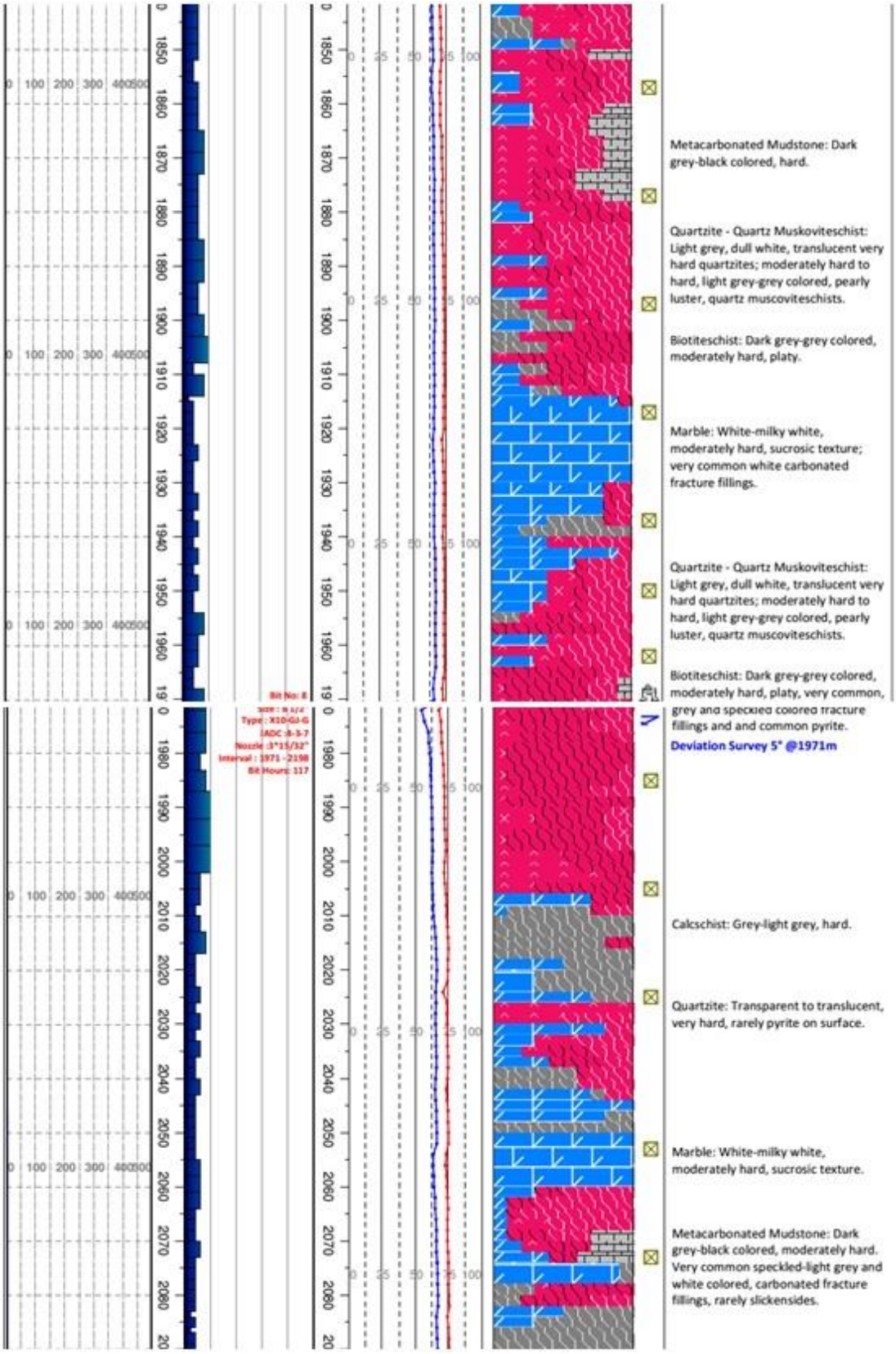
Bit No: 8
Type : X10-GJ-G
IADC :8-3-7
Nozzle :3*15/32"
Interval : 1971 - 2198
Bit Hours: 117
Metacarbonated Mudstone: Dark grey-black colored, hard.
Quartzite - Quartz Muskoviteschist: Light grey, dull white, translucent very hard quartzites; moderately hard to hard, light grey-grey colored, pearly luster, quartz muscoviteschists.
Biotiteschist: Dark grey-grey colored, moderately hard, platy.
Marble: White-milky white, moderately hard, sucrosic texture; very common white carbonated fracture fillings.
Quartzite - Quartz Muskoviteschist: Light grey, dull white, translucent very hard quartzites; moderately hard to hard, light grey-grey colored, pearly luster, quartz muscoviteschists.
Biotiteschist: Dark grey-grey colored, moderately hard, platy, very common, grey and speckled colored fracture fillings and and common pyrite.
Deviation Survey 5° @1971m
Calcschist: Grey-light grey, hard.
Quartzite: Transparent to translucent, very hard, rarely pyrite on surface.
Marble: White-milky white, moderately hard, sucrosic texture.
Metacarbonated Mudstone: Dark grey-black colored, moderately hard. Very common speckled-light grey and white colored, carbonated fracture fillings, rarely slickensides.

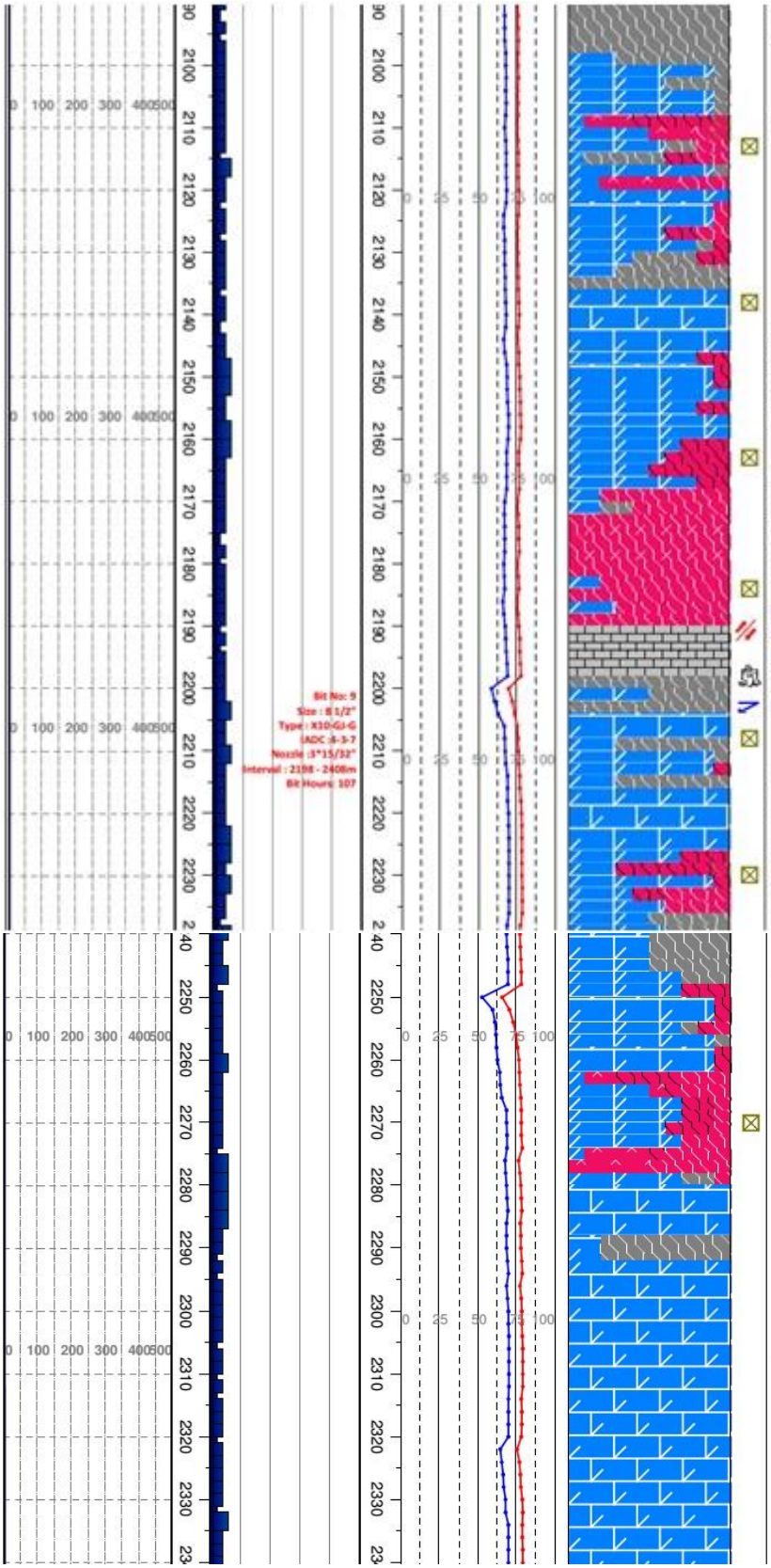

Calcschist: Grey-light grey colored, hard, partially chalky calcite fillings.

Chloriteschist: Green-light green, moderately hard.

Marble: Off white-cream-light grey colored, moderately hard, sucrosic texture. Very common (%40-50) white-cream colored, carbonated fracture fillings, pyrite and slickensides on surface, rarely chloritization.

Quartzite - Quartz Muskoviteschist: Dull white, translucent very hard quartzites; light grey-grey colored, moderately hard to hard, pearly luster quartz muscoviteschists, partially calcschist, partially chalky and pyrite.

Basin Boundry Fault Zone @ 2190 - 2198
Metacarbonated Mudstone: Dark grey-black colored, moderately hard, common fault clay.
Deviation Survey 9° @2198m

Marble: White-milky white, moderately hard to hard, sucrosic texture.

Muscoviteschist: Pearly-light grey colored, moderately hard, platy, peraly luster, rarely chloritization.

Calcschist: light grey-off white, grey colored, hard, partially chalky calcite fillings.

Quartzite - Quartz Muskoviteschist: Dull white, translucent very hard quartzites; light grey-grey colored, moderately hard to hard, pearly luster quartz muscoviteschists, partially chalky and pyrite.

Marble: White-milky white, moderately hard to hard, sucrosic texture.

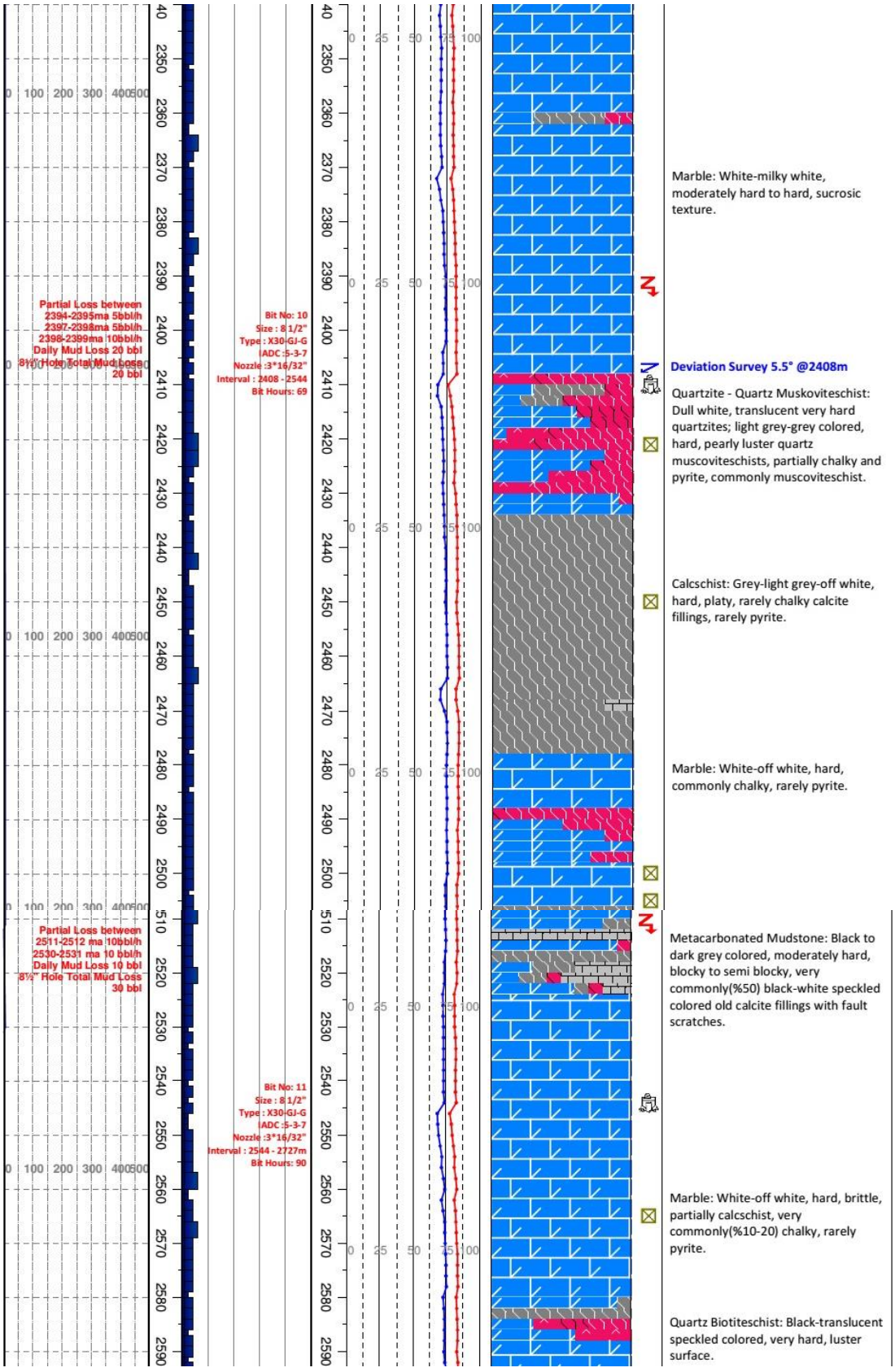
Partial Loss between
2394-2395ma 5bbl/h
2397-2398ma 5bbl/h
2398-2399ma 10bbl/h
Daily Mud Loss 20 bbl
8½" Hole Total Mud Loss
20 bbl
Bit No: 10
Size : 8 1/2"
Type : X30-GJ-G
ADC :5-3-7
Nozzle :3*16/32"
Interval : 2408 - 2544
Bit Hours: 69
Deviation Survey 5.5° @2408m
Marble: White-milky white, moderately hard to hard, sucrosic texture.
Quartzite - Quartz Muskoviteschist: Dull white, translucent very hard quartzites; light grey-grey colored, hard, pearly luster quartz muscoviteschists, partially chalky and pyrite, commonly muscoviteschist.
Calcschist: Grey-light grey-off white, hard, platy, rarely chalky calcite fillings, rarely pyrite.
Marble: White-off white, hard, commonly chalky, rarely pyrite.
Partial Loss between
2511-2512 ma 10bbl/h
2530-2531 ma 10 bbl/h
Daily Mud Loss 10 bbl
8½" Hole Total Mud Loss
30 bbl
Metacarbonated Mudstone: Black to dark grey colored, moderately hard, blocky to semi blocky, very commonly(%50) black-white speckled colored old calcite fillings with fault scratches.
Bit No: 11
Size : 8 1/2"
Type : X30-GJ-G
ADC :5-3-7
Nozzle :3*16/32"
Interval : 2544 - 2727m
Bit Hours: 90
Marble: White-off white, hard, brittle, partially calcschist, very commonly(%10-20) chalky, rarely pyrite.
Quartz Biotiteschist: Black-translucent speckled colored, very hard, luster surface.

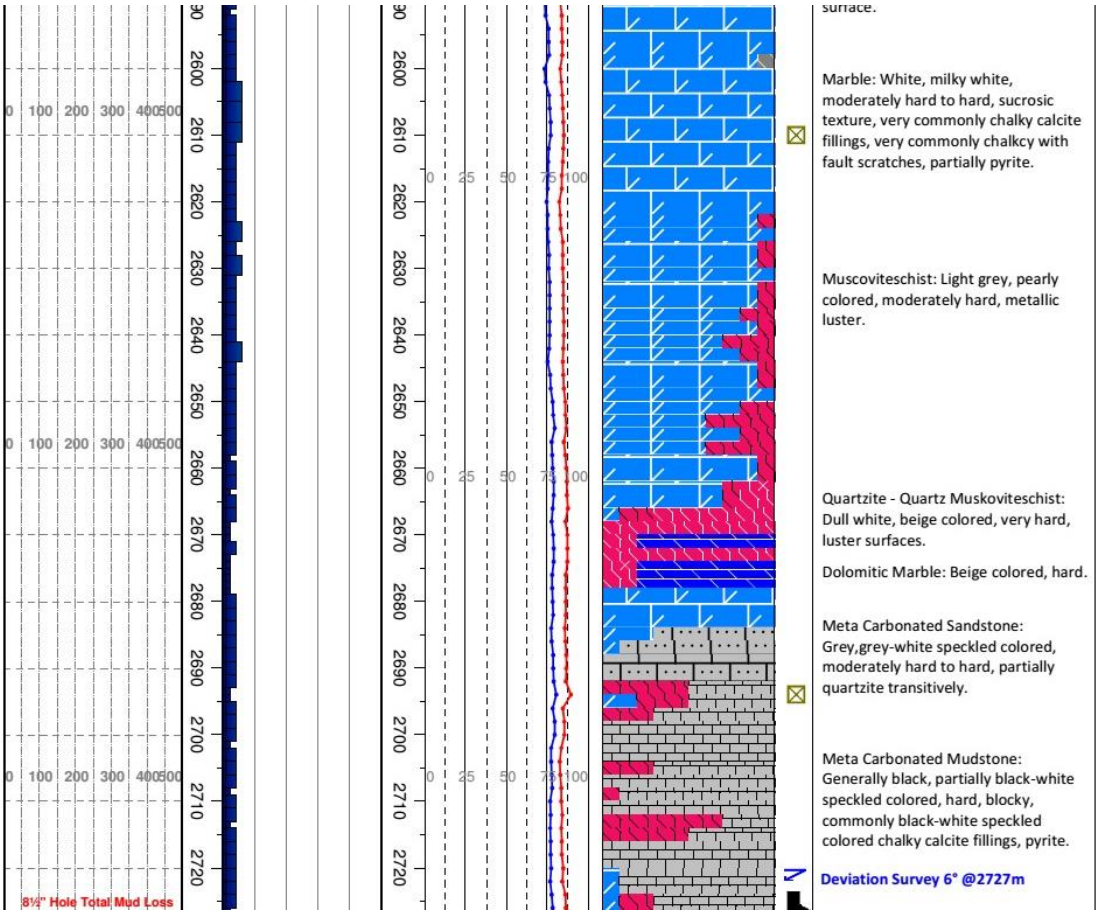

D.4 CUTTING SAMPLE LOG FOR X-8

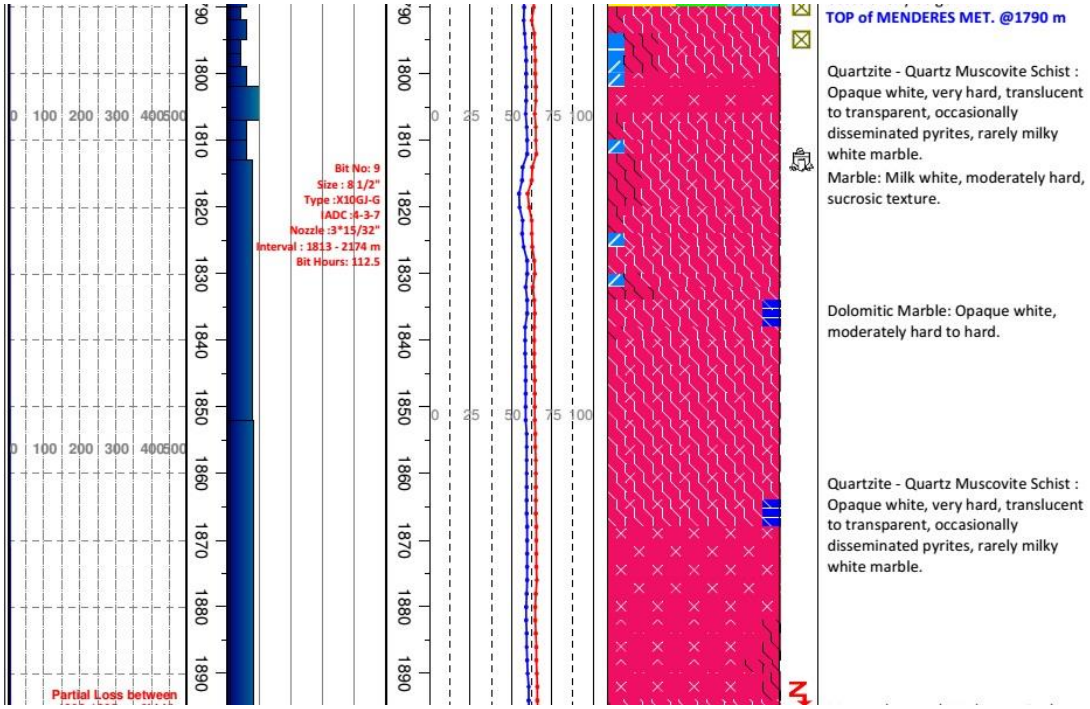

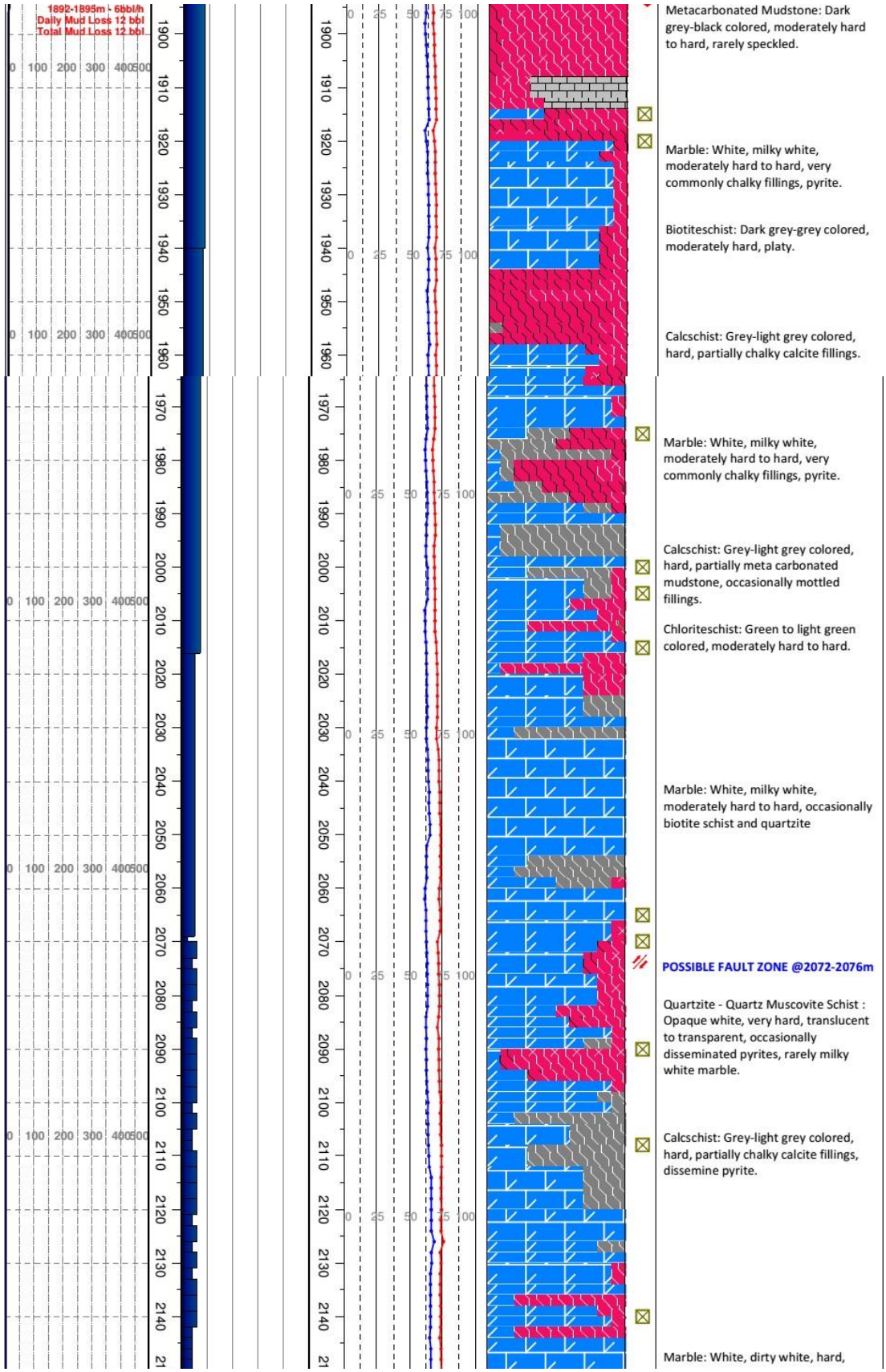
1892-1895m - 6bbl/h
Daily Mud Loss 12 bbl
Total Mud Loss 12 bbl
Metacarbonated Mudstone: Dark grey-black colored, moderately hard to hard, rarely speckled.
Marble: White, milky white, moderately hard to hard, very commonly chalky fillings, pyrite.
Biotiteschist: Dark grey-grey colored, moderately hard, platy.
Calcschist: Grey-light grey colored, hard, partially chalky calcite fillings.
Marble: White, milky white, moderately hard to hard, very commonly chalky fillings, pyrite.
Calcschist: Grey-light grey colored, hard, partially meta carbonated mudstone, occasionally mottled fillings.
Chloriteschist: Green to light green colored, moderately hard to hard.
Marble: White, milky white, moderately hard to hard, occasionally biotite schist and quartzite
POSSIBLE FAULT ZONE @2072-2076m
Quartzite - Quartz Muscovite Schist : Opaque white, very hard, translucent to transparent, occasionally disseminated pyrites, rarely milky white marble.
Calcschist: Grey-light grey colored, hard, partially chalky calcite fillings, dissemine pyrite.
Marble: White, dirty white, hard,

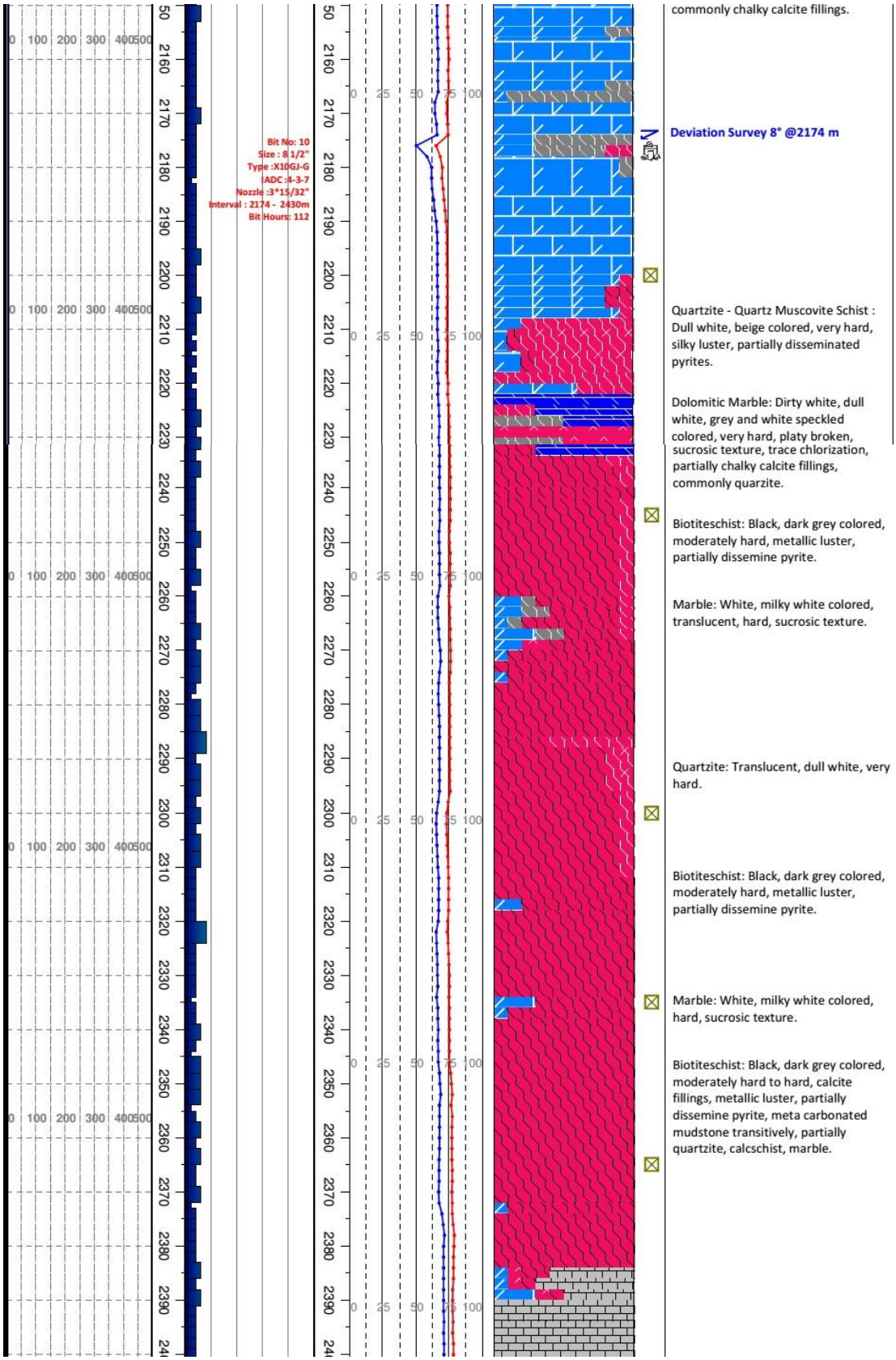

commonly chalky calcite fillings.

Quartzite - Quartz Muscovite Schist : Dull white, beige colored, very hard, silky luster, partially disseminated pyrites.

Dolomitic Marble: Dirty white, dull white, grey and white speckled colored, very hard, platy broken, sucrosic texture, trace chlorization, partially chalky calcite fillings, commonly quarzite.

Biotiteschist: Black, dark grey colored, moderately hard, metallic luster, partially dissemine pyrite.

Marble: White, milky white colored, translucent, hard, sucrosic texture.

Quartzite: Translucent, dull white, very hard.

Biotiteschist: Black, dark grey colored, moderately hard, metallic luster, partially dissemine pyrite.

Marble: White, milky white colored, hard, sucrosic texture.

Biotiteschist: Black, dark grey colored, moderately hard to hard, calcite fillings, metallic luster, partially dissemine pyrite, meta carbonated mudstone transitively, partially quartzite, calcschist, marble.

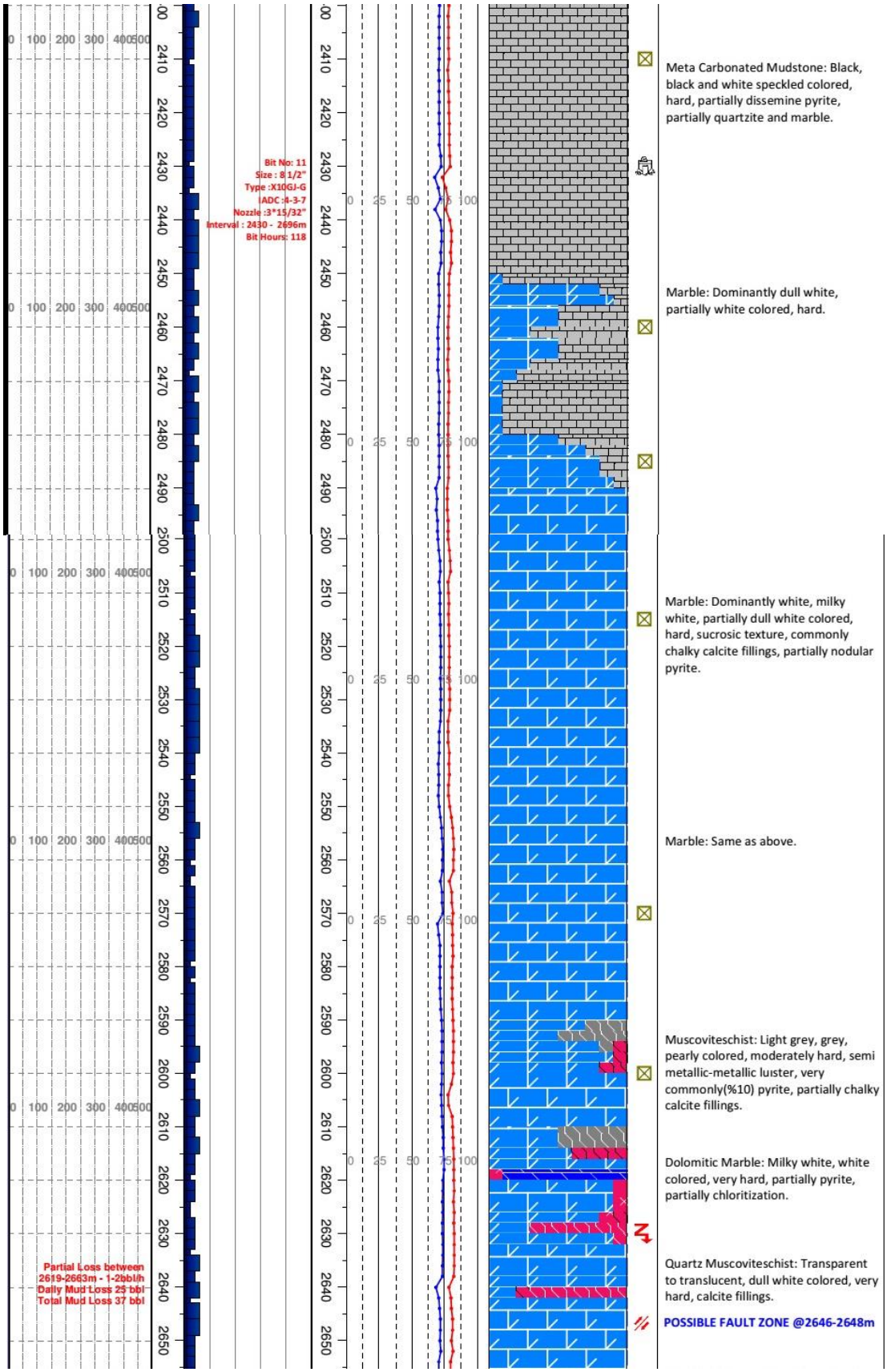
Bit No: 11
Size : 8 1/2"
Type :X10GJ-G
IADC :4-3-7
Nozzle :3*15/32"
Interval : 2430 - 2696m
Bit Hours: 118
Partial Loss between
2619-2663m - 1-2bbl/h
Daily Mud Loss 25 bbl
Total Mud Loss 37 bbl
Meta Carbonated Mudstone: Black, black and white speckled colored, hard, partially dissemine pyrite, partially quartzite and marble.
Marble: Dominantly dull white, partially white colored, hard.
Marble: Dominantly white, milky white, partially dull white colored, hard, sucrosic texture, commonly chalky calcite fillings, partially nodular pyrite.
Marble: Same as above.
Muscoviteschist: Light grey, grey, pearly colored, moderately hard, semi metallic-metallic luıster, very commonly(%10) pyrite, partially chalky calcite fillings.
Dolomitic Marble: Milky white, white colored, very hard, partially pyrite, partially chloritization.
Quartz Muscoviteschist: Transparent to translucent, dull white colored, very hard, calcite fillings.
POSSIBLE FAULT ZONE @2646-2648m

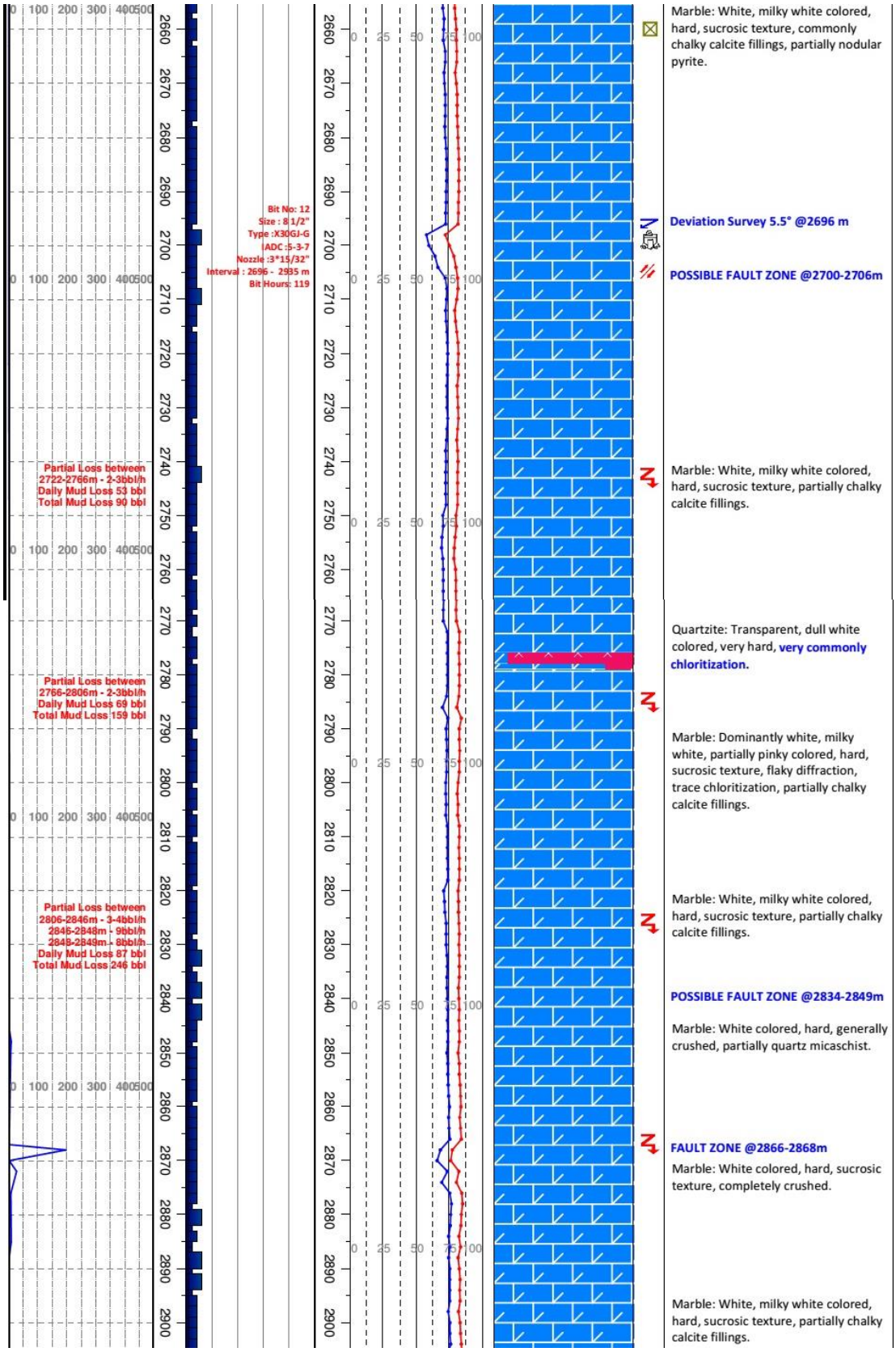
Bit No: 12
Size : 8 1/2"
Type :X30GJ-G
IADC :5-3-7
Nozzle :3*15/32"
Interval : 2696 - 2935 m
Bit Hours: 119
Partial Loss between
2722-2766m - 2-3bbl/h
Daily Mud Loss 53 bbl
Total Mud Loss 90 bbl
Partial Loss between
2766-2806m - 2-3bbl/h
Daily Mud Loss 69 bbl
Total Mud Loss 159 bbl
Partial Loss between
2806-2846m - 3-4bbl/h
2846-2848m - 9bbl/h
2848-2849m - 8bbl/h
Daily Mud Loss 87 bbl
Total Mud Loss 246 bbl
Marble: White, milky white colored, hard, sucrosic texture, commonly chalky calcite fillings, partially nodular pyrite.
Deviation Survey 5.5° @2696 m
POSSIBLE FAULT ZONE @2700-2706m
Marble: White, milky white colored, hard, sucrosic texture, partially chalky calcite fillings.
Quartzite: Transparent, dull white colored, very hard, very commonly chloritization.
Marble: Dominantly white, milky white, partially pinky colored, hard, sucrosic texture, flaky diffraction, trace chloritization, partially chalky calcite fillings.
Marble: White, milky white colored, hard, sucrosic texture, partially chalky calcite fillings.
POSSIBLE FAULT ZONE @2834-2849m
Marble: White colored, hard, generally crushed, partially quartz micaschist.
FAULT ZONE @2866-2868m
Marble: White colored, hard, sucrosic texture, completely crushed.
Marble: White, milky white colored, hard, sucrosic texture, partially chalky calcite fillings.

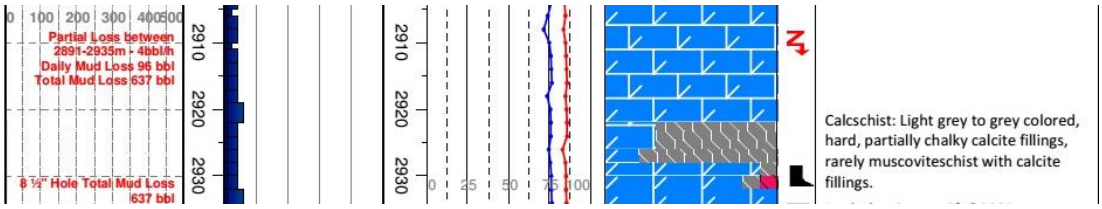
0 100 200 300 400 500
Partial Loss between 2891-2935m - 4bbl/h
Daily Mud Loss 96 bbl
Total Mud Loss 637 bbl
8 ½" Hole Total Mud Loss 637 bbl
2910
2920
2930
0 25 50 75 100
N
Calcschist: Light grey to grey colored, hard, partially chalky calcite fillings, rarely muscoviteschist with calcite fillings.